

**INTEGRATION OF CORE AND PETROPHYSICAL DATA TO EVALUATE
THE RESERVOIR HETEROGENEITIES IN THE LOWER GORU
FORMATION, SOUTHERN INDUS BASIN, PAKISTAN**



AMNA JAVED

01-262222-012

**DEPARTMENT OF EARTH AND ENVIRONMENTAL SCIENCES
BAHRIA UNIVERSITY ISLAMABAD
OCTOBER 2024**

INTEGRATION OF CORE AND PETROPHYSICAL DATA TO EVALUATE THE
RESERVOIR HETEROGENEITIES IN THE LOWER GORU FORMATION,
SOUTHERN INDUS BASIN, PAKISTAN



AMNA JAVED

01-262222-012

A thesis submitted in fulfilment of the requirements for the award of the degree of
Master of Science (Geology)

DEPARTMENT OF EARTH AND ENVIRONMENTAL SCIENCES

BAHRIA UNIVERSITY ISLAMABAD

OCTOBER 2024


Bahria University

Department of Earth & Environmental Sciences
Islamabad Campus, Islamabad

Dated: 30-10-2024

Certificate

A thesis submitted by **Ms. Amna Javed** to the Department of Earth & Environmental Sciences, Bahria University, Islamabad in partial fulfillment of the requirements for the degree of **Masters in Geology** (Session 2022-2024).

Committee Member	Name	Signature
Supervisor	Mr. Adeeb Ahmed	
Internal Examiner	Mr. Tausif Ahmad	
External Examiner	Dr. Abdus Saboor	
Post Graduate Coordinator	Dr. Muhammad Iqbal Hajana	
Head of Department (E&ES)	Dr. Syed Umair Ullah Jamil	

APPROVAL FOR EXAMINATIONScholar's Name: Amna JavedRegistration No: 82947Program of Study: MS GeologyThesis Title: Integration of Core and Petrophysical Data to Evaluate the Reservoir Heterogeneities in the Lower Goru Formation, Southern Indus Basin, Pakistan

It is to certify that the above scholar's thesis has been completed to my satisfaction and, to my belief, its standard is appropriate for submission for examination. I have also conducted plagiarism test of this thesis using HEC prescribed software and found similarity index at 10% and from single source is 1% that is within the permissible limit set by the HEC for the MS degree thesis. I have also found the thesis in a format recognized by the BU for the MS thesis.

Principal Supervisor's Signature: _____

Date: _____

Name: Adeeb Ahmed

AUTHOR'S DECLARATION

I, Amna Javed is hereby state that my MS thesis titled “Integration of Core and Petrophysical Data to Evaluate the Reservoir Heterogeneities in the Lower Goru Formation, Southern Indus Basin, Pakistan” is my own work and has not been submitted previously by me of taking any degree from this university “Bahria University Islamabad” or anywhere else in the country/world. At any time if my statement is found to be incorrect even after my graduation, the University has the right to withdraw/cancel my MS degree.

Name of the Scholar: Amna Javed

Date: _____

PLAGIARISM UNDERTAKING

I solemnly declare that research work presented in the thesis titled “Integration of Core and Petrophysical Data to Evaluate the Reservoir Heterogeneities in the Lower Goru Formation, Southern Indus Basin, Pakistan” is solely my research work with no significant contribution from any other person. Small contribution/help wherever taken has been duly acknowledged and that complete thesis has been written by me.

I understand the zero-tolerance policy of the HEC and Bahria University towards plagiarism. Therefore, I as an Author of the above titled thesis declare that no portion of my thesis has been plagiarized and any material used as reference is properly referred/ cited.

I understand that if I am found guilty of any formal plagiarism in the above titled thesis even after award of MS degree, the university reserves the right to withdraw, revoke my MS degree and that HEC and the University has the right to publish my name on the HEC/University website on which names of the scholars are placed who submitted plagiarized thesis.

Scholar / Author’s Sign: _____

Name of the Scholar: Amna Javed

DEDICATION

I dedicate my work to my father Ch. Javed Iqbal. Thank you for guiding me, inspiring me and making me what I am today. You deserve endless gratitude.

ACKNOWLEDGMENTS

First and foremost, I would like to express my gratitude to Almighty Allah for His supremacy, countless blessings, and for being the redeemer of my soul.

This project would not have been possible without the support of many people. Many thanks to my supervisor, Mr. Adeeb Ahmed, Senior Lecturer, Department of Earth and Environmental Sciences, Bahria University, for helping me throughout my thesis/research work. I have benefited greatly from your wealth of knowledge. I am extremely grateful that you took me on as a student and continued to have faith in me. Also, thanks to my father, Mr. Javed Iqbal, for guiding and helping me. I would like to express my sincere gratitude to all the staff of G & R lab I-9 Islamabad for their invaluable support. I would like to express my appreciation to Dr. Muhammad Iqbal Hajana, PGP Coordinator, and Dr. Syed Umair Ullah Jamil, Head of the Department of Earth and Environmental Sciences, Bahria University, Islamabad. I am indebted to the Oil and Gas Development Company Limited and the Bahria University for support throughout my research work. I also thank my colleagues for several valuable suggestions.

My sincere thanks to Mr. Momin Ahmad Butt, Ms. Laiba Khan, and my baby brother (Arslan Javed) and friends for their invaluable assistance throughout the project and during my state of affliction.

ABSTRACT

Integrating core and petrophysical data to evaluate reservoir heterogeneities in the Lower Goru Formation of the Southern Indus Basin, Pakistan provides a comprehensive understanding of the formation's complexities. This study aims to identify facies and mineralogical variations within the reservoir, examining how these factors contribute to its heterogeneity and affect reservoir properties. The research seeks to illuminate the interplay between geological characteristics and reservoir quality by correlating core data with petrophysical measurements.

Methodologically, this study involved a comprehensive analysis of three cores from basal sands of the Lower Goru Formation, extracted from Wells A, B, and C. The cores were thoroughly logged for sedimentological, lithological, and ichnological features, followed by detailed slab and thin section studies to assess mineralogical composition and textural properties. Core plug samples were subjected to porosity, permeability, and water saturation measurements using advanced techniques. Additionally, gamma-ray logging and well log analysis provided further insights into the formation's petrophysical attributes.

The analysis reveals a diverse sedimentary sequence, characterized by very fine to coarse granule-sized sandstones with varying sedimentary structures such as cross laminations and mud-drapes. The facies indicate a shoaling-up sequence from offshore to shoreface environments. Core plug analysis highlights significant reservoir heterogeneity, with variable porosity and permeability, suggesting complex spatial distribution and potential sweet spots for hydrocarbon production. Well-log data corroborate these findings, showing moderate porosity but extremely low permeability and high water saturation, challenging hydrocarbon extraction.

In conclusion, the study underscores the Lower Goru Formation's complex reservoir characteristics, marked by significant heterogeneity in facies, mineralogy, and petrophysical properties. The integration of core and well log data highlights the need for tailored recovery strategies to manage the reservoir's tight nature and high water content, aiming to optimize hydrocarbon extraction and improve reservoir management practices.

TABLE OF CONTENTS

CHAPTER	TITLE	PAGE
	APPROVAL FOR EXAMINATION	iii
	AUTHOR'S DECLARATION	iv
	PLAGIARISM UNDERTAKING	v
	DEDICATION	vi
	ACKNOWLEDGEMENTS	vii
	ABSTRACT	viii
	TABLE OF CONTENTS	ix
	LIST OF TABLES	xv
	LIST OF FIGURES	xvi
	LIST OF ABBREVIATIONS	xxi
1	INTRODUCTION	1
	1.1 Background of the Study	1
	1.2 Location and Accessibility to the Study Area	2
	1.2.1 Location	2
	1.2.2 Accessibility to the study area	2
	1.3 Previous Work	4
	1.3.1 Research gap	6
	1.4 Problem Statement	6
	1.5 Aims and Objectives	7
	1.6 Significance of the Study	8
	1.7 Data Acquired	8

2	REGIONAL GEOLOGY	9
	2.1 Introduction	9
	2.2 Regional Tectonics	10
	2.3 Paleogeographic Evolution and Depositional Style	12
	2.4 Stratigraphy of the Study Area	15
	2.5 Petroleum System	15
	2.5.1 Petroleum play of the study area	16
	2.5.1.1 Source rock	16
	2.5.1.2 Reservoir rock	16
	2.5.1.3 Seal rock	16
3	METHODOLOGY	19
	3.1 Introduction	19
	3.2 Data Set	20
	3.3 Core Sampling and Description	20
	3.4 Slab and Thin Section Studies	21
	3.5 Porosity, Permeability, and Water Saturation Measurements	21
	3.6 Gamma Ray Logging and Core Log Preparation	22
	3.7 Well Log Analysis	22
	3.7.1 Porosity calculation	23
	3.7.2 Permeability estimation	23
	3.7.3 Water saturation determination	23
	3.8 Correlation and Integration of Data	24
4	CORE ANALYSIS	25
	4.1 Background	25

4.2	Core Analysis of Well A	26
4.2.1	Core 1 (Well A)	26
4.2.2	Panoramic view of the Core 1	27
4.2.3	General description of the Core 1	28
4.2.4	Findings	34
4.3	Core analysis of Well B	36
4.3.1	Core 2 (Well B)	36
4.3.2	Panoramic view of the Core 2	37
4.3.3	General description of the Core 2	38
4.3.4	Findings	44
4.4	Core analysis of Well C	46
4.4.1	Core 3 (Well C)	46
4.4.2	Panoramic view of the Core 3	47
4.4.3	General description of the Core 3	48
4.4.4	Findings	53
4.5	Sedimentary Texture	53
4.5.1	Grain size	53
4.5.2	Grain shape and sorting	53
4.6	Physical Sedimentary Structures	54
4.7	Biogenic Sedimentary Structures	55
4.7.1	Biologic description	56
4.7.1.1	Ophiomorpha	56
4.7.1.2	Asterosoma	57
4.7.1.3	Planolites	57
4.7.1.4	Macaronichnus	58
4.7.1.5	Conichnus	58

4.8	Core Logs	64
4.9	Gamma-Ray Logs	69
4.9.1	Gamma Ray Spectroscopy	69
4.9.2	GR-Spectroscopy analyses results	70
4.9.3	GR-Spectroscopy analyses correlation	72
5	DEPOSITIONAL SEDIMENTARY FACIES AND THE ENVIRONMENTS	74
5.1	Background	74
5.2	Sedimentary Facies	75
5.2.1	Facies-A (intense biodegradation)	75
5.2.2	Facies-B (moderate biodegradation)	76
5.2.3	Facies-C (finer to very coarse-grained sandstone)	77
5.2.4	Facies-D (extensive biogenic activity)	79
5.2.5	Facies-E (less bioturbation)	80
5.2.6	Facies-F (coarse grained sandstone)	80
5.2.7	Facies-G (medium-grained sandstone)	81
5.2.8	Facies-H (medium-lower to fine-upper grained sandstone)	82
5.2.9	Facies-I (shaley patch)	83
5.2.10	Facies-J (lenticular shaley laminations)	84
5.2.11	Facies-K (unconsolidated massive sandstone)	84
6	PETROGRAPHIC ANALYSIS	87
6.1	Introduction	87
6.2	Petrographic Analysis of the Core Sections Studied	88

6.3	Slab Studies	88
6.3.1	Findings	90
6.4	Thin Section Studies	97
6.4.1	Thin section properties	98
6.4.2	Mineralogical properties	99
6.4.2.1	Detrital constituents	99
6.4.2.2	Cementing materials	99
6.4.2.3	Compaction and porosity reduction	100
6.4.3	Findings	104
7	RESERVOIR HETEROGENEITIES THROUGH CORE ANALYSIS AND PETROPHYSICAL ANALYSIS	106
7.1	Introduction	106
7.2	Horizontal Core Plug Analysis	108
7.2.1	Introduction	108
7.2.2	Calculated parameters	109
7.2.2.1	Porosity	109
7.2.2.1	Permeability	111
7.2.2.1	Water saturation	112
7.2.3	Results	113
7.3	Petrophysical Analysis	114
7.3.1	Introduction	114
7.3.2	Logs used in petrophysical analysis	116
7.3.3	Calculated parameters	122
7.3.3.1	Volume of shale (VSH-GR)	122
7.3.3.2	Neutron Density porosity (PHIT-ND)	122

7.3.3.3 Sonic porosity (PHIT-S)	123
7.3.3.4 Average total porosity (PHIT-FINAL)	124
7.3.3.5 Effective porosity through Neutron Density Log (PHIE-ND)	124
7.3.3.6 Effective porosity through Sonic log (PHIE-S)	125
7.3.3.7 Average Effective Porosity (PHI-FINAL)	126
7.3.3.8 Permeability through well regression (PERM-WR)	126
7.3.3.9 Saturation of water (SW)	127
7.3.4 Porosity, permeability and water saturation determined through Well logs	128
7.3.5 Picket plot creation	128
7.3.6 Results	131
CONCLUSIONS	133
FUTURE SUGGESTIONS	135
REFERENCES	136
APPENDICES	144-159

LIST OF TABLES

TABLE NO.	TITLE	PAGE
2.1	Estimated General Stratigraphy of the Study Area.	17
7.1	Average results from the Horizontal Core Plug Analysis.	113
7.2	Average results from the Well log Analysis.	131
7.3	Calculated parameters from the samples through core and petrophysical analysis.	132

LIST OF FIGURES

FIGURE NO.	TITLE	PAGE
1.1	Location of Bitrism Block with Study Area marked in Blue and Wells marked in red.	3
1.2	The Satellite image of study area (Bitrism block).	4
2.1	Photographs (left) showing tectonic map of Pakistan (Kazmi and Rana, 1982), while right side displays tectonic features exposed in the study area (Raza et al., 1990).	10
2.2	(A) Photograph showing Cretaceous shoreline across the territory of Pakistan (B) Tethys shoreline during Late Paleocene to Late Pliocene (C) General trend of Paleo-Vitakri River from East to West, transporting sediment from Indian shield rock and depositing them in Proto-Indus system (D) General trend of Paleo Indus River system from North to South, transporting sediments from Himalayan mountains to Indus basin (E) Geodynamics of Indian plate.	14
2.3	General stratigraphic succession of the lower Indus Basin-Pakistan (after Zaigham and Mallick 2000).	18
3.1	Complete Workflow of Thesis.	19
4.1	Position of the Core 1 within Basal Sand of Lower Goru Formation, in Well A.	26
4.2	Panoramic view of Core 1 Well A	27
4.3	Position of the Core 2 within Basal Sand of Lower Goru Formation, in Well B.	36
4.4	Panoramic view of Core 2 Well B.	37
4.5	Position of the Core 3 within Basal Sand of Lower Goru Formation, in Well C.	46
4.6	Panoramic view of Core 3 Well C.	47
4.7	Photographs showing Intense bioturbation fabric in a medium fine-grained sandstone. Large sub-horizontal burrows have destroyed most of the original bedding. (A) Ichnofacies Macaconichus, Thalassinoids, Ophiomorpha and Planolites are visible. (B) Ichnofacies Skolithos and Planolites are visible. (C)	59

- Whitish grey coarser sand particles are observed that are calcareous in nature with Ichnofacies Planolites and Ophiomorpha. (D) Ichnofacies Macaconichus, Ophiomorpha and Planolites are visible.
- 4.8 Photographs showing Intense bioturbation fabric in a medium fine-grained sandstone. Large sub-horizontal burrows have destroyed most of the original bedding. (A) Ichnofacies Macaconichus, Thalassinoids, Ophiomorpha and Planolites are visible. (B) Ichnofacies Macaconichus, Thalassinoids, Ophiomorpha and Planolites are visible. (C) Ichnofacies Thalassinoids can be observed. (D) Ichnofacies Skolithos, Conichus, Thalassinoids, Ophiomorpha and Planolites are visible. 59
- 4.9 (A) Ichnofacies Macaconichus, Thalassinoids, Ophiomorpha and Planolites are visible. (B) Brownish grey sandstone with wavy planar laminations and calcareous patch with a sub vertical ophiomorpha. (C) Brownish grey sandstone with calcareous granules and a shift in grain size from medium fine to lower coarse grains is noticeably visible with abundance of burrows. (D) Brownish grey fine to medium fine sandstone with a few horizontal burrows (Thalassinoides) can be observed. 60
- 4.10 (A, B, C and D) Brownish grey to yellowish grey compact sandstone with carbonaceous filled wavy planar laminations including flaser and lenticular bedding. 60
- 4.11 (A) Photograph showing Flaser bedding. (B and C) Photograph showing Pebbly lags. (D) Photograph showing Slightly angular shaley laminations. 61
- 4.12 (A, B and C) Intensely bioturbated sandstone with no preserved sedimentary structures. 61
- 4.13 Photograph showing Finer grained sandstone at the top, fracture filled with carbonaceous material in the middle and coarser grained sandstone rock at the bottom. 61
- 4.14 (A, B, C and D) photographs showing whitish grey sandstone with visible fractures filled with carbonaceous material. 62
- 4.15 (A, B, C and D) photographs showing whitish grey medium grained sandstone showing carbonaceous material filled laminations (planar laminations, slightly angled laminations, wavy angular laminations and trough-cross laminations). 62
- 4.16 Photographs showing (A) Pebbly lags with cross laminations filled with carbonaceous material. (B) Shaley laminas. 62

4.17	Photograph showing (A, B and C) Medium coarse to upper coarse sandstone Showing planner laminations, slightly angled laminations, wavy angular laminations and cross laminations. Some are filled with carbonaceous material. (D) Perfect visual display of trogh-cross bedding.	63
4.18	(A and B) Brownish grey unconsolidated coarse grained fissile sandstone present with Sulphur i.e. greenish yellow in color and organic matter/ coaly material i.e. blackish in color.	63
4.19	(A to H) Marked stains showing rigorous bubbling when reacted with 10% HCl due to the presence of calcareous material. Coarse to vary coarse grained brownish grey unconsolidated sandstone is visible.	63
4.20	Core log of Core-1 Well A generated by using Easycore software.	66
4.21	Core log of Core-2 Well B generated by using WellCAD software.	67
4.22	Core log of Core-3 Well C generated by using Easycore software.	68
5.1	(A): Sub-environments of a Barrier Island System (From Reinson G. E., 1984).	85
5.2	(B): Generalized profile of the Beach and Nearshore Zone. (From Reinson, G. E., 1984).	86
6.1	Microphotographs of Slabs showing (A) Quartz Vein and a lithic fragment. (B) fairly porous and permeable sandstone with Iron oxide (brown spots) and biotite/mafic (black spots) material. (C and D) Compact hard sandstone with shale/sand laminas. (E and F) fairly porous and permeable sandstone with carbonaceous matrix.	91
6.2	Microphotographs of Slabs showing (G) Compact sandstone with blueish green colored Gluconite and calcareous cementation. (H) poorly sorted sandstone with mineral Gluconite and lithic rock fragment. (I) Hard sandstone rock with medium to lower coarser grains, different cementing material is visible. (J) Poorly sorted greyish sandstone with a black spot maybe iron oxide. (K and L) Sandstone with fracture filled with probably Iron matrix.	92
6.3	Microphotographs of Slabs showing (M) Sub rounded to angular grains with a vein of probabbly carbonaceous or micaceous material. (N) Fine to very fine compact hard rock with micaceous material and laminations. (O and P) Poorly too fairly sorted sandstone with fair visible porosity. (Q and R) Carbonaceous matrix is present with a hint of Mica.	93

- 6.4 Microphotographs of Slabs showing (S) Fine to medium grained sandstone with abundance of iron oxide. (T) fairly sorted sandstone with whitish lithic fragment. (U and V) Fine to coarse sub rounded to angular grained compact rock with fair sorting. (W) Cross laminations are visible with maybe an oil stain in the left. (X) coarse grained sandstone rock with greenish/blueish spots representing maybe gluconite. 94
- 6.5 Microphotographs of Slabs showing (Y) Medium to coarse grain compact rock with micaceous material and maybe Gluconite. (Z) Quartz fragments with red spots representing Iron minerals. (A1 and B1) Medium to fine grained sandstone with calcareous matrix. (C1) Quartz fragments and micaceous material is present. (D1) fairly sorted sandstone with laminations. 95
- 6.6 Microphotographs of Slabs showing (F1) Brownish laminations in the upper part which are non-calcareous while rest of the matrix is highly calcareous. (F1) Rigorous reaction with 10% HCl, visible bubbling due to presence calcareous material. (G1) Black carbonaceous/Organic matter is present with good to fair sorting of grains. (H1) Sub rounded to angular Quartz grains. (I1) thin pebbly lags layer present in finer sediments. (J1) Ichnofacie is visible on the left bottom corner filled with some whitish material. 96
- 6.7 Microphotographs of Slabs showing (K1 and L1) trace fossils/burrows filled with carbonaceous organic matter. 97
- 6.8 Microphotographs under XPL with 4X magnification, showing (A) polycrystalline quartz, (B) fractured quartz granules (C) tourmaline (D) algal fragment (E) bioclast (F) bivalve shell (G) gastropode (H) recrystallized calcite filled shell fragment (I, J) oyster shells (K) pyretized shell (L) pyrite cement (M) pyrite cement under (PPL) (N) pyrite grain on quartz granule and (O) pyrite cement with a polycrystalline granule in medium grained sandstone. 101
- 6.9 (A) Microphotograph showing Quartz, mica and a green mineral. (B) Microphotograph showing the same minerals under PPL. (C) Microphotograph showing sutured Quartz grains. (D) Microphotograph showing excellent quartz overgrowth. (E) Microphotograph showing plagioclase with albite twinning under PPL. (F) Microphotograph showing the quartz grain surrounded and corroded by ferroan calcite cement. (G and H) Microphotograph showing ferroan calcite cementing material. 102
- 6.10 Microphotograph showing (A) the coarse size Quartz grains which are rounded to sub rounded and are moderately sorted. (B) Quartz mineral with clear edges and corner with some microfractures on the surface. (C) moderately to fairly sorted Quartz grains (10X). (D) Texturally and mineralogically matured closely packed Quartz 103

grains showing moderate visual porosity. (E) Closely packed and fairly sorted Quartz arenite with green color Glauconite mineral. (F). fine grained Quartz arenite closely packed with dark brown material most probably organic/ carbonaceous material.

7.1	Calculated parameters from Well log of Well A, B and C.	118
7.2	Well Log data of Well A.	119
7.3	Well Log data of Well B.	120
7.4	Well Log data of Well C.	121
7.5	Picket Plot of Well A.	129
7.6	Picket Plot of Well B.	130
7.7	Picket Plot of Well C.	130

LIST OF ABBREVIATIONS

PL	-	Planolites
SK	-	Skolithos
OP	-	Ophiomorpha
MC	-	Macaronichnus
CO	-	Conichnus
TH	-	Thalassinoides
GR	-	Gamma Ray Log
DT	-	Sonic Log
CALI	-	Caliper Log
SFLU	-	Spherically Focused Log
LLD	-	Laterolog Deep
RHOB	-	Bulk Density Log
PHIN	-	Neutron Log
SP	-	Spontaneous Potential Log
VSH-GR	-	Volume of Shale
PHIT-ND	-	Total Neutron and Density Porosity
PHIT-S	-	Total Sonic Porosity
PHIT-FINAL	-	Average Total Porosity
PHIE-ND	-	Effective Neutron and Density Porosity
PHIE-S	-	Effective Sonic Porosity
PHI-FINAL	-	Average Effective Porosity
PERM-WR	-	Permeability through Well Regression
SW	-	Saturation of Water
HCL	-	Hydrochloric Acid

RCA	-	Regular Core Analysis
SCAL	-	Special Core Analysis
XPL	-	Cross Polarized Light
PPL	-	Plain Polarized Light
NMR	-	Nuclear magnetic Resonance
SW-AR	-	Saturation of Water through Archie's Equation

CHAPTER 1

INTRODUCTION

1.1 Background of the Study

Reservoir heterogeneity, as described by Alpay (1972), captures the geological complexities of a reservoir and their impact on fluid flow within the subsurface formation. This phenomenon includes a range of variations in reservoir properties, particularly porosity, permeability, and water saturation, occurring across scales from the microscopic to the large-scale (Weber, 1982). The composition and depositional processes, including bioturbation, are key factors influencing reservoir heterogeneities. The mineralogical makeup of the framework minerals reflects the mechanical and chemical stability of the reservoir, while depositional and diagenetic processes significantly influence properties such as sandstone body shape, sorting, and levels of organic activity (Morad et al., 2000).

This study focuses on the Lower Goru Sandstone of the Cretaceous in the Lower Indus Basin, Pakistan, aiming to elucidate reservoir heterogeneities resulting from compositional and depositional differences. The sedimentary basins of Pakistan, ranging from the Cambrian to the Miocene and Pliocene epochs, contain petroleum-rich sedimentary rocks, primarily composed of clastic and non-clastic types. Notably, the hydrocarbon potential is mainly concentrated in carbonates and sandstones. Within the Indus Basin, the Lower Goru Sandstone, deposited during the Cretaceous period, is a significant reservoir rock, widely distributed throughout the Central and Southern Indus Basins (Kadri, 1995). Variations in reservoir performance within the Lower Goru Formation are attributed to changes in sediment supply dynamics due to tectonic activity and climatic conditions during the Cretaceous. Consequently, this study seeks to uncover the depositional details and associated reservoir heterogeneities within the Lower Goru Sandstone.

In essence, this research aims to contribute to a comprehensive understanding of the geological and petrophysical complexities characterizing the Lower Goru Sandstone reservoir, thereby facilitating more informed exploration and exploitation strategies in similar geological contexts.

1.2 Location and Accessibility to the Study Area

1.2.1 Location

The research area is located within the Thar Platform in the southern part of the Indus Basin in Pakistan as shown in the Figure 1.1. To the north, the southern Indus Basin is defined by the Sukkur Rift, which separates it from the central Indus Basin. The eastern border of the southern Indus Basin is adjacent to the Indian Shield, while the western border is marked by the marginal zone of the Indian Plate. The southward extension of this basin is restricted by the offshore Murray Ridge-Oven Fracture plate boundary (Kadri, 1995). The key geological units in the southern Indus Basin include the Thar Platform, Karachi Trough, Kirthar Foredeep, Kirthar Fold Belt, and Offshore Indus (Kadri, 1995).

1.2.2 Accessibility to the study area

The study area is situated within the Khairpur district of Sindh Province, spanning coordinates between 26°16' and 26°29' N Latitude and 68°54' to 69°0' E Longitude as shown in the figure 1.2. The primary urban center nearby is Sanghar, positioned approximately 40 kilometers to the south of the study site. Geographically, the area falls within Central Sindh Province, bordered to the north by the Jacobabad High (Sukkar Ridge), to the east by the Jaisalmir High, to the south by the Thar Slope and Nagarparkar Ridge, and to the west by the Thatha and Hyderabad High. (Kadri, 1995).

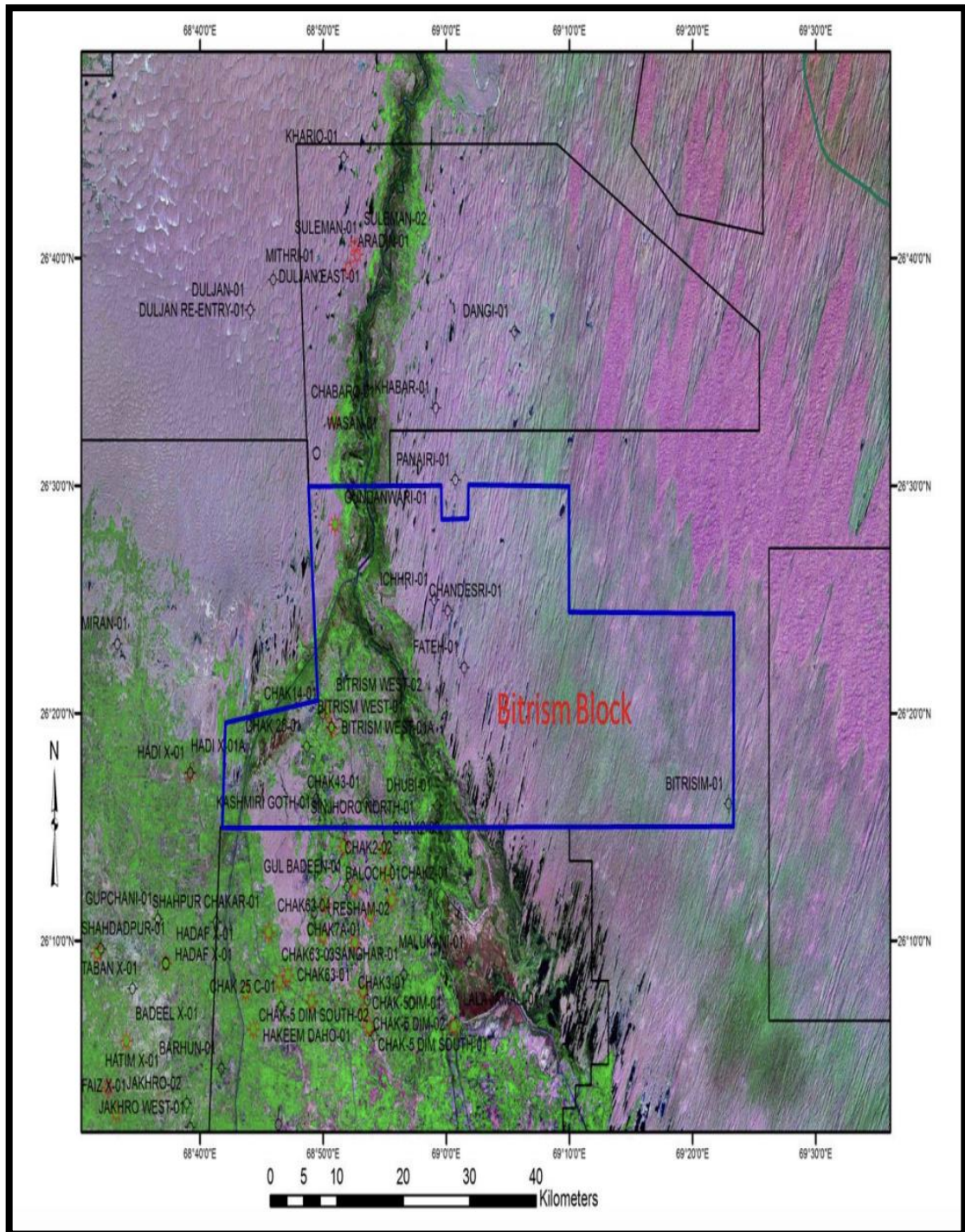


Figure 1.2 The Satellite image of study area (Bitrism block) (Ilyas, 2019).

1.3 Previous Work

Williams (1959) provided an early overview of the Goru Formation, building on Oldham's (1892) observations of the "Belemnite Beds." Jones (1961) later

categorized the lithological components within the "Parh group." The Goru Formation is named after the village of Gorm in the Kirthar range, near the Nar River, and has been divided into the Upper and Lower Goru Formations (Kadri, 1995). The Upper Goru Formation primarily consists of fine-grained sedimentary rocks, while the Lower Goru Formation is characterized by sandstone layers subdivided into upper, middle, and basal sands, with intercalated shale units such as the Turk shale, Badin shale, and Jhol shale. In the hydrocarbon-rich upper sand layers, further subdivisions like A-sand, B-sand, C-sand, and D-sand have been identified based on intermittent lithologies (Quadri and Shuaib, 1986).

Raza et al. (2020) conducted a detailed study using synthetic seismograms and well logs to calculate petrophysical parameters and rock physics properties. Their findings revealed that the B-interval of Miano 9 and 10 holds high hydrocarbon saturation, porosity, and permeability, indicating a promising hydrocarbon zone. Dar et al. (2021) focused on petrophysical and SEM analyses, interpreting gamma-ray log data to define five electrofacies, each representing distinct depositional environments such as shoreface, tidal flats, and transgressive shelves. Ahmed et al. (2021) employed TOC and Rock-Eval pyrolysis to evaluate source rock potential, while Khalid et al. (2022) used 2D seismic synthetic modeling to map the Talhar Shales and Sembar Formation, which dip towards the northeast and overlay the Chilton limestone reservoir.

Ali et al. (2022) utilized petrophysical modeling techniques, including Picket plot charts and cross-plots, to identify lithological zones in KGF, confirming its potential as a rich gas zone. Waqar et al. (2022) explored the stratigraphic model of six wells, highlighting how lateral facies changes, driven by sea-level fluctuations, influence the pinching of pay zones towards the northeast. Similarly, Khaskheli et al. (2022) and Khan et al. (2023) examined the depositional and diagenetic processes impacting reservoir quality, finding that key factors like carbonate cementation, quartz overgrowth, and authigenic chlorite significantly influence porosity and permeability.

Ashraf et al. (2020) utilized an integrative approach combining petrophysical parameters, geostatistical analysis, and rock physics with Constrained Sparse Spike

Inversion (CSSI) to evaluate reservoir quality and spatial heterogeneity in the B-Sand and C-Sand of the Lower Goru Formation within the Sawan Gas Field, highlighting spatial heterogeneities in sand ratio and porosity. Hussain et al. (2017) assessed hydrocarbon prospects in the Lower Goru Formation's basal sand units using well log data, revealing significant commercial hydrocarbon potential in net pay zones, with up to 95% hydrocarbon saturation. Khan et al. (2017) analyzed gamma-ray log data from the Hakeem Daho well to examine depositional facies, identifying lithological heterogeneities related to eustatic sea-level changes. Siyar et al. (2017) characterized the Lower Goru Formation's reservoirs in the central Indus Basin, identifying fine-grained silty sandstone as a good reservoir based on petrophysical parameters.

Nisar et al. (2016) used seismic and well log data to study the structural style and reservoir properties of the Lower Goru Formation, finding water-saturated zones due to hydrophobic effects. Baig et al. (2016) investigated reservoir diagenesis in the Lower Goru Formation, emphasizing the impact of chlorite coatings and quartz overgrowth on porosity and permeability. Abbas et al. (2015) utilized geophysical techniques for 3D modeling of the Sawan Gas Field, identifying stratigraphic-cum-structural traps with excellent reservoir properties. Sahito et al. (2013) examined the depositional environment of the Upper Sands in the Lower Goru Formation, indicating fluctuating energy near-shore deposition. Munir et al. (2011) used seismic stratigraphy and rock physics to locate hydrocarbon sands in the Sawan field, confirming gas presence and saturation. Mohsin et al. (2010) performed a diagenetic analysis of the Lower Goru Formation's basal sands, highlighting the role of quartz cement in porosity. Berger et al. (2009) studied chlorite cement's influence on porosity preservation in feldspathic litharenite at depth in the Sawan gas field.

These studies collectively underscore the intricate geological heterogeneities within the Goru Formation, emphasizing the interplay between lithology, structure, and diagenesis in determining its hydrocarbon potential.

1.3.1 Research gap

While these studies have significantly advanced the understanding of the Lower Goru Formation's reservoir potential, gaps remain in fully comprehending the interplay between depositional processes, diagenetic alterations, and their collective impact on reservoir heterogeneities, particularly in deeper and less explored sections of the formation. Future research should focus on integrating high-resolution geophysical techniques with advanced diagenetic studies to unravel these complexities.

1.4 Problem Statement

The Lower Goru Formation, a key hydrocarbon reservoir within the Lower Indus Basin of Pakistan, exhibits complex heterogeneities due to its varied depositional environments, mineralogical compositions, and diagenetic alterations. Despite extensive research on its reservoir characteristics, significant challenges remain in understanding the detailed spatial distribution and influence of these heterogeneities on reservoir performance. Current methods often inadequately correlate core data with petrophysical analysis, leading to gaps in accurately predicting reservoir behavior and optimizing exploration and production strategies. This research seeks to address these challenges by integrating core analysis with advanced petrophysical techniques to systematically investigate the facies, mineralogy, and their contributions to reservoir heterogeneity in the Lower Goru Formation. By refining the understanding of these factors, this study aims to enhance the prediction accuracy of reservoir properties, thereby supporting more effective hydrocarbon exploration and extraction in similar geological settings.

1.5 Aims and Objectives

The objectives of this research are as follows

- a) To identify facies and mineralogy using core data, with a focus on understanding their contributions to reservoir heterogeneity.

b) To correlate core data with petrophysical data, examining how these relationships influence various reservoir properties and their associated heterogeneities.

1.6 Significance of the Study

The current research presents a novel approach that uniquely links the provenance and depositional styles to the reservoir heterogeneities of the Cretaceous sandstone units. Integral to this study is the examination of ichnology, which provides a foundational methodology for Interpreting depositional processes and their subsequent effects on reservoir quality. The observed variations in reservoir properties significantly influence overall reservoir performance. Therefore, this investigation is poised to offer valuable insights into the reservoir heterogeneity of the Lower Goru Formation, which is critical for the strategic exploration and production of hydrocarbons. This research aims to develop comprehensive strategies that enhance our understanding and management of reservoir heterogeneity, ultimately supporting more efficient hydrocarbon extraction and resource utilization.

1.7 Data Acquired

Data have been obtained from three cores extracted from Wells A, B, and C, targeting the basal sands of the Lower Goru Formation. Additionally, the corresponding well logs for these wells have been acquired in LAS format.

CHAPTER 2

REGIONAL GEOLOGY

2.1 Introduction

This chapter is structured to focus on the regional geology of the study area, covering aspects such as tectonics, basin evolution, and the stratigraphic framework. Regional tectonics play a crucial role in shaping basin architecture, which in turn significantly influences the development of the stratigraphic framework. To gain insights into sediment types, sediment supply rates, and drainage patterns influenced by topography, a comprehensive understanding of regional tectonics is essential. Beyond tectonic factors, basin evolution and the stratigraphic framework offer a detailed depiction of the paleoenvironment and paleoclimate at the time of stratigraphic deposition. Thus, an in-depth understanding of regional geology is necessary to comprehend the source and depositional styles of lithostratigraphic units, which is valuable for highlighting their economic significance, such as reservoir heterogeneities in this study. The study area is part of the Sindh Monocline in the Southern Indus Basin within the Gondwanan domain of the Indian plate, showcasing a complete Cretaceous stratigraphic sequence (Raza et al., 1990) (Fig. 2.1).

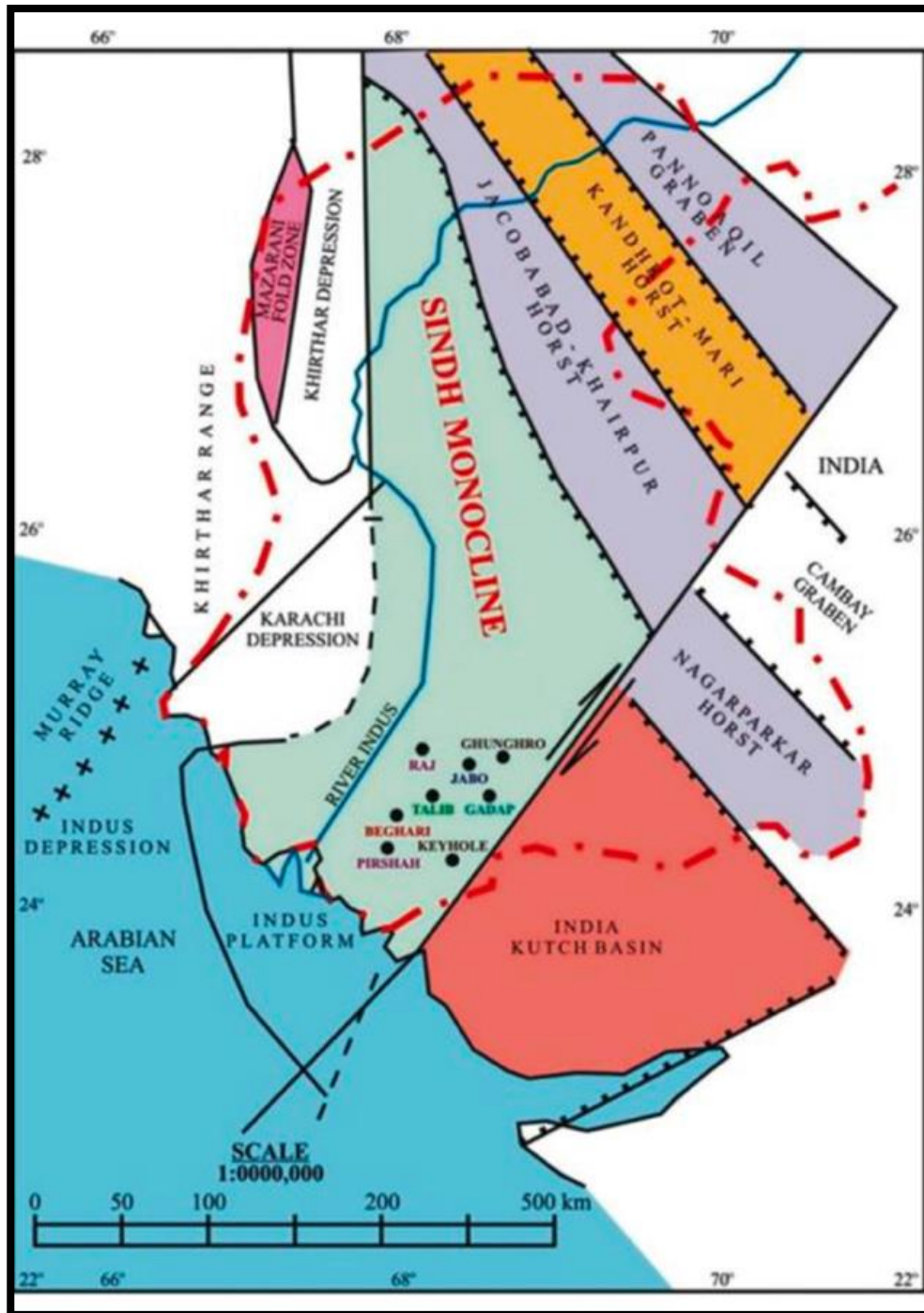


Figure 2.1 Photographs displays tectonic features exposed in the study area (Raza et al., 1990).

2.2 Regional Tectonics

Situated in the northwestern part of the Indian plate, Pakistan's territory reflects a tertiary convergence zone of the Indo-Asian plate, representing a

combination of the Gondwanian, Tethyan, and Laurasian domains (from south to north) (Kazmi and Jan, 1997; Sheikh and Naseem, 1999). Regionally, Pakistan's geological boundaries include the Arabian plate to the south, the Eurasian plate to the north, and the Afghan/Lut/Iran block to the west (Molnar and Tapponnier, 1975). Interactions with these tectonic plates have resulted in Pakistan's distinctive geology and physiography, showcasing a prime example of plate tectonics. The Main Karakoram Thrust (MKT) and the Main Mantle Thrust (MMT) define the convergent boundary between the Indian plate, Kohistan Island Arc (KIA), and the Karakoram block in the north. Additionally, the subduction of the Arabian plate beneath the southern margin of the Eurasian plate along the Makran coast exemplifies an oceanic-continent convergent boundary, while the north-south striking Chaman transform boundary delineates the western boundary with the Afghan block (Kazmi and Jan, 1997).

The complex interaction and tectonic evolution began with early rifting in the Gondwana supercontinent, leading to the formation of a passive continental margin, notably of the Atlantic type, during the Permo-Triassic period (Searle, 1983). Effective rifting caused the Indo-Australian plate to separate from the Madagascar plate during the Cretaceous period (Powell, 1979). Interaction between the Indo-Asian plates occurred in the Late Cretaceous, with collision and subsequent orogeny starting in the Middle Eocene (Molnar and Tapponnier, 1975; Powell, 1979). During its northward journey, the Indian plate rotated counterclockwise, introducing extensional tectonic features (Powell, 1979). Consequently, the Indo-Pakistan plate experienced both extensional and collisional regimes (Fig. 2.2). Geological structures such as the hill ranges, Cis and Trans Indus ranges, and the Sulaiman and Kirthar mountains reflect these evolutionary phases. Jurassic-Early Paleocene extensional tectonics influenced much of the Gondwanian domain, including the study region. The northward drift and counterclockwise rotation of the Indian plate created an extensional regime in the west and a compressional regime in the north, causing the uplift of Indian shield rocks and subsidence of platform regions, forming horsts and grabens along with volcanic activities (Sheikh and Naseem, 1999). Moreover, tilted faults in the platform regions led to the formation of the Sindh monocline (Kemal, 1991). The study area, part of the Sindh monocline, is bordered by tectonic features

such as the Jacobabad-Khairpur horst to the northeast, the Karachi depression and Indus platform to the southwest, the Nagarparkar horst and Indian Kuch basin to the southeast, and the Kirthar depression to the northwest (Raza and Ahmed, 1990) (Fig. 2.1).

2.3 Paleogeographic Evolution and Depositional Style

In addition to the intermontane basins and the recently identified Pishin basin/Kaker Khorasa basin (Pishin Basin) (Ahmed, 1991), Pakistan's physiography features two primary evolutionary basins that encapsulate the majority of the country's depositional history. These two basins are the Baluchistan basin and the Indus basin, separated by the Chaman transform boundary, marked by the Ornach Nal and Chaman strike-slip faults (Kadri, 1995; Sheikh and Naseem, 1999). The Indus basin is particularly renowned for its sedimentary rock sequence, which spans from the Precambrian to the recent period, although it notably lacks strata from the Carboniferous, Devonian, Silurian, and Ordovician periods (Shah, 2009).

During the basin's evolutionary stages, post-Jurassic upwarping of the Indian shield led to the formation of the Sargodha highs, Jacobabad highs, and Mari Kandkhot highs (Siddiqui, 2004). These highs significantly influenced sedimentation, acting as barriers and creating shelf or neritic regions within the sedimentary basin (Shah, 2009). Consequently, the Indus basin is divided into two tectonostratigraphic provinces: The Kirthar-Sulaiman (Lower Indus basin) and the Kohat-Potwar provinces (Upper Indus basin). The Lower Indus basin is bordered by the Indian shield and the marginal zone of the Indian plate to the east and west, respectively, with the Murray Ridge-Oven Fracture Zone to the south and the Sukker Rift to the north. The Jacobabad-Mari-Kandhkot highs further subdivide the Lower Indus basin into the Central and Southern Indus basin during the late Cretaceous (Raza and Ahmed, 1990).

Physiographically, the Southern Indus basin comprises the Offshore Indus, Kirthar Fold Belt and Foredeep, Karachi Trough, and Thar Platform (Khattak et al., 2004). The Indus basin is an ideal site for sediment deposition, receiving sediments from various regions, particularly from the hinterland in the north and northwest and

the shield rocks in the east and southeast (Malkani and Mahmood, 2016). The unique depositional style of the basin is attributed to shifting sedimentation sites throughout the tectonic history of the Indian plate. During the Paleozoic era, the Indian plate experienced a pyrogenic style of sedimentation, functioning as a stable platform with the northern passive margin serving as the primary site for sediment deposition (Shah, 2009).

In the Permian period, the rifting led to the opening of the Neotethys Ocean, shifting sedimentation to the north and northwestern passive margins (Kazmi and Jan, 1997). Throughout the Mesozoic era, the northwestern part of the Indian plate remained the principal site of sedimentation, while the rest of the plate, functioning as an island, saw no sedimentation (Shah, 2009). The Cretaceous period marked significant tectonic instability and seaward progradation of the Indian plate, with various sites acting as depocenters. During the Early Cretaceous, sedimentation occurred in the Upper Indus Basin, the Sulaiman range area, and parts of the southern Axial belt, including the Quetta region (Shah, 2009).

A prograding delta during this time was represented by parts of the Cis and Trans Indus ranges and regions of the Sargodha highs, while other regions were characterized by shallow marine environments. In the Late Cretaceous, tectonic upwarping of the Indian shield resulted in the formation of the Sargodha highs, Sanjawi arc, and Jacobabad highs. The intervening areas continued to be sites of clastic sedimentation, whereas shallow marine regions facilitated carbonate deposition (Shah, 2009).

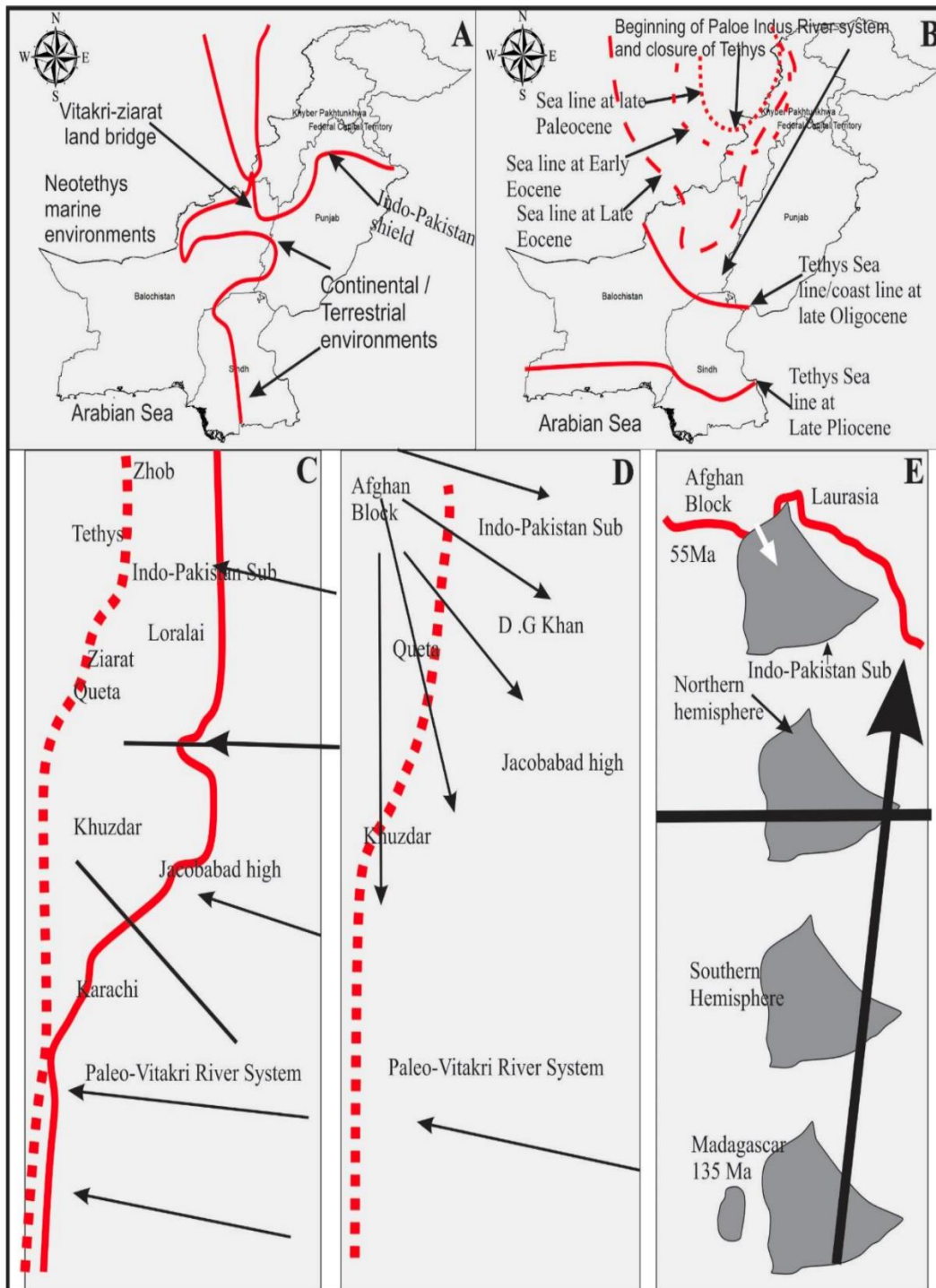


Figure 2.2 (A) Photograph showing Cretaceous shoreline across the territory of Pakistan (B) Tethys shoreline during Late Paleocene to Late Pliocene (C) General trend of Pale-Vitakri River from East to West, transporting sediment from Indian shield rock and depositing them in Proto-Indus system (D) General trend of Pale Indus River system from North to South, transporting sediments from Himalayan mountains to Indus basin (E) Geodynamics of Indian plate.

2.4 Stratigraphy of the Study Area

The study area is situated in the Southern Indus basin, containing a substantial Mesozoic-Tertiary sedimentary sequence overlain by recent deposits (Kadri, 1995). The Cretaceous rocks, the focus of the current study, include a thick and complete stratigraphic sequence spanning from the Berriasian to the Late Maastrichtian and are present in various regions of the Southern Indus basin as shown in Figure 2.3 (Kadri, 1995; Kazmi and Jan, 1997).

The Lower Goru Formation, a prominent stratigraphic unit within the Lower Indus Basin of Pakistan, is part of the Cretaceous succession, characterized by a complex depositional environment indicative of significant paleoenvironmental shifts. This formation, primarily composed of interbedded sandstones, shales, and siltstones, represents a significant hydrocarbon reservoir in the region. The depositional environment of the Lower Goru is interpreted as a transition from fluvial to deltaic and shallow marine settings, reflecting variations in sediment supply and relative sea level changes during the Cretaceous period (Khan et al., 2007). The sandstones within this formation are often well-sorted and display significant lateral and vertical heterogeneity, suggesting a high-energy depositional setting influenced by channel and deltaic processes (Ahmed et al., 2012). The shales, on the other hand, are indicative of low-energy, offshore marine conditions, often rich in organic content, which are crucial for the generation and preservation of hydrocarbons (Farooq et al., 2015). Stratigraphically, the Lower Goru is subdivided into several members (Table 2.1), each representing distinct depositional episodes and environments, thus providing a detailed record of the Cretaceous sedimentation within the basin (Zaigham and Mallick, 2000).

2.5 Petroleum System

The petroleum system consists of a mature source rock, pathway, reservoir, trap and seal. Appropriate relative timing of formation of these elements and the processes of generation, migration and accumulation are necessary for hydrocarbons to accumulate and be preserved. Exploration plays and prospects are typically

developed in basins or regions in which a complete petroleum system has some likelihood of existing. (Kadri, 1995).

2.5.1 Petroleum play of the study area

A play is “a group of geologically related prospects having similar conditions of source, reservoir and trap. (Kadri, 1995). Within a basin the presence of play elements plays an important role in hydrocarbon accumulation. The petroleum system consists of a mature source rock, migration pathway, reservoir rock, trap and seal appropriate relative timing of formation of these elements and processes of generation. Lower Indus basin is the main hydrocarbon producing basin of Pakistan 37% hydrocarbon is extracted from lower Indus basin.

2.5.1.1 Source rock

The lower Cretaceous Shale of Sembar Formation is a proven source for oil and gas discovered in the lower Indus basin because of its organic richness in oil-prone kerogen and thermal maturity. The lower part of the Goru Formation (Talhar shale) is moderately rich in organic shale having fair to good genetic potential. Studies based on virginities reflectance infer that the kerogen is a virginities dominated and mature up to a depth of 2977 m in lower Goru Formation. Where amorphous organic matter rich oil prone kerogen become dominant and can be regarded as “potential source rock”. (Thompson, 1976).

2.5.1.2 Reservoir rock

Basal sands of Lower Goru (Cretaceous) Formation are the primary objective in this area. These sands are proven producers in several fields. Average porosities for these sands are around 13% in the prospect area (Thompson, 1976).

2.5.1.2 Seal rock

A thick stratigraphic sequence of shale and marl of upper Goru Formation serves as cap rock for underlying Lower Goru Sand Reservoir. The shale of Lower Goru Formation also has the same properties (Thompson, 1976).

Table 2.1 Estimated General Stratigraphy of the Study Area.

Age	Formation	Formation top	Thickness	Lithology
Post Eocene	Alluvium	Surface	625	Sandstone with subordinate claystone.
~~~~~ UNCONFIRMITY ~~~~~ ~				
Eocene	Laki	610	531	Limestone with subordinate Shale.
~~~~~ UNCONFIRMITY ~~~~~ ~				
Palaeocene	Ranikot	1160	362	Sandstone with subordinate Shale.
	Khadro	1522	105	Claystone with sandstone and basalt.
~~~~~ UNCONFIRMITY ~~~~~ ~				
Cretaceous	Parh	1624	255	Chalk
	Upper Goru	1880	301	Marl with subordinate Shale.
	Lower Goru	2183	1335	Sandstone with interbeds of Shale.
	Lower Goru Shale unit	2183	798	Shale, Marl with subordinate Sandstone.
	Basal sand	2993	38	Sandstone with interbeds of Shale.
	Talhar shale	3023	76	Shale with minor Sandstone.
	Massive sand	3095	423	Sandstone with interbeds of Shale.
	Sembar	3514	86+	Shale.



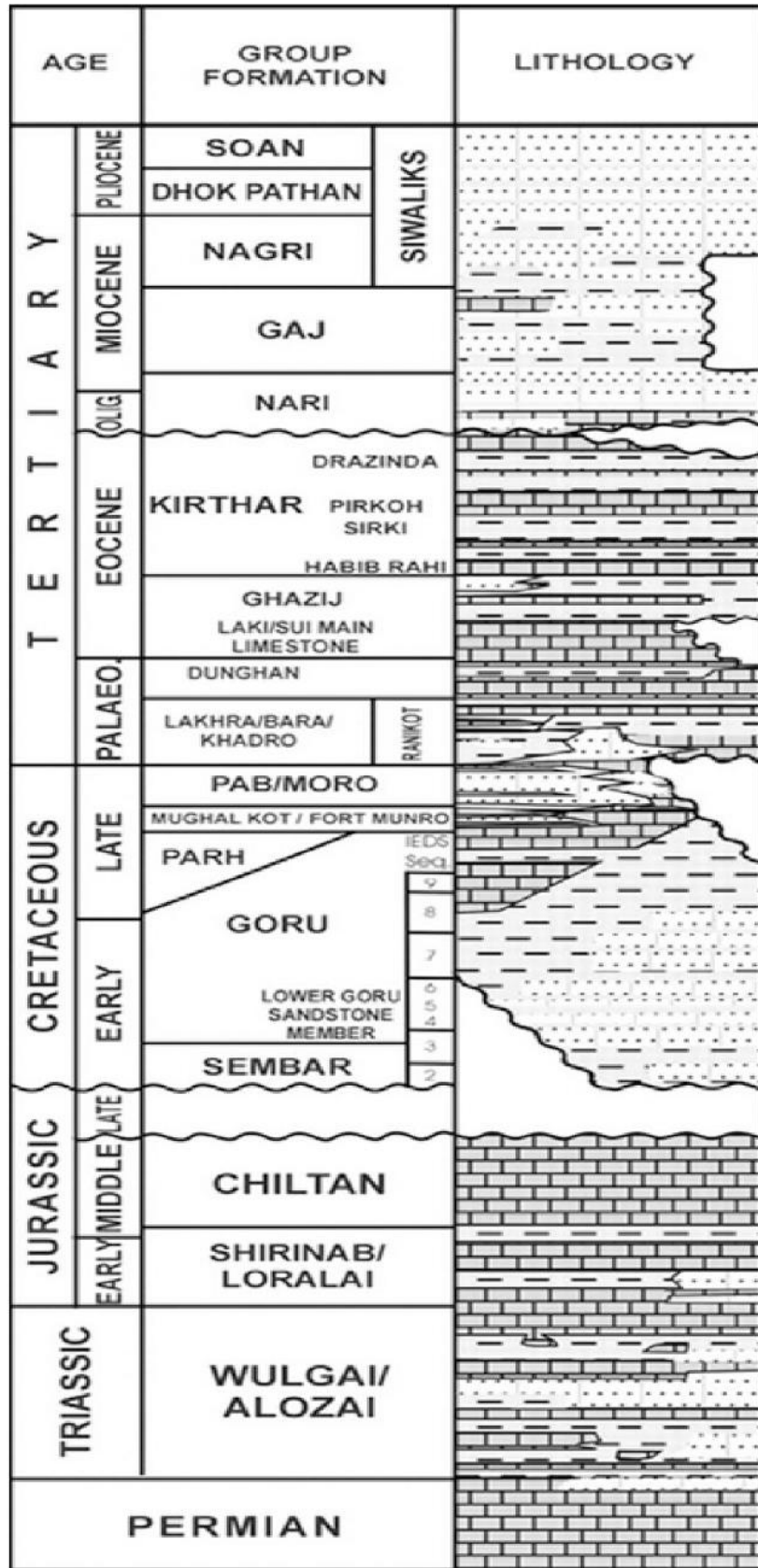


**Figure 2.3** General stratigraphic succession of the lower Indus Basin-Pakistan (after Zaigham and Mallick, 2000).

## CHAPTER 3

### METHODOLOGY

#### 3.1 Introduction

This chapter outlines the methodology employed to analyze core data and petrophysical well logs for the purpose of evaluating reservoir properties, specifically porosity, permeability, and water saturation. The methodology encompasses a series of steps beginning with the collection and description of core samples, followed by laboratory analyses, digital processing of well logs, and integration of data using specialized software. Each step is meticulously designed to ensure the accuracy and reliability of the results, facilitating a comprehensive understanding of the subsurface reservoir characteristics. A complete workflow is described below in Figure 3.1.

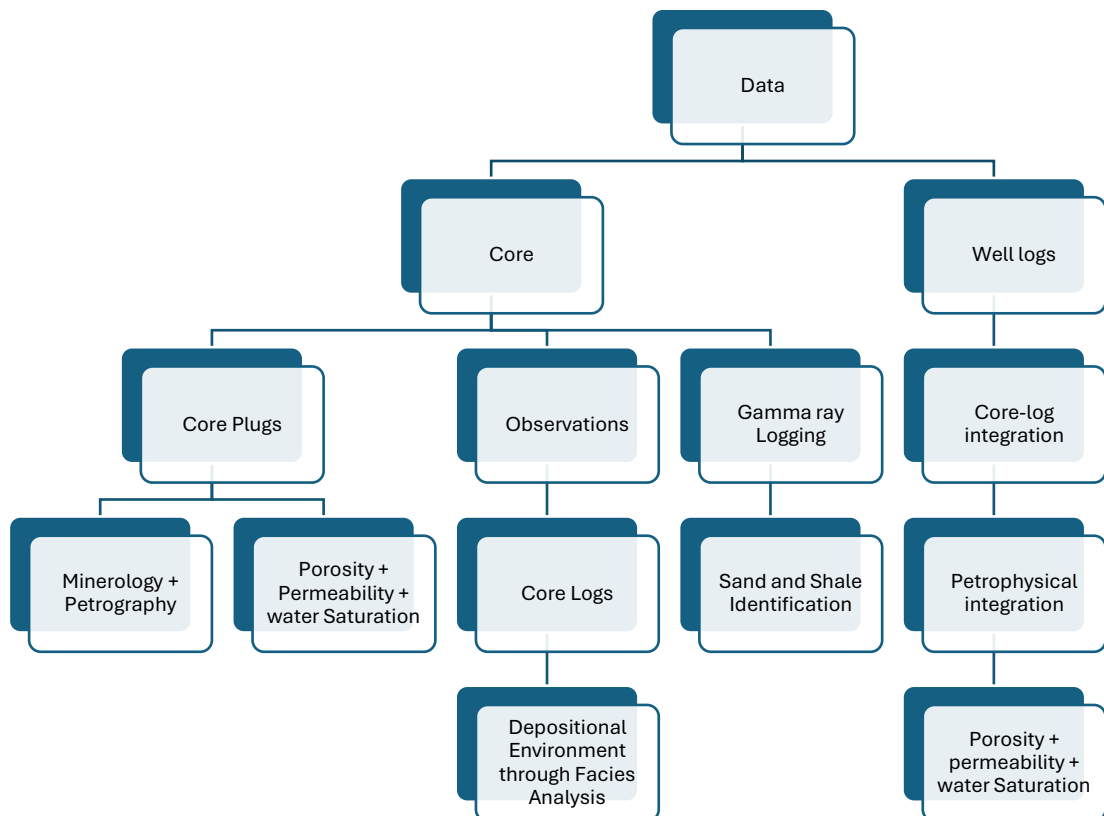


**Figure 3.1** Complete Workflow of Thesis.

### **3.2 Data Set**

In this study, three cores were analyzed, all extracted from the basal sands of the Lower Goru Formation. Core-1 was obtained from Well A, Core-2 from Well B, and Core-3 from Well C. The core recovery rates were excellent, with 100% recovery from Well A, 90% from Well B, and 95% from Well C. These cores provide a robust dataset for evaluating the petrophysical characteristics of the basal sands. Additionally, raw well log data from these wells was utilized for comprehensive petrophysical analysis, ensuring a detailed understanding of porosity, permeability, and water saturation across the studied intervals.

### **3.3 Core Sampling and Description**

The study commenced with comprehensive logging of nine-meter-long cores obtained from each well, focusing on sedimentological, lithological, and ichnological characteristics. Sedimentological and lithological properties, encompassing textural and structural attributes of lithological units, were meticulously documented, while ichnological features, including traces of various fossils, were also recorded. The lithological units were measured using a measuring tape, with each meter of core examined individually to identify facies variations. Core logging was conducted at a centimeter scale, and differentiation between carbonate and non-carbonate lithologies and fossils was achieved using a 10% dilute HCL solution. Textural and mineralogical properties of lithological units were assessed using a hand lens, and millimetric to centimetric scale trace fossils were identified and documented. Various facies, along with distinct depositional and compositional characteristics, were thoroughly photographed. The core was first subjected to a general visual description, wherein lithological features, sedimentary structures, and any visible evidence of porosity were documented. This initial assessment provided a macroscopic understanding of the core, enabling the identification of key intervals for further detailed study.

The core was then logged by hand, with the following parameters recorded: lithology, color, grain size, sorting, cementation, porosity type, and any notable

features such as fractures or bioturbation. These logs served as a foundational dataset, allowing for a preliminary correlation with well logs and aiding in the selection of samples for laboratory analysis.

### **3.4 Slab and Thin Section Studies**

Following the hand logging, 30 core samples were selected for slab and thin section studies. These samples were chosen based on their representativeness of the different lithologies and intervals identified during the core description phase. The slab samples were prepared by cutting the cores into thin slices, providing a larger surface area for detailed visual inspection and analysis. Thin sections for petrographic studies were created by initially polishing one surface of each sample slab. Subsequently, textural properties within each slab were meticulously analyzed, and zones of interest were identified for thin section preparation. The slabs were then thinned into chips and polished using silicon carbide (400, 600, 800, 1000 grit). Proper glass was scraped and polished on one side to embed the chip, following which the chip was grounded and polished to a thickness of 30 micrometers. These thin sections were analyzed using a petrographic microscope, enabling the identification of mineralogical composition, grain size distribution, pore types, and cementation patterns. These observations were critical for understanding the depositional environment and diagenetic history of the reservoir, as well as for estimating porosity at a micro-scale.

### **3.5 Porosity, Permeability, and Water Saturation Measurements**

Core plugs were extracted from the selected samples for quantitative analysis of porosity, permeability, and water saturation. These core plugs, typically cylindrical in shape, were subjected to laboratory measurements using standard industry technique i.e. CMS-300 Horizontal Core Plug Analysis.

Porosity was measured using the Helium Porosimetry method. This technique involves the injection of helium gas into the core plug under controlled pressure, and

the resulting volume displacement is used to calculate the porosity of the sample. This method is favored for its accuracy and non-destructive nature.

Permeability was determined using a gas permeameter, where nitrogen gas was flowed through the core plug under a known pressure differential. The permeability was then calculated based on the flow rate and pressure drop, using Darcy's law.

Water saturation was measured using the Dean-Stark apparatus, a technique that involves the extraction of fluids from the core plug via distillation. The volume of water recovered is compared to the pore volume to calculate the water saturation. This method is particularly effective for accurately determining the amount of water present in the pore spaces of the rock.

### **3.6 Gamma Ray Logging and Core Log Preparation**

A gamma-ray (GR) machine was used to generate the gamma-ray log for the cores. This involved measuring the natural radioactivity of the core samples, which provides an indication of the shale content and helps in identifying lithological boundaries.

The gamma-ray log was then integrated with the core description data to prepare a comprehensive core log. This integration was performed using EasyCore and WellCAD software. EasyCore was utilized for initial log preparation, offering a user-friendly interface for digitizing the core data. WellCAD was employed for further refinement and integration of the data, allowing for the creation of detailed, high-resolution logs. These logs were essential for correlating core data with well logs and for providing a visual representation of the subsurface geology.

### **3.7 Well Log Analysis**

To complement the core data, well logs in LAS (Log ASCII Standard) format were imported into Techlog software for digital processing and analysis. The LAS

files included a suite of logs such as gamma-ray (GR), resistivity, neutron porosity, density, and sonic logs.

Within Techlog, the well logs were first calibrated and corrected for any environmental effects to ensure the accuracy of the data. Following this, a petrophysical interpretation was conducted to calculate porosity, permeability, and water saturation across the wellbore. The interpretation process involved the following steps:

### **3.7.1 Porosity calculation**

Porosity was calculated using the density and neutron logs. The density log provided a direct measure of the bulk density of the formation, from which porosity was derived using a matrix density appropriate for the lithology. The neutron log, which measures the hydrogen content of the formation, was used to cross-check the porosity values and correct for any lithological effects.

### **3.7.2 Permeability estimation**

Permeability was estimated using empirical correlations that relate porosity and other log-derived parameters to permeability. The Timur-Coates and Coates-Dumanoir models were applied, depending on the availability and quality of the data, to provide a robust estimation of permeability.

### **3.7.3 Water saturation determination**

Water saturation was calculated using the resistivity logs in conjunction with the Archie equation. The resistivity log measures the ability of the formation to conduct electrical current, which is influenced by the water content and salinity. By applying the Archie equation, the water saturation was determined for various intervals within the well.

### **3.8 Correlation and Integration of Data**

The final step was the correlation and integration of the core and well log data. Correlation was done by comparing the core-derived properties with those obtained from well logs. This involved correlating the values of porosity, permeability, and water saturation, allowing for a detailed comparison and validation of the results and ensuring a consistent interpretation across different data sets. The integration of core and well log data provided a comprehensive understanding of the reservoir properties, with the core data serving as ground truth for calibrating and validating the well log interpretations.

## CHAPTER 4

### CORE ANALYSIS

#### 4.1 Background

Core analysis is a fundamental practice in geological and petroleum engineering that involves the detailed examination of rock samples, or cores, extracted from subsurface formations to characterize their physical and chemical properties. This analysis provides crucial insights into reservoir properties, including porosity, permeability, and fluid saturation, which are essential for accurate reservoir modeling and hydrocarbon recovery optimization (Tiab and Donaldson, 2012). Core analysis is typically divided into routine core analysis (RCA) and special core analysis (SCAL), with RCA focusing on basic properties like porosity and permeability, while SCAL delves into more complex parameters such as capillary pressure and relative permeability (Dullien, 1992). The data obtained from core analysis is instrumental in calibrating and validating well log interpretations, thus enhancing the reliability of reservoir characterization and simulation models (Johnson, 2010). Furthermore, core analysis is vital for understanding diagenetic processes that affect reservoir quality over geological time, such as cementation, compaction, and dissolution, which directly influence the storage and flow capacity of hydrocarbon reservoirs (Pittman, 1992).

Various characteristics observed in the studied cores have been classified into respective categories that follow in the forthcoming descriptions.



4.2 Core Analysis of Well A

4.2.1 Core 1 (Well A)

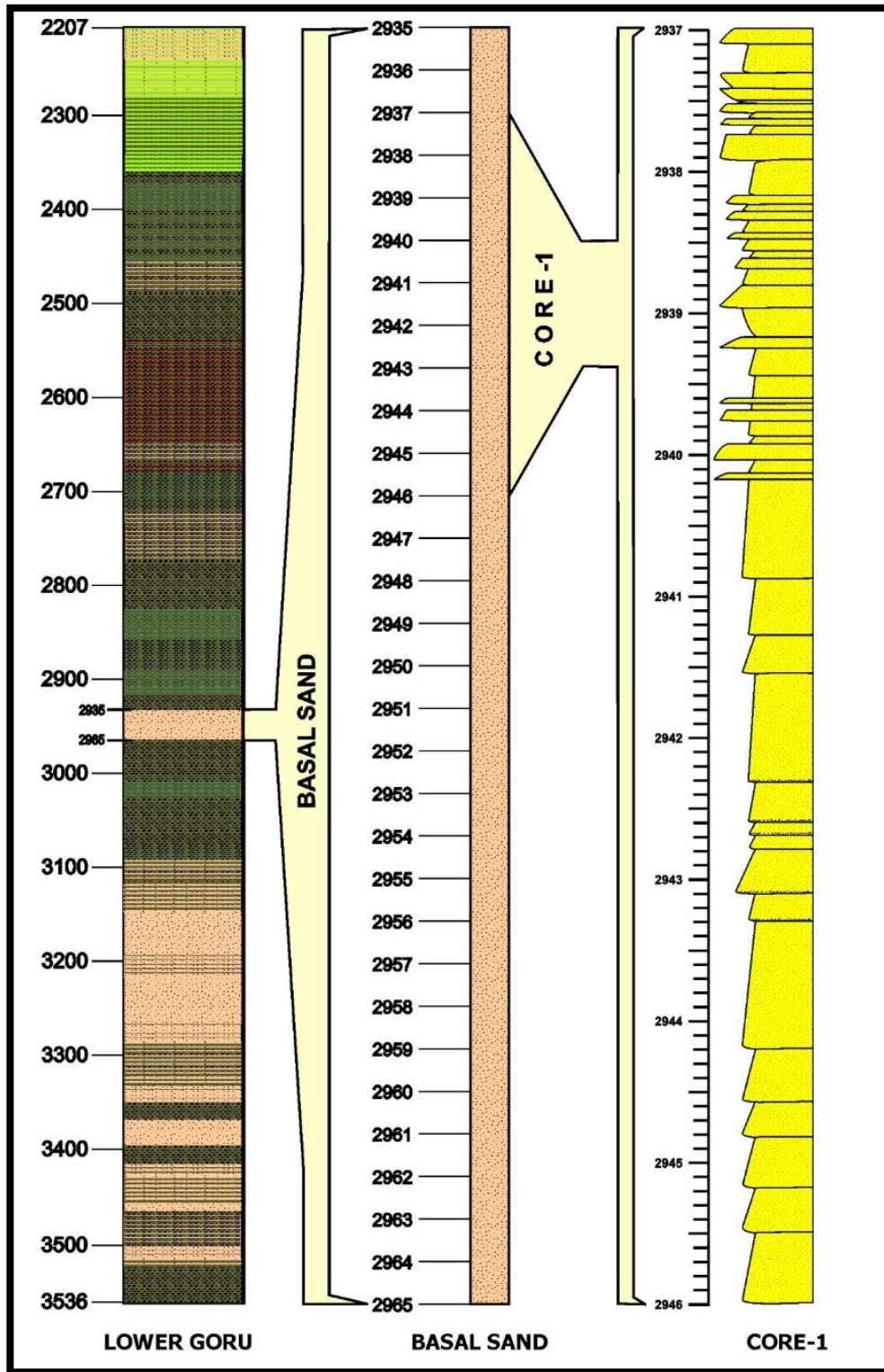


Figure 4.1 Position of the core 1 within Basal Sand of Lower Goru Formation, in Well A.

### 4.2.2 Panoramic view of the core 1

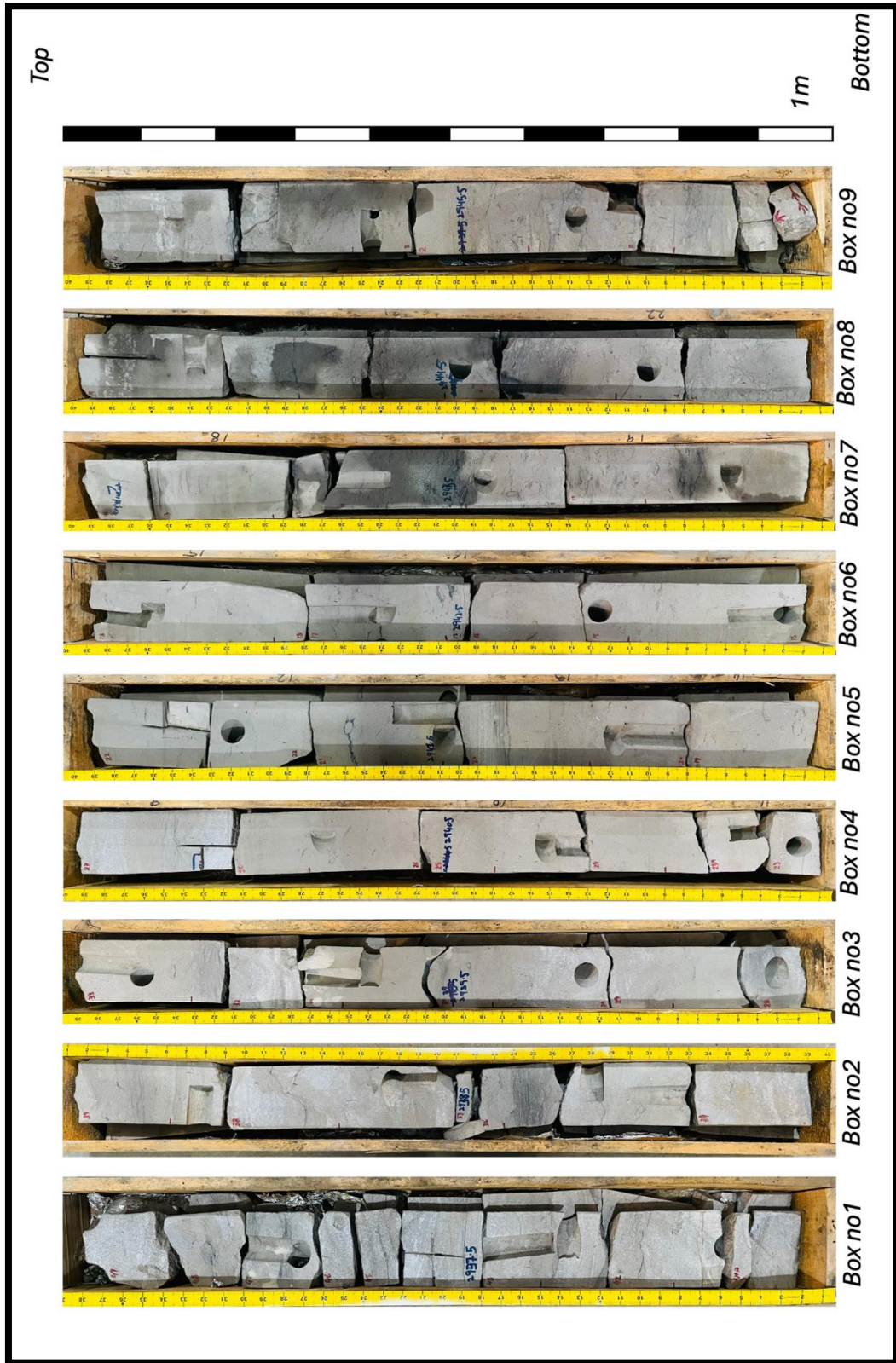


Figure 4.2 Panoramic view of core 1 (Well A)

### 4.2.3 General description of the core 1

The observations are outlined in one-meter interval, beginning from the bottom and continuing towards top as per stratigraphic convention.

2946m-2945m (Box No-9): The core begins with coarse to medium-grained, light greenish-grey sandstone that is slightly to moderately calcareous. The basal 7 cm section contains a few horizontal burrows and weak laminations. As you move upward, the sediments become more bioturbated and burrowed, with faintly preserved mud drapes. The burrows, primarily horizontal and sub-vertical, are most abundant in the middle part of the unit and are filled with dirty white, cleaner sand. Due to biogenic reworking, no primary sedimentary structures have been preserved.

The overlying unit consists of coarse to medium-grained, light greenish-grey sandstone with occasional dark grey to black shale stringers near the top. The basal part of this unit is massive, with a few laminations and very few burrows. Two noticeable horizontal laminations of white leached calcite, marking separate sediment deposition episodes, are present and act as an eye-catching feature. The upper part of the unit is moderately to highly burrowed, with most burrows being horizontal to sub-horizontal thalassinoides filled with light brownish-grey, non-calcareous sandstone. A burrowed horizontal shale lamina is present at the top.

The uppermost unit in this box consists of coarse to medium-grained, light greenish to whitish-grey sandstone with an erosive base. The lower part is massive, with a few Skolithos burrows and concentrated lenses of calcite cement in a horizontal bedding trend. The basal 2 cm is coarse-grained with faint horizontal laminations. The upper part of this unit continues into the bottom of the next box, where it becomes highly burrowed and bioturbated, with burrows primarily horizontal, along with a few sub-vertical ones, filled with cleaner sand.

2945m-2944m (Box No-8): This interval begins with coarse to medium-grained, light greenish grey to light brownish-grey sandstone. The lower portion is massive, with a few Skolithos burrows that are vertical to sub-vertical and horizontal, filled with cleaner sand. The upper part is heavily burrowed and bioturbated, with a non-erosive base. As you move upward, the sandstone transitions from light greenish

grey to light brownish grey, becoming coarser toward the top. There are a few horizontal burrows present, including two well-preserved vertical Skolithos burrows. The unit exhibits weak horizontal laminations due to differences in grain size and is capped by a calcite-leached lamina.

The middle unit (pieces 7 and 8) consists of coarse to medium-grained, light greenish to light brownish-grey sandstone. The lower part is massive with a few horizontal to sub-horizontal burrows and weak laminations, while the upper part is heavily burrowed and bioturbated with no preserved sedimentary structures.

The overlying unit (pieces 9-12) is composed of coarse to medium-grained, light greenish to whitish-grey sandstone. The basal 30 cm section is massive, with minimal vertical to sub-vertical burrows and a few weak shaly fragments. Near the base, concentrated lenses of calcite, about 2 cm thick, are present in a horizontal bedding shape. The grain size in this section ranges from coarse to very coarse, with a brownish-grey color. An oblique sub-vertical burrow lined with black shaly material and filled with sand crosscuts the calcite-leached horizon, indicating post-calcite leaching biogenic activity. A large, 5 cm long vertical Skolithos burrow is present on the backside of piece 9.

The upper part of this interval consists of light greenish grey, moderately burrowed, and bioturbated sandstone with black-colored wavy shale stringers. In piece 11, Siphonichnus burrows, primarily of horizontal orientation with black shaly linings and clean sand fills, are preserved. Wavy mud drapes are also present throughout the upper part of the unit.

2944m-2943m (Box No-7): The majority of this box (about 70%) has already been described in connection with the previous box (No. 8). The remaining section begins with medium to fine, slightly brownish-grey, massive sandstone, featuring a lag or granular lamina of coarse to very coarse sand grains at the base. The lower part includes a few horizontal burrows and shaly structures resembling shells. Near the top, wavy, curvy, and slightly convex shale laminations or mud drapes are preserved, which transition to horizontal laminations at the top of the unit.

The last section of this box consists of medium to coarse, slightly greenish-grey, massive sandstone with a lag or granular lamina of coarse to very coarse sand

grains at the base. This section also contains horizontal burrows and shaly structures resembling shells. The upper part of this section (extending into the bottom of box No. 6) is light brownish-grey and coarsens upward. Horizontal burrows are present here as well, including two well-preserved vertical ones (Skolithos). The unit also contains weak horizontal laminations, which are visible due to differences in grain size and are capped by a calcite-leached lamina.

2943m-2942m (Box No-6): This box is described as a continuation of the previous one, beginning with medium to fine, light greenish-grey sandstone that is slightly bioturbated. The lower and upper parts contain shaly black fragments, with the base of this unit being erosive and planar horizontal. The overlying unit is also medium to fine, light brownish grey, but consists of massive sandstone with a lag or granular discontinuous lamina of coarse to very coarse sand grains at the base, continuing upward with the same characteristics. Two wavy mud drapes are observed in the basal part, along with very few horizontal burrows at the base of piece no. 16. A few mud-dominated fragments are present in both the upper and lower parts.

The final interval leading into box no. 5 consists of sandstone with the same grain size, slightly bioturbated, and massive, with a lag or granular base of coarse to very coarse sand grains. Scattered coarse grains, along with a few horizontal and a single vertical burrow, are also present. The upper part of this unit, extending into the basal part of box 5, is light greenish-grey sandstone with no visible sedimentary structures. Larger horizontal and smaller vertical burrows are present, with occasional disseminated coarse grains in the central part. Mud-dominated or shaly fragments are observed throughout. Near the top, weak laminations are preserved, capped by a 2 cm thick burrowed interval that also contains horizontal interlaminations or mud drapes of fine sand and shale.

2942m-2941m (Box No-5): This interval is less bioturbated and contains coarser material compared to the lower one. Nearly half of this box was described in the preceding section. The remaining half consists of two units. The lower unit is composed of coarse to medium, light greenish grey to light brownish-grey sandstone. The basal 5 cm part is laminated and contains disseminated coarse grains. Above this, the sandstone is massive and fines upward, with a single horizontal burrow. A few small sub-horizontal burrows and small shale fragments are also observed.

The upper unit is medium to fine, light brownish grey to light greenish-grey massive sandstone with a weakly preserved erosive base. There are a few horizontal burrows (*Thalassinoides*) and a single vertical burrow (*Skolithos*). No disseminated grains are observed, but a black shale lamina is present at the top. *Skolithos* burrows are also visible on the back side of this piece. A few shaly fragments are present, and this unit continues into the basal part of the next box.

2941m-2940m (Box No-4): Adjacent to the basal piece, there is a larger unit composed of coarse to medium, light greenish-grey sandstone that fines upward. The basal 2 cm of this unit features laminations permeated with calcite, while the rest of the unit is massive. The lower half contains disseminated coarse grains, arranged more or less in a horizontal bedding or lamination style. Slightly shaly fragments are present throughout the interval, and the entire unit has very few horizontal to sub-horizontal burrows.

Above this, a small bed of granular to very coarse, whitish-grey sandstone overlies the unit. The whitish color is due to calcite cement, and the bed's top is wavy. The second-to-last piece in this box is medium to fine, light brownish-grey sandstone with weak, wavy, and irregular mud drapes and scattered coarse grains. A flame or escape-like structure is preserved near the base, over the gritty unit. The top of the box contains granular to very coarse, whitish-grey sandstone, which is wedge-shaped at the front and appears as trough-cross bedded from the back. The top of this unit continues into the next box, showing a wavy, gritty, and undulated bedding surface with slightly calcareous cementing material.

2940m-2939m (Box No-3): The basal unit of this box consists of medium to fine, light grey, horizontally laminated sandstone, which contains a horizontal burrow filled with coarse-grained sandstone. Above this, the larger unit in the lower half of the box is composed of medium to fine, light greenish grey to light brownish-grey sandstone, with a few horizontal to sub-vertical burrows preserved near the top and just below the fine shaly laminae. The basal part contains very coarse disseminated sand grains, and a vertical burrow is observed in the central part. Although there are two small, very coarse-grained sandstone beds, each about 2 to 3 cm thick and fining upward, the interval is treated as a single unit. This is due to the presence of a large

Conichnus burrow or a collapsed Ophiomorpha tunnel-shaped structure, which creates converging laminae where the sediments appear reworked and slightly mixed.

The lower coarse unit consists of grit to very coarse sandstone with a wedge shape, while the upper unit is made up of similar grit to very coarse sandstone with coarser grains and calcite cement. Both gritty units are mottled, slumped, or reworked, and possibly contain isolated trough cross beds. A 5 cm long vertical Skolithos or Ophiomorpha burrow is also present. Above this, medium to fine, light greenish grey to light brownish-grey sandstone is found, with poorly preserved thinning upward beds. Scattered very coarse grains and shaly fragments are also present.

This unit is overlain by very coarse to coarse, whitish-grey, calcite-cemented sandstone beds, which feature symmetrical wave-topped beds and interlaminations of white, very coarse sandstone with coarse brownish-grey sandstone. The upper part of this box contains coarse to fine, light brownish-grey sandstone. The basal part is very fine-grained, with a single horizontal burrow preserved in the centre. Small Macaronichnus burrows, filled with brownish material, are present in the light grey, fine-grained lower part's groundmass. The upper part is massive, with disseminated coarse grains and lacks laminations or other sedimentary structures.

2939m-2938m (Box No-2): This box has been divided into several small units, starting at the bottom with very coarse to coarse, whitish-grey, clean, well-sorted sandstone. The sandstone is calcite-cemented and consists of three horizontal beds, each internally featuring trough cross-interlaminations of very coarse whitish-grey and coarse light brownish-grey sandstone. The grains are sub-angular to sub-rounded, indicating reworking by water or physical processes. The overlying unit is coarse to medium, light brownish-grey, massive sandstone, capped by a wavy shale stringer with a few horizontal burrows and scattered very coarse grains. This unit grades upward into a coarse, whitish-grey, massive, well-sorted sandstone bed with a single wedge shape.

The next finer-grained unit is medium to fine, light grey, shaly sandstone, containing disseminated coarse to very coarse grains, wavy shale laminae, and a horizontal burrow near the base. Macaronichnus burrows filled with light brown sand and coarse quartz grains are also present. This unit grades into a coarse to medium,

light brownish-grey sandstone, featuring scattered very coarse grains, wavy shale mud drapes, and weak horizontal laminations at the base. It is overlain by very coarse to coarse, whitish-grey, well-sorted, bedded sandstone with a few grits. In this section, a *Conichnus* burrow or collapsed structure over an *Ophiomorpha* tunnel is observed, which is overlain by coarse to medium, light brownish-grey sandstone, also containing scattered very coarse grains. Shale laminae and weak horizontal laminations are present near the base.

Further upward, there is a very coarse to coarse, whitish-grey, well-sorted sandstone unit with a few grits. This grades into coarse to medium, light brownish-grey sandstone, with scattered very coarse grains. A concave shale lamina is present at the top, with a horizontal burrow preserved below it. The second-to-last unit in this core is comprised of very coarse to coarse, whitish-grey sandstone, which is well-sorted and bedded, with a few grits and a wedge-shaped top.

The last unit in this box is medium to fine, very light brownish-grey sandstone with a few mud drapes and laminae near the top. There are a few small vertical burrows, along with one horizontal burrow at the base and another in the central part. Disseminated coarse sand grains and a 5 mm thick black shale lamina are found near the top. The black shale lamina is capped by a 2 cm thick medium to fine, light brownish-grey sandstone containing a few mud drapes.

2938m-2937m (Box No-1): Box No-1 of this core is characterized by its coarser grain size compared to the other boxes and is divided into several smaller units. It begins with a very coarse to coarse sandstone that is thinly trough cross-bedded with curving bases and contains a significant amount of calcite cement. The lower section includes interbeds of medium to fine-grained, very light brownish-grey sandstone, while the upper part is massive and shows a graded bedding pattern. Above this, there is a medium to fine-grained, very light brownish-grey sandstone unit, featuring a thicker shale lamina and mud drapes near the top, along with scattered coarse sand grains.

Next, a very coarse to coarse, laminated, whitish-grey trough cross-bedded sandstone unit is present, which grades into medium to fine-grained, very light brownish-grey, laminated sandstone with shell clasts at the centre and a concave shale lamina at the base. Another unit consists of very coarse to coarse, whitish-grey



sandstone interlaminated with medium to fine-grained, light brownish-grey sandstone. This unit fines upward into a slightly brownish grey, thinly bedded/laminated sandstone with well-developed horizontal mud drapes on each bed.

This is followed by a coarser unit of very coarse to coarse, coarsening upward sandstone, which is whitish-grey and has a clear wedge shape. It grades into another coarse to very coarse, well-preserved, trough cross-bedded, whitish-grey unit, which also coarsens upward and has slightly concave bed bases. The second-to-last unit in this box is composed of coarse to medium-grained, slightly brownish-grey sandstone, with patches of very coarse sand. A medium-sized horizontal burrow and wavy mud drape are preserved in the centre, with a curving base.

The final unit in this box consists of very coarse to coarse, whitish-grey sandstone, featuring a very coarse, wedge-shaped bed in the lower part. A sub-vertical to vertical burrow, identified as *Ophiomorpha*, is also present in this unit. The upper half of this last unit is mostly massive, with a basal bedded nature.

#### **4.2.4 Findings**

The brief summary of the Core-1, drilled out from the Basal Sand of Lower Goru Formation is concluded as:

1. The rocks in the core are light greenish to light brownish and whitish grey, very fine to very coarse upper and granule sized sandstone with few dark grey mud-drapes.
2. The rocks show abundant physical sedimentary structures, dominant of which are cross laminations (wave and current ripple formed), horizontal laminations, irregular planar laminations, low angle cross bedding, mud-drapes, muddy seams, slump like structures, wedge shaped bedding and trough cross bedding.
3. Common biogenic materials are shell like fragments in few intervals of the lower part of the core.
4. The sediments display abundant identified and described biogenic traces and burrows, including *Thalassinoides*, *Ophiomorpha*, *Siphonichnus*, *Macaronichnus* and *Conichnus*.

5. The core consists of one mega coarsening-up cycle, breakable into several smaller fining-up cycles.
6. It can be safely suggested that the studied sediments were deposited in a shallow marine depositional environment.
7. The facies interpreted in the core is shoreface which has been divided into its lower shoreface, middle shoreface and upper shoreface, representing a wave-dominated prograding beach/barrier bar environment.

### 4.3 Core Analysis of Well B

#### 4.3.1 Core 2 (Well B)

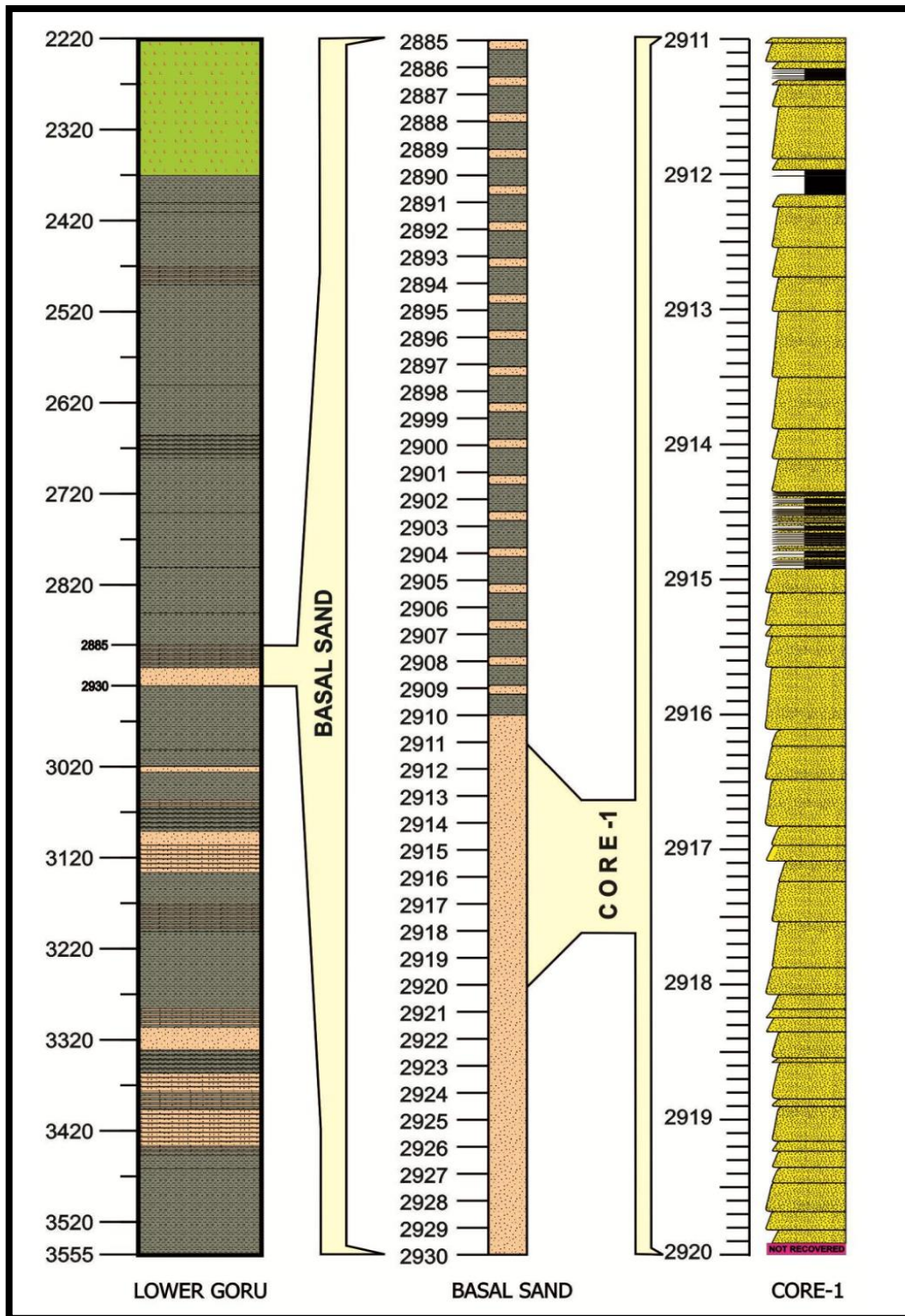


**Figure 4.3** Position of the Core 2 within Basal Sand of Lower Goru Formation, in Well B.

## 4.3.2 Panoramic view of the core 2

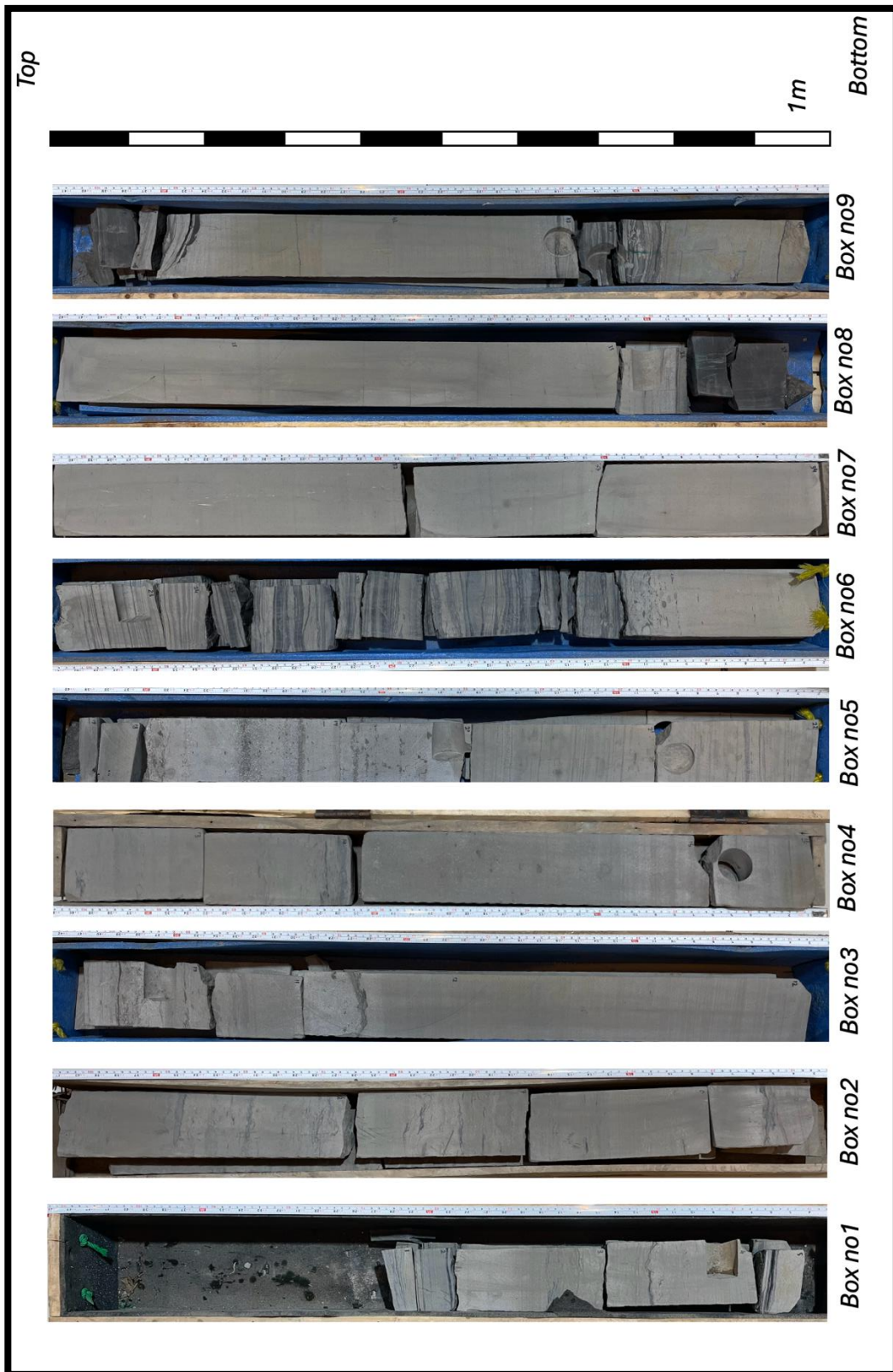


**Figure 4.4** Panoramic view of core 2 (Well B)

### 4.3.3 General description of the core 2

The observations are outlined in one-meter interval, beginning from the bottom and continuing towards top as per stratigraphic convention.

2920m-2919m (Box No-9): The core begins with medium lower to fine upper, greenish-grey, mica-rich sandstone that features mud-drapes or laminae. The upper part of this unit has horizontal black shale laminae or drapes, while the lower part is sub-horizontal, wavy, and curvy or swaly. At the top, there is a 3 mm thick wavy black shale lamina.

This is followed by a unit of the same grain size, very light grey, and massive sandstone. It shows weakly preserved plane bed laminations near the top and base, with a massive middle section.

The overlying unit is medium upper to medium lower, light grey, and highly bioturbated with mottling but no preserved sedimentary structures. It features a wavy black shale lamina near the top. This unit contains a few vertical burrows of *Ophiomorpha nodosa*, horizontal burrows of *Ophiomorpha irregularis*, and an *Asterosoma* burrow, with scattered *Macaronichnus* burrows also present. Above a shale lamina, the sandstone becomes less bioturbated and more highly micaceous.

The second-to-last unit of this box consists of medium lower to fine upper, very light grey sandstone that fines upward and displays horizontal to sub-horizontal laminae. It is capped by very thin interlaminated black shale and very fine sand.

2919m-2918m (Box No-8): This box or interval continues from the previous one and begins with medium lower to fine upper, light greyish sandstone that is moderately burrowed. It contains a few *Macaronichnus* burrows but lacks physical sedimentary structures.

Moving upward, there is a light greyish, horizontally laminated sandstone unit that is preserved between two bioturbated zones. The overlying sandstone is also light grey and moderately burrowed, with mostly horizontal burrows filled with the same sand and outlined by black shale. A notable feature is a large, 6 cm long horizontal burrow filled with silty material. Scattered *Macaronichnus* burrows are present, and bioturbation increases upward, with the entire unit showing signs of

bioturbation. It is capped by medium lower to fine upper, light grey sandstone with horizontal laminations and a single vertical burrow.

The next thick unit maintains the same grain size and light grey color, with its lower part being moderately mottled and containing a single vertical burrow. The upper part features small horizontal burrows and a larger burrow with sutured structures. *Macaronichnus* burrows are also present in the central part, and remnants of horizontal laminations are visible. This unit is capped by a 4 cm thick, horizontally laminated sandstone layer.

Near the top of the box, the grain size decreases from medium upper to medium lower. This unit is light grey, massive, and contains small horizontal burrows in the central part. It is capped by a thick, irregularly shaped black shale lamina or mud-drape. Pervasive *Macaronichnus segregatis* burrows are present throughout. The topmost unit extends into the next box.

2918m-2917m (Box No-7): The basal unit of this box extends from the previous box and consists of medium upper to medium lower, whitish grey sandstone, divided into two sub-units. The lower sub-unit features horizontal and slightly swaly laminations, a few horizontal burrows, and a single sub-vertical burrow, topped by a thick black shale lamina or mud-drape.

The upper sub-unit is mottled and contains numerous horizontal burrows, with a thick black shale lamina or mud-drape situated in the centre. As you move upward, the grain size decreases to medium lower to fine upper sandstone, with weakly preserved horizontal laminations. The upper half also features a few *Macaronichnus* burrows and two *Asterosoma* burrows.

In the next section, the sandstone is medium upper to medium lower in grain size, light grey, and fining upward. It is a massive sandstone unit with no preserved sedimentary structures, except for a wavy and irregular shaly band near the top.

The upper half of this box is characterized by finer, medium lower to fine upper, very light grey sandstone with thin horizontal laminations. The laminae are thicker at the base, gradually thinning upward from 7 mm at the base to 3 mm at the top. The laminations are visible due to slight changes in grain size and color. The

thinning laminae trend reflects decreasing energy conditions toward the top, with the entire unit being horizontally bedded and laminated.

2917m-2916m (Box No-6): The medium lower to fine upper sandstone from the lower box transitions into fine upper to fine lower, light grey sandstone in the current box. This sandstone is horizontally thin bedded in the upper part and shows very slight bioturbation, with a few small and two large horizontal Ophiomorpha irregulare burrows filled with cleaner sand and outlined by black shaly material. Macaronichnus burrows are also observed near the top of this unit.

Above this, the next two units have medium lower to fine upper grain sizes. The lower unit is light grey and massive, lacking physical sedimentary structures. In contrast, the upper unit is light grey sandstone that is moderately to highly bioturbated. It features mainly horizontal burrows, with a few Macaronichnus burrows as well. The middle part of this unit shows remnants of horizontal laminations and a grey lamina, while the upper and lower parts lack sedimentary structures, with mottling increasing towards the top.

The upper half of this box contains medium upper to medium lower, light grey sandstone with thin horizontal laminations. The lower part is massive, while the upper part features thick laminae that thin upward. Framboidal or lens-shaped pyrites are present in the massive lower part, and a shale drape is found near the top. The basal 2 cm consists of coarse lower to medium upper grained material.

2916m-2915m (Box No-5): This box extends from the previous box and begins with a few centimetres of medium lower to fine upper, light grey sandstone that is highly micaceous and muddy/silty. It features horizontal laminations with a few mud-drapes in the central part. Some laminae exhibit a pyritic shade due to fine pyrite grains.

The overlying unit, which constitutes almost the lower half of this box, is medium upper to medium lower, whitish grey sandstone and represents the coarsest interval in this core. This interval starts with a 3 cm thick sandstone layer containing mud clasts (up to 1 cm in diameter), quartz granules, and pebbles, with an erosive base. It is followed by a 2 cm thick massive sandstone layer with no sedimentary

structures. Above this, a 1 cm band of very coarse lower to granule-sized quartz grains and small bivalve shells is present, topped by a 4 cm thick massive sand unit.

Moving upward, there is a 10 cm thick zone with 3 to 4 patches of granule to very coarse upper-sized quartz grains and pyritized shells. The lower two patches contain well-rounded quartz pebbles. The patches decrease in thickness and fineness of grain size upward, with the upper two patches consisting of granule to very coarse lower grains. The uppermost patch is mostly cemented with pyrite.

Above this pyrite-cemented patch is a 6 cm thick massive unit with disseminated coarse quartz grains. This is followed by a 7 cm thick unit containing 3 to 4 bands (10 mm to 5 mm thick) that thin upward and include mud clasts/bioclasts and abundant very coarse quartz grains. The upper part of this unit contains disseminated coarse quartz grains, intraclasts, and pyrite nodules or framboids, with pyrite also precipitated among the coarser grains.

The upper half of this box features medium upper to medium lower, light greenish grey sandstone. It starts with low-angle planar crossbedding or laminations at the base, transitioning to planar and horizontal bedding or laminations with mud-drapes at the top. The lower part of this unit has a few pyrite nodules or clasts.

This section includes 6-7 smaller units with both low-angle cross-bedding and horizontal planar bedding, which start with bedding at the base and end with laminations at the top, showing a thinning upward trend indicative of decreasing energy conditions. Siderite granules or clasts are present at the back of this section. Disrupted mud-rich laminae suggest crypto-bioturbation. A 5 cm thick part of this unit extends into the next box and has already been described.

2915m-2914m (Box No-4): This zone begins with medium upper to medium lower, greyish-white sandstone interbedded with dark grey silty shale. The laminations are sub-horizontal to swaly and slightly wavy in nature. Some sand laminae exhibit sideritic staining, while the shale laminae contain mica and pyrite grains. These laminae also show slight inverse grading, possibly due to crypto bioturbation, resembling graded rhythmites deposited by a storm sand layer in an offshore transition zone.



Overlying this unit are heterolithic or tidal beds consisting of dark grey shale and medium lower to fine upper, light grey sandstone. This section features a slightly erosive base with a 2 mm thick siderite lamina and pyrite content.

The heterolithic unit, which comprises most of the box, contains two cycles. The lower cycle begins with wavy bedding and transitions upward into lenticular bedding and tidal rhythmic laminations. The sandstone intervals in this cycle contain siderite but no burrows. The upper cycle starts with wavy flaser bedding and grades upward into wavy and lenticular bedding. This cycle includes a few horizontal burrows and small gutter-cast-like structures at the bases of the sandstone beds or laminae. The unit concludes with thin horizontal interlaminations of sandstone and dark grey shale. In the upper cycle's sandstone, there is a clear horizontal burrow filled with calcareous sand and bordered by siderite. Most sandstone beds exhibit swaly and hummocky laminae in convex and concave upward positions, which have been truncated by mud layers.

2914m-2913m (Box No-3): This zone encompasses the uppermost part of box no. 4, the entirety of box no. 3, and 90% of box no. 2. It features medium lower to fine upper, light brownish to light greenish grey sandstone and is approximately 2 meters thick. The unit contains 6 to 7 low-angle, bi-directional cross-bedded layers separated by horizontally laminated zones.

The base of the unit is distinctly erosive and includes siderite-brown grains. The basal 7 cm are filled with clasts, well-rounded sand balls, and mud balls, all surrounded by siderite grains. The larger clasts are mostly well-rounded, up to 1 cm in diameter. Additionally, foraminifera or bivalve-like clasts of dark brownish grey to dark grey and pyrite-containing material, up to 1 cm in length and 2 to 3 mm in thickness, are present. Some clasts are encased in rusty siderite grains, which are coarser than the clasts and slightly calcareous. Black, elongated, medium to coarse-grained pyritic particles are aligned linearly and parallel to the bedding. A few medium-sized (up to 7 mm diameter) horizontal burrows are observed in a 10 cm thick layer above the clast-containing zone.

As you move upward through the unit to the top of piece no. 35, the grain size remains consistent (medium lower to fine upper) with a slight fining upward trend. There are no biogenic sedimentary structures present. The only sedimentary

structures are low-angle, bi-directional planar cross-bedding and horizontal bedding, which are only weakly preserved. The final 5 cm of the unit consists of greyish-white, calcareous sandstone with parallel and horizontal lamination, capped by a black shale lamina with fine sandstone lenticels and light grey sand laminae. Re-activation surfaces and horizontal laminations are noted among the unidirectional and bi-directional low-angle cross-bedded units.

2913m-2912m (Box No-2): This box closely resembles the previous one, except for its topmost unit, which consists of dark grey to black shale with faint lamination and a few lens-shaped pyrite deposits in the lower part. Additionally, there are very few pyritized and interconnected lenses of fine-grained sandstone near the top of this unit, which extends to the base of the next box. No other physical or biogenic structures are observed in this black shale unit. The lack of biogenic activity suggests deposition below the storm wave base in an anoxic offshore environment, while the presence of pyrite clasts and nodules indicates reducing conditions.

2912m-2911m (Box No-1): The basal and smaller unit of the core consists of an 8 cm thick sandstone that ranges from fine upper to medium lower grain size and has a coarsening upward trend. This whitish grey sandstone features low-angle and swaly cross-lamination with a slight coarsening upward trend. At the top, there is a 3 mm thick, black, curvy, convex-upward mud-drape or seam with an anticlinal bump and rightward dip, resembling a load structure or mud blanket. The inter-laminated layers show a decrease in swaly and wave ripple-like cross-laminae upward. This unit also includes flaser-bedded sandstone with dark grey, organic-rich mud-draperes and small interbeds of medium-fine flaser laminated sandstone and dark grey mudstone/shale.

The heterolithic unit is composed of four larger flaser-bedded units and three smaller flaser-laminated units. Above this, a thicker unit of medium lower to fine upper, light greenish grey sandstone is observed. This unit features sub-horizontal laminated beds in the upper part and low-angle planar cross-laminated and leftward-dipping beds in the lower part. Two units with similar characteristics, grain size, and lithology are separated by a reactivation surface indicating two storm or wave phases. This unit is capped by a 4 mm thick black shale lamina with a sand lamina beneath

it. Near the base, a vertical fracture filled with grey material or sand is noted, along with load cast structures disturbing the black shale lamina.

The following unit consists of fine upper to medium lower, whitish grey to light grey sandstone with two sets of opposite-dipping cross-laminated thin beds that truncate each other. Above this, there is a dark grey to black shale unit with heterolithic tidal bedding and well-preserved sandstone injectites. This is followed by a thin unit of medium lower to fine upper, whitish to brownish grey, fining upward, laminated sandstone with subordinate black shale laminations. A thick shale lamina with fine sand lenses is present in the centre.

The penultimate unit is medium upper to medium lower, fining upward, light greenish grey sandstone. Its basal and upper parts show rightward-dipping, thin cross-laminated beds, while the lower cross-laminae are disturbed in places by burrows. The middle part contains two large *Conichnus* burrows and a few *Ophiomorpha* burrows. This unit is topped by a 2 mm thick blackish, curvy shale lamina that truncates the underlying swaly laminae or climbing ripples.

The final piece of the core, 3 cm thick, consists of medium upper to medium lower, light greenish grey sandstone with shale stringers. It appears bioturbated and contains an *Ophiomorpha* collapsed tunnel structure, with a *Conichnus* burrow-like structure near the top.

#### **4.3.4 Findings**

The brief summary of the Core-2, drilled out from the Basal Sand of Lower Goru Formation is concluded as:

1. The rocks in the core are light greenish to light brownish and whitish grey, very fine to very coarse upper and granule sized sandstone and well-rounded mudclasts with few dark grey mud-drapes.
2. The rocks show abundant physical sedimentary structures, dominant of which are cross laminations, horizontal laminations, irregular planar laminations, low angle unidirectional and bidirectional cross bedding, mud-drapes, muddy seams, sandstone injectites, wedge shaped bedding, flaser, wavy and lenticular bedding.

3. Common biogenic comminuted oyster shell fragments in the coarsest zone of box no 5 of the core observed.
4. The sediments display abundant identified and described biogenic traces and burrows including *Ophiomorpha*, *Macaronichnus*, *Planolites*, *Asterosoma* and *Conichnus*.
5. The core consists of two mega coarsening-up cycles, breakable into several smaller fining-up cycles.
6. It can be safely suggested that most of the studied sediments were deposited in a shallow marine depositional environment.
7. The facies interpreted in the core shows shoreface to offshore settings which has been divided into offshore, offshore sand bars, offshore transition zone, lower shoreface, middle shoreface and upper shoreface, representing a wave-dominated prograding beach/barrier bar environment.

4.4 Core Analysis of Well C

4.4.1 Core 3 (Well C)

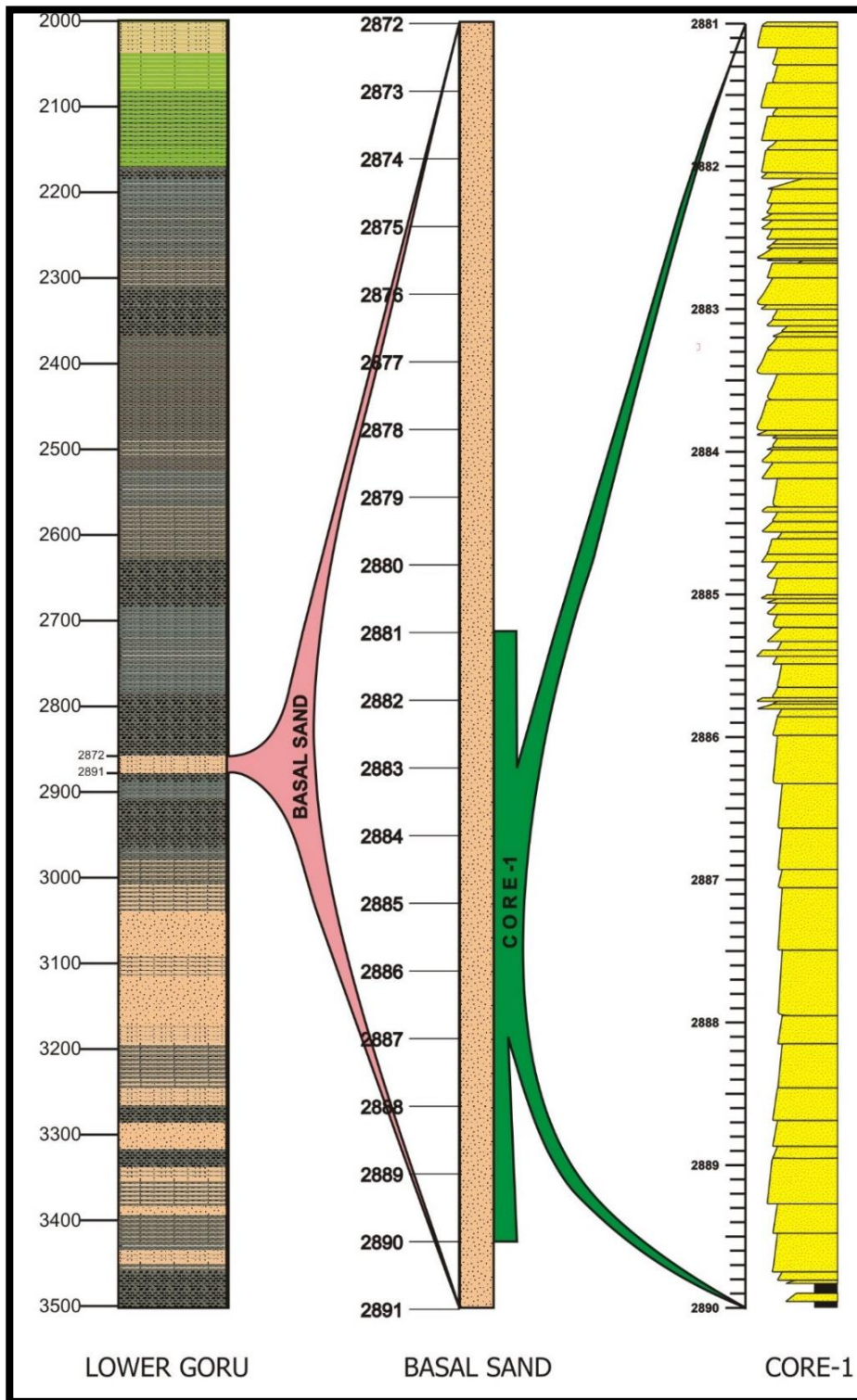


Figure 4.5 Position of the Core 3 within Basal Sand of Lower Goru Formation, in Well C.

### 4.4.2 Panoramic view of the core 3

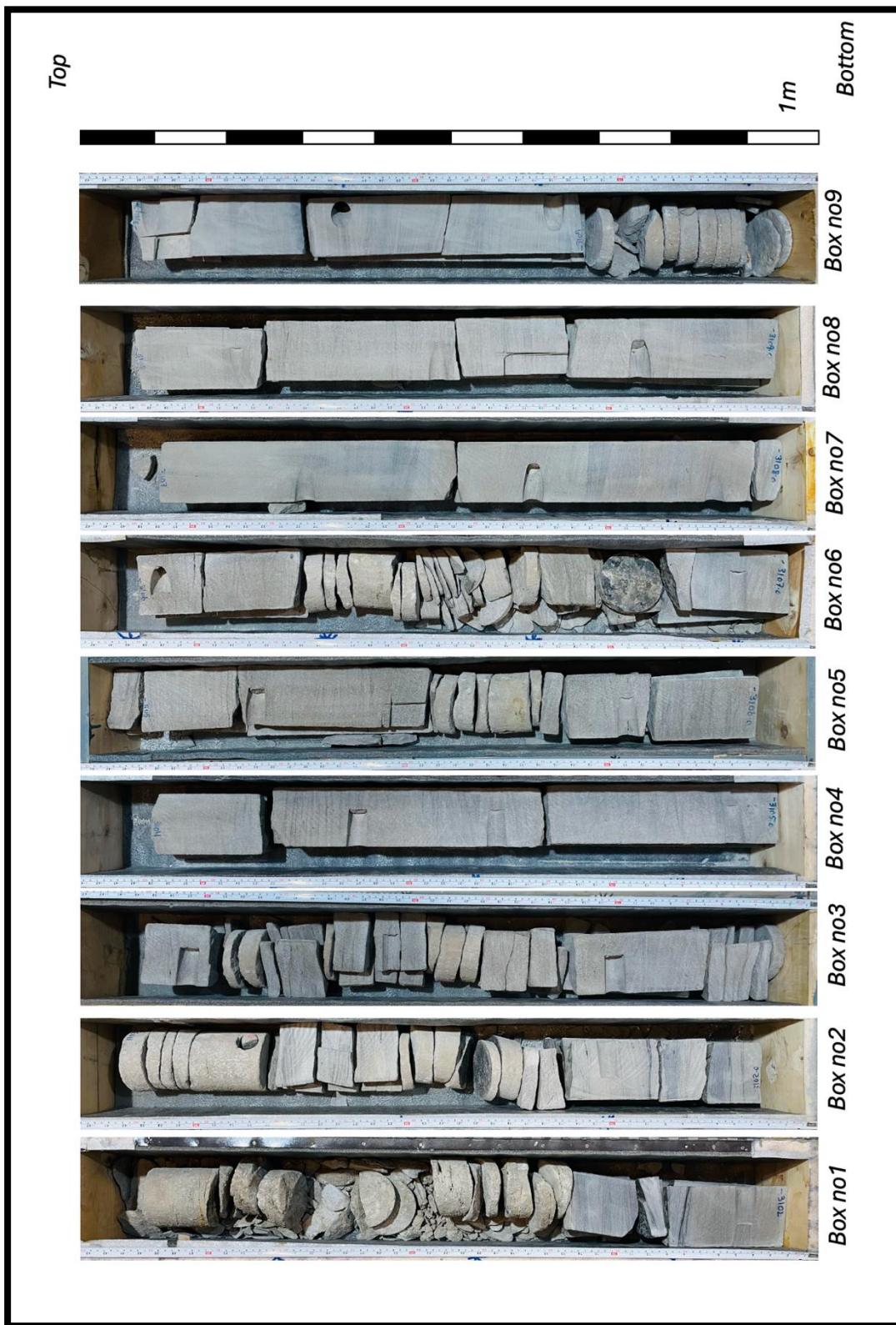


Figure 4.6 Panoramic view of Core 3 (Well C)

### 4.4.3 General description of the core 3

The observations are outlined in one-meter interval, beginning from the bottom and continuing towards top as per stratigraphic convention.

3310m-3309m (Box No-9): The core sample exhibits a sedimentary sequence predominantly characterized by cross-lamination, with a notable gradation in sandstone grain size from moderately fine in the upper sections to moderately coarse towards the base. The stratigraphy commences with a 14 cm interval featuring parallel lamination, which is indicative of relatively stable depositional conditions with uniform sediment accumulation.

This is followed by a 6 cm layer of low-angle lamination, inclined at approximately 45 degrees, suggesting a transition to slightly higher energy conditions. The core then progresses into another 6 cm of parallel lamination, demonstrating a return to a more stable depositional environment. This is succeeded by a 6 to 7 cm section of low-angle lamination, indicating renewed variations in sedimentation energy, and is followed by an additional interval of parallel lamination. The sequence concludes with a final 3 cm of low-angle lamination, providing further evidence of the fluctuating depositional dynamics within this section of the core.

In the lower part of the core, where the grain size transitions to moderately coarse, the sandstone becomes unconsolidated, reflecting a shift in sedimentary conditions. This section of the core is characterized by highly calcareous cementation, consistent with the observed increase in grain size and changes in sediment texture. The progression from fine to coarse-grained sandstone, coupled with the alternating patterns of lamination, underscores the complex depositional environment and varying energy conditions that influenced sediment accumulation in this core section.

3309m-3307m (Box No-7 and 8): This section of the core features compact, moderately fine sandstone with a well-defined sequence of sedimentary structures. In the upper 40 cm, the sandstone exhibits planar laminations interspersed with wavy laminations, reflecting variations in depositional energy and sedimentary conditions.

This is followed by a 4 cm interval characterized by low-angle laminations, which transitions into a subsequent 8 cm sequence of planar laminations.

Above this, cross-lamination extends for another 8 cm, culminating in trough crossbedding that continues through to the end of the core. The presence of trough crossbedding throughout this interval strongly suggests deposition in a shoreface environment, characterized by high-energy conditions and dynamic sediment transport.

Chemical testing with 10% HCl confirms that the cementation is non-calcareous, consistent with the observed sedimentary features. Both the core sections exhibit notably non-micaceous rocks, further emphasizing the nature of the sedimentary environment. The sequence of sedimentary structures, including planar laminations, wavy laminations, low-angle laminations, cross-lamination, and trough crossbedding, provides valuable insights into the depositional processes and environmental conditions that influenced the formation of this core section.

3307m-3306m (Box No-6): The upper 18 cm of this box is characterized by a compact texture with parallel and low-angle laminations. Within this interval, the grain size progressively increases from medium coarser to coarser, reflecting a gradual change in sedimentary deposition.

From 18 cm to 78 cm, the core transitions to an unconsolidated state, containing notable quantities of sulphur and organic matter. This section exhibits a color range from whitish grey to brownish grey and is distinguished by its micaceous composition and highly calcareous cementation. The sediment within this interval is loose and exhibits significant variability in texture and color, indicative of dynamic depositional processes.

Below 78 cm, the basal part of the core reveals well-defined trough crossbedding, which is characteristic of a shoreface depositional environment. In this lower section, the sandstone texture becomes finer, with a gradual decrease in grain size to moderately fine towards the bottom. The color of the sandstone shifts to a greenish-brownish grey, and both cross-lamination and parallel lamination are present. These sedimentary structures and compositional changes provide insight into the evolving depositional conditions and environmental setting of the core sample.



3306m-3305m (Box No-5): In this section of the core, the grain size transitions to a moderately coarse texture, with the material displaying a color range from whitish grey to brownish grey. This change becomes particularly evident in the middle interval, where the sediment turns unconsolidated and fissile, making it difficult to cut. Below this interval, the presence of granules underscores the variability in sediment composition.

Chemical testing with 10% HCl confirms that the cement is non-calcareous, and the material is distinctly micaceous. The core reveals trough crossbedding, a sedimentary feature indicative of deposition in a shoreface environment. This structure suggests a high-energy depositional setting where sediment transport and sorting were significant.

Throughout the core, thin laminations are consistently observed, although less frequent than in previous sections. The combination of moderately coarse grain size, non-calcareous cementation, micaceous composition, and the presence of trough crossbedding all provide strong evidence of a dynamic and energetic depositional environment. The observed sedimentary structures and grain characteristics offer valuable insights into the conditions that influenced sediment deposition in this part of the core.

3305m-3304m (Box No-4): Continuing from Box 3, this core sample is characterized by notably coarse grain size and a compact composition. Chemical analysis using 10% HCl confirms that the cement is non-calcareous, and the material is micaceous. Throughout the core, thin laminations are present, though less frequently than in previous sections. Parallel low-angle and cross-laminations are consistently observed, indicating a dynamic depositional environment.

The material exhibits fair to moderate sorting, suggesting that deposition occurred close to the sediment source. The presence of granules further highlights the coarser nature of this sample. Despite these features, there is a noticeable absence of bioturbation throughout this section of the core. This lack of biological disturbance suggests relatively stable conditions during deposition, with sediment primarily influenced by physical processes rather than biological activity.

The combination of coarse grain size, non-calcareous cement, micaceous composition, and the presence of granules all point to a high-energy depositional environment, similar to that observed in Box 3. The sedimentary structures, including thin laminations, parallel low-angle laminations, and cross-laminations, reinforce the interpretation of a dynamic setting with minimal bioturbation, providing a clear indication of the depositional processes that shaped this part of the core.

3304m-3303m (Box No-3): In contrast to box one and two, this core consistently exhibits a coarser grain size throughout, indicating a high-energy shoreface depositional environment. The core is notably compact, with 10% HCl tests conducted at two different intervals confirming that the cement is highly calcareous, and the material is non-micaceous. Thin laminations are present throughout the core, accompanied by parallel and low-angle laminations in the middle section, and cross-laminations at the bottom, suggesting a dynamic depositional setting.

The core displays fair to moderate sorting, which indicates its close proximity to the source material. Additionally, the presence of granules further highlights the coarser nature of this sample. The brown patches observed within the core are indicative of magnetite. The combination of these characteristics coarse grain size, high calcareous cementation, thin laminations, and the presence of granules provides strong evidence of a high-energy environment where sediment transport and deposition were significant.

3303m-3302m (Box No-2): The core sample exhibits a distinct variation in grain size, transitioning from coarse at the top to moderately fine toward the bottom. The uppermost 16 cm is made up of loose, fissile, unconsolidated material with highly calcareous cementation and no visible bedding structures. Beneath this, a 10-12 cm section shows low-angle laminations, followed by a 14 cm interval of unconsolidated material with calcareous cementation and minimal mica content. In the core's central portion, loosely packed granules are present. Towards the lower end, the material becomes non-calcareous and micaceous, featuring several parallel laminations. This section also includes a fracture filled with carbonaceous material. At the very end of the core, a complex pattern of laminations is observed, including

low-angle, wavy-angle, and parallel-angle laminations, as well as a single high-angle lamination.

3302m-3301m (Box No-1): The core sample, extending up to 66 cm, primarily consists of loose, unconsolidated sandstone that was too soft to be cut and fissile in nature. This section is notable for its high sulphur and organic matter content, indicating a rich chemical composition. The sandstone shows trough crossbedding, suggesting deposition in a shoreface environment. The sandstone color ranges from whitish to brownish-grey, and chemical testing with 10% HCl confirms that the cement is non-calcareous.

Below this unit, the core exhibits more defined stratification. This begins with 2 cm of low-angle laminations, followed by 1 cm of parallel laminations, and then 1 cm of cross-lamination. This is succeeded by another sequence of low-angle laminations and trough cross-bedding similar to the upper section. Additionally, a fracture filled with carbonaceous material and a micaceous composition is present in the lower part of the core.

Grain size varies noticeably; the upper section contains coarser unconsolidated material, while the basal part transitions to finer grains, ranging from fine to moderately fine at the bottom. The changes in grain size and sedimentary structures provide valuable insights into the depositional processes and environments that shaped this core.

#### **4.3.4 Findings**

The brief summary of the Core-2, drilled out from the Basal Sand of Lower Goru Formation is concluded as:

1. The rocks in the core are light greenish to light brownish and whitish grey, very fine to very coarse upper and granule sized sandstone and several intervals of unconsolidated massive sandstone.
2. The rocks show abundant physical sedimentary structures, dominant of which are cross laminations, horizontal laminations, irregular planar laminations, low angle unidirectional and bidirectional cross bedding.
3. No biogenic activity observed throughout the core.

4. The core consists of several coarsening-up cycles, breakable into smaller fining-up cycles.
5. It can be safely suggested that most of the studied sediments were deposited in a shoreface depositional environment.
6. The facies interpreted in the core shows shoreface to offshore settings which has been divided into offshore, offshore sand bars, offshore transition zone, lower shoreface, middle shoreface and upper shoreface, representing a wave-dominated prograding beach/barrier bar environment.

## **4.5 Sedimentary Texture**

### **4.5.1 Grain size**

The grain-size profile of the cores reveals a predominant coarsening-upward trend with major coarsening-up cycles observed throughout the cores. On a finer scale, however, the cores exhibit well-defined fining-upward cycles interspersed with fewer coarsening-upward intervals. A few units of cores contain medium fine sands which transition upward to medium, coarse, and very coarse grains, forming prominent coarsening-up cycles. Notably, a few intervals of the cores even grade into granules. The longest of these cycles extends approximately 2.1 meters in thickness. The base of several cycles is characterized by very coarse to gritty sand grains and erosive bases, suggesting high-energy depositional conditions and potential tidal surge-induced sediment transport. Additionally, few smaller-scale intervals within the cores are dominated by shale and heterolithic beddings, reflecting a more varied sedimentary environment.

### **4.5.2 Grain shape and sorting**

The sedimentary quartz grains, which constitute the bulk of the material, are generally moderate to well-rounded, with quartz granules and mud clasts exhibiting even better rounding. The degree of rounding diminishes with smaller grain sizes, a typical characteristic of sediments. This rounding indicates textural maturity, which

could result from aeolian or wave-dominated aqueous processes. Alternatively, textural maturity may also be achieved through polycycling. The grain-size profile of the cores indicates an increase in environmental energy from the bottom to the top, featuring a transgressive phase and cyclic maxima in energy levels. Sediment sorting ranges from moderate to good. Despite the core exhibiting a broad spectrum of grain sizes, from very fine to very coarse, and including granules, the overall sorting remains commendable. This effective sorting supports the hypothesis of textural evolution occurring on ocean beaches.

#### **4.6 Physical Sedimentary Structures**

Fabric of the cores shows several physical sedimentary structures that include cross laminations (wave and current ripple formed), plane laminations, irregular planar laminations, low angle cross bedding, mud-drapes, fine muddy seams, sand injectites, slump-like structures, wedge shaped, swaly, curve, flaser, wavy and lenticular bedding. Besides bioturbation, the good sorting of the sediments can be responsible for visual lack of physical sedimentary structures. Most laminations form due to size grading of sediments at some scale with few due to change in sediments color. Good sorting may discourage formation of physical sedimentary structures. However, Sedimentological analysis of core that shows the presence of physical and biogenic structures even in visually barren rocks. Thin muddy drapes and mud-seams in sand suggest changing of hydrodynamic conditions between those of sand deposition and mud settling. The sediment depositional interface is rarely flat and is covered with small and large bedforms. Most familiar of these are small current and wave ripples. The bedforms range in size from small, few centimetres across ripples to large sand waves that are many hundreds of meters across. The bedforms are few centimetres high in ripples but are up to 15 meters high in sand waves. These bedforms move and in so doing make many kinds of internal laminations and bedding that bear clues to the hydrodynamics of the environment. Current produced bedforms are asymmetrical with steeper slope facing the down-current side (Sam Boggs, Jr. Principles of Sedimentology and Stratigraphy). In active sediment transport, sediments are moved largely as bedload up the shallower slope and avalanches down

the steeper slope. In this way the bedform moves and makes X-laminations or X-bedding internally. The kind of current-made bedform is related to the current speed. Also, grain size of sediment and water depth influence the size and shape of the bedforms. Relationship have been established empirically between current-made bedforms, mean flow velocity and sediment grain size for a flow depth of about 0.4 meter. It suggests current ripples form in slow currents in sediments finer than 0.6 mm in grain size. These ripples make small cross-laminations in the sediments. At higher current speeds in coarser sediments somewhat larger bedforms, subaqueous dunes or sand waves are formed. When current speed is high (from 0.6 to over 1 m/s) than sediment bed is flattened and laminae parallel to the depositional interface are formed. Such lamination is called upper-flow-regime plane-bed. Wave ripples are common bedforms in shallow marine sediments and these makes many kinds of internal cross laminations (Sam Boggs, Jr. Principles of Sedimentology and Stratigraphy).

#### **4.7 Biogenic Sedimentary Structures**

The sediments exhibit significant biogenic activity and a range of burrows, indicating a rich fauna in the depositional environment that has extensively reworked the sediments. The infauna, predominantly soft-bodied, has left minimal traces. The burrow characteristics suggest the presence of suspension and deposit feeders, especially in the lower sections of the core. The nature of these biogenic traces aligns with the physical attributes of the sediments. Numerous small, mud-dominated specimens are noted within the core.

Most of the burrows are Ophiomorpha, which are typically horizontal or gently inclined to the bedding and circular in cross-section. These burrows generally range from 0.5 to 1.5 cm in diameter, with an average of about 1 cm. The walls of these burrows are lined with a distinct, darker rim of finer muddy material, contrasting with the cleaner, lighter-colored quartz sand found within the burrows and in the surrounding matrix. Some burrows exhibit crossovers and interpenetrations. The presence of Ophiomorpha suggests relatively high wave or current energy and is indicative of clean, well-sorted, and shifting particulate

substrates, where deposition and erosion rates can fluctuate rapidly, commonly found in foreshore or shoreface environments.

In addition, *Macaronichnus* burrows are prominently present in certain intervals, appearing as clusters of mostly horizontal, cylindrical burrows with winding paths, and are identifiable by their elongate to elliptical and circular cross-sections. These burrows are distinguished from the surrounding sediment by their pale color and a darker mantle of mica or heavy minerals. Near the top of the core, *Conichnus*, a relatively large, conical burrow with a sub-circular cross-section and sub-vertical orientation, is observed. Other biogenic structures present in the core include *Asterosoma* and *Planolites*.

#### **4.7.1 Biologic description**

Five (05) ichnogenre/trace fossils have been found and identified in these cores as shown in figures 4.7, 4.8 and 4.9. A little detail, regarding observed and identified burrows, has been taken from the (Atlas of Trace Fossils in Well Core (2017) by Dirk Knaust). These ichnofacies are described below:

##### **4.7.1.1 Ophiomorpha**

Ophiomorpha consists of boxworks that create a horizontal maze with vertical shafts. The burrows are typically circular to elliptical in cross-section, with passive fill being common, though some segments may exhibit active meniscate fill. The burrow linings are distinctive, featuring pellets of sand and/or mud along the walls. Diameters of Ophiomorpha burrows range from 3 to 30 mm, and complete systems can extend several meters in length and more than 1 meter in depth. This trace fossil is commonly found in clean sandstone, both homogeneous and cross-bedded, where its activity introduces significant amounts of organic matter and fine sediment, potentially leading to sediment heterogenization. Thin mudstone layers may be fully penetrated due to the producer's search for food. The pelleted wall makes Ophiomorpha relatively easy to identify in core samples. While horizontal burrow parts are predominant, vertical shafts can also be visible. Open Ophiomorpha tunnels

may collapse, causing downward deflection of laminae, which can mimic *Conichnus*. Ophiomorpha is prevalent in high-energy environments and helps differentiate sandy shoreline settings. It is more common in lowstand systems tracts compared to transgressive systems tracts due to the favourable conditions for its producers in marginal and nearshore marine settings.

#### **4.7.1.2 Asterosoma**

Asterosoma is a morphologically variable trace fossil characterized by multiple arm-like burrows radiating from a central axis, tapering towards blind ends, which may extend into fine galleries. It occurs in both siliciclastic and carbonate substrates, with a preference for sandy environments. Typically, only fragments of the burrow system are visible in core sections, appearing as clusters of bulbous forms surrounded by mud laminae and often passively filled with sand. Asterosoma can be mistaken for other burrows with concentric laminations such as *Cylindrichnus*, *Rosselia*, *Artichnus*, or *Hillichnus*. It is generally regarded as the feeding trace of deposit-feeding or suspension-feeding organisms. Asterosoma is found across a range of marine environments from paralic to deep marine settings and is common in deltaic successions, particularly in delta front and prodelta deposits. It is associated with well-oxygenated environments and is a typical component of the *Cruziana* Ichnofacies, though it also appears in the *Skolithos*, *Zoophycos*, and *Nereites* ichnofacies.

#### **4.7.1.3 Planolites**

Planolites is a simple, horizontal to slightly inclined cylindrical burrow without branching or lining, characterized by an active, homogeneous fill. In plain view, Planolites appears as straight to tortuous burrows, and in cross-section, they are circular to elliptical, depending on compaction. Dimensions vary widely from millimetres to centimetres. Planolites is commonly found in soft-ground environments and occurs in siliciclastic and carbonate sediments. In core samples, Planolites appears as elongate horizontal tubes with circular to elliptical sections and is typically filled with sand, which contrasts with surrounding mud-dominated



lithologies. Its simplicity can lead to confusion with other trace fossils, such as thinly lined *Palaeophycus*, which differs by having a passive fill. *Planolites* is attributed to a variety of organisms, including worms, arthropods, and mollusks, and is interpreted as a product of deposit-feeding, active sediment processing. It is prevalent in all aquatic environments and is a common element of shallow tier ichnofabrics.

#### **4.7.1.4 Macaronichnus**

*Macaronichnus* consists of predominantly horizontal, cylindrical burrows of indefinite length with straight, winding, meandering, or spiral-like courses, although oblique and vertical burrows can also occur. These burrows are characterized by an active fill of pale sand and an outer mantle of dark mineral grains. They are unbranched and typically appear in high density, with diameters ranging from 0.2 to 2.0 cm and lengths of several centimetres. *Macaronichnus* is typically found in sandy substrates and is recognized in core samples as crowds of horizontal cylindrical burrows with winding courses, identifiable by their pale fill and dark mantle of mica or heavy minerals. It is a common trace fossil in shallow marine settings such as foreshore, shoreface, and delta-front deposits, as well as intertidal and shallow subtidal environments. *Macaronichnus* assemblages are typical of the *Skolithos* Ichnofacies.

#### **4.7.1.5 Conichnus**

*Conichnus* is a relatively large, conical burrow with a sub-circular cross-section and sub-vertical orientation. The internal fill is mainly passive, with a thin lining along the burrow walls. *Conichnus* may be related to internal convex-down structures or be located above such structures. Burrow depths typically range from a few centimetres to several decimetres. The burrow features an upper dish-shaped depression above the cone-shaped lower section. Complete specimens are rare in core samples due to their large size, with length-to-diameter ratios ranging from 3:1 to 10:1 or more. Internally, *Conichnus* often shows downward-deflected laminae, which can also affect adjacent sediments, leading to listric faults or collapsed sediment. The fill of *Conichnus* may be re-burrowed to various extents. It is commonly found in

high-energy, nearshore to shallow-marine environments with high sediment supply and shifting substrates, including intertidal zones, tidal flats, estuaries, sand waves, dunes, mega ripples, and flood-tidal deltas. *Conichnus* is a characteristic trace fossil of the Skolithos Ichnofacies.

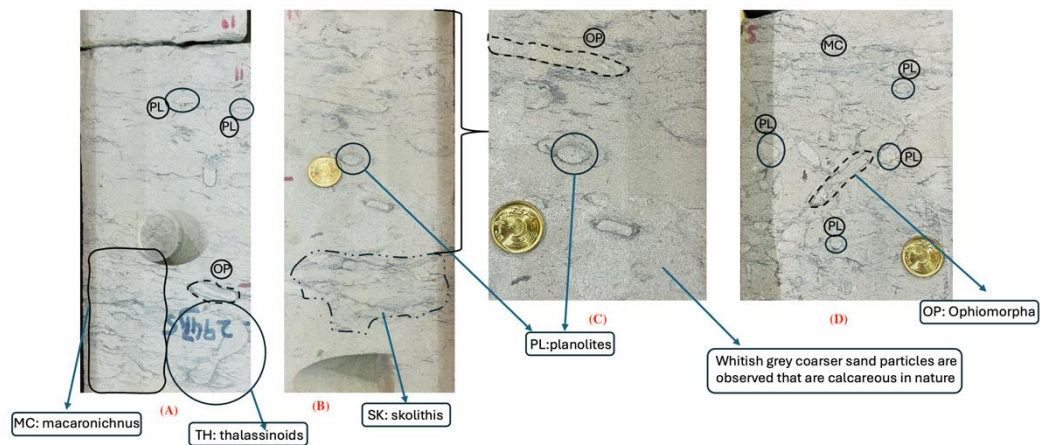


**Figure 4.7** Photographs showing Intense bioturbation fabric in a medium fine-grained sandstone. Large sub-horizontal burrows have destroyed most of the original bedding. (A) Ichnofacies Macaronichnus, Thalassinoids, Ophiomorpha and Planolites are visible. (B) Ichnofacies Skolithos and Planolites are visible. (C) Whitish grey coarser sand particles are observed that are calcareous in nature with Ichnofacies Planolites and Ophiomorpha. (D) Ichnofacies Macaronichnus, Ophiomorpha and Planolites are visible.

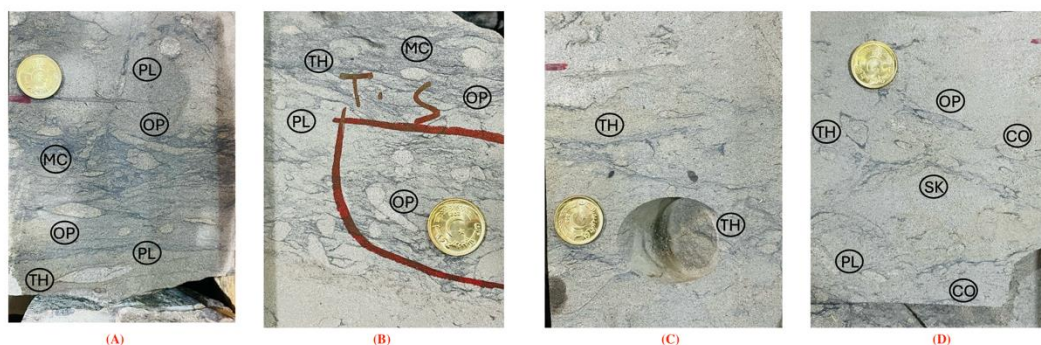


**Figure 4.8** Photographs showing Intense bioturbation fabric in a medium fine-grained sandstone. Large sub-horizontal burrows have destroyed most of the original bedding. (A) Ichnofacies Macaronichnus, Thalassinoids, Ophiomorpha and Planolites are visible. (B) Ichnofacies Macaronichnus, Thalassinoids, Ophiomorpha and Planolites are visible. (C) Ichnofacies Thalassinoids can be observed. (D) Ichnofacies Skolithos, Conichnus, Thalassinoids, Ophiomorpha and Planolites are visible.



**Figure 4.9** (A) Ichnofacies *Macaconichus*, *Thalassinoids*, *Ophiomorpha* and *Planolites* are visible. (B) Brownish grey sandstone with wavy planar laminations and calcareous patch with a sub vertical ophiomorpha. (C) Brownish grey sandstone with calcareous granules and a shift in grain size from medium fine to lower coarse grains is noticeably visible with abundance of burrows. (D) Brownish grey fine to medium fine sandstone with a few horizontal burrows (*Thalassinoides*) can be observed.

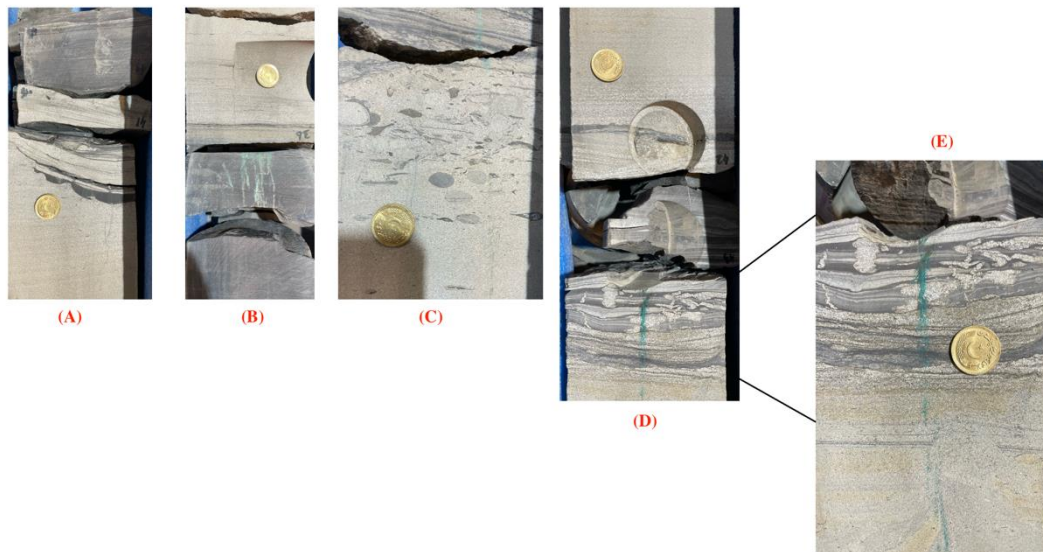


**Figure 4.10** (A) Shaley patch on top and a shaley lamina in the middle greyish brown sandstone with planar and cross laminations (B) Greyish brown sandstone with planar laminations and shaley patch on bottom (C) Intensely bioturbated whitish grey sandstone with shaley laminas on top (D and E) Moderately bioturbated with flaser bedding and shaley planar and cross laminations brownish yellow compact sandstone.

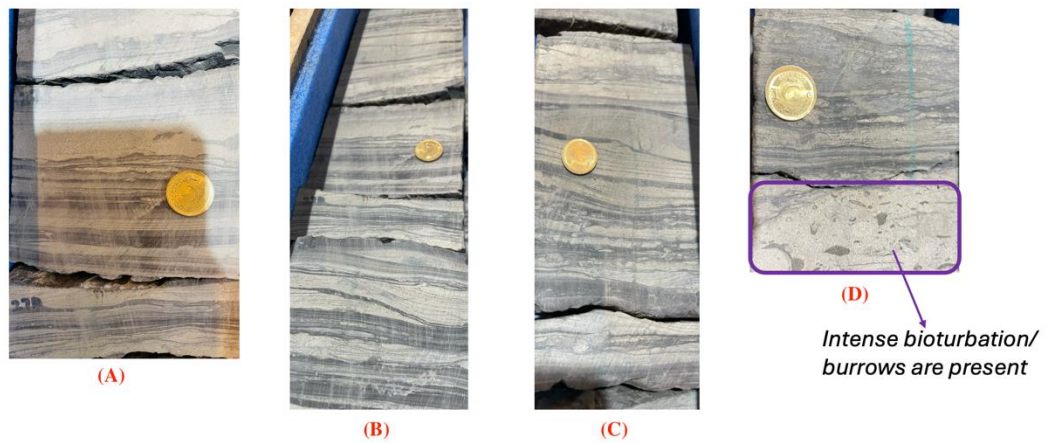


**Figure 4.11** (A, B, C and D) Brownish grey to yellowish grey compact sandstone with carbonaceous filled wavy planar laminations including flaser and lenticular bedding.

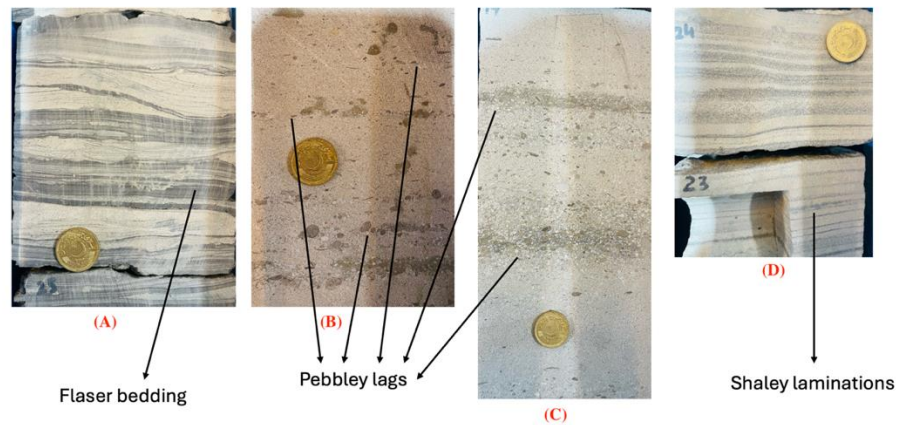


**Figure 4.12** (A) Photograph showing Flaser bedding. (B and C) Photograph showing Pebbly lags. (D) Photograph showing Slightly angular shaley laminations.

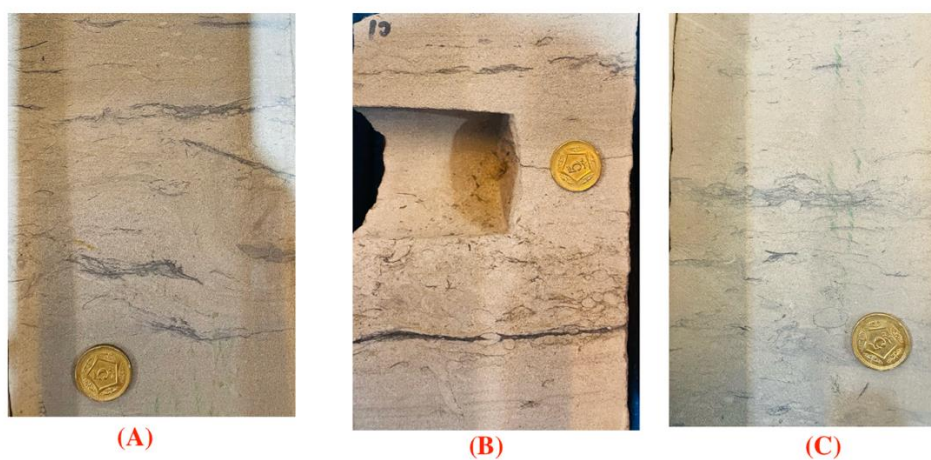


**Figure 4.13** (A, B and C) Intensely bioturbated sandstone with no preserved sedimentary structures.

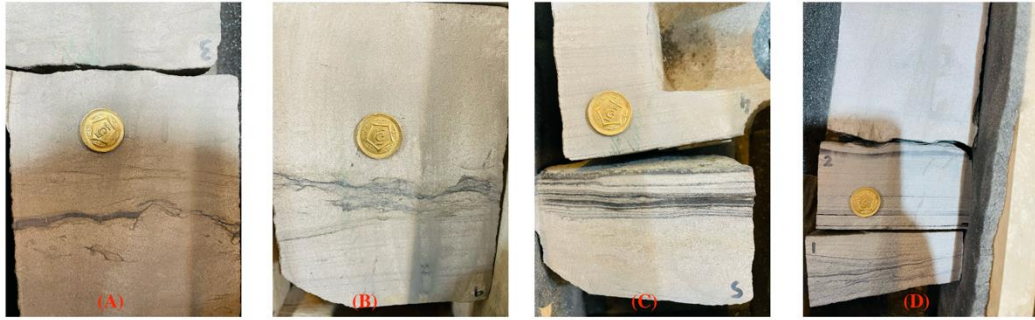


**Figure 4.14** (A, B, C and D) photographs showing whitish grey sandstone with visible fractures filled with carbonaceous material.

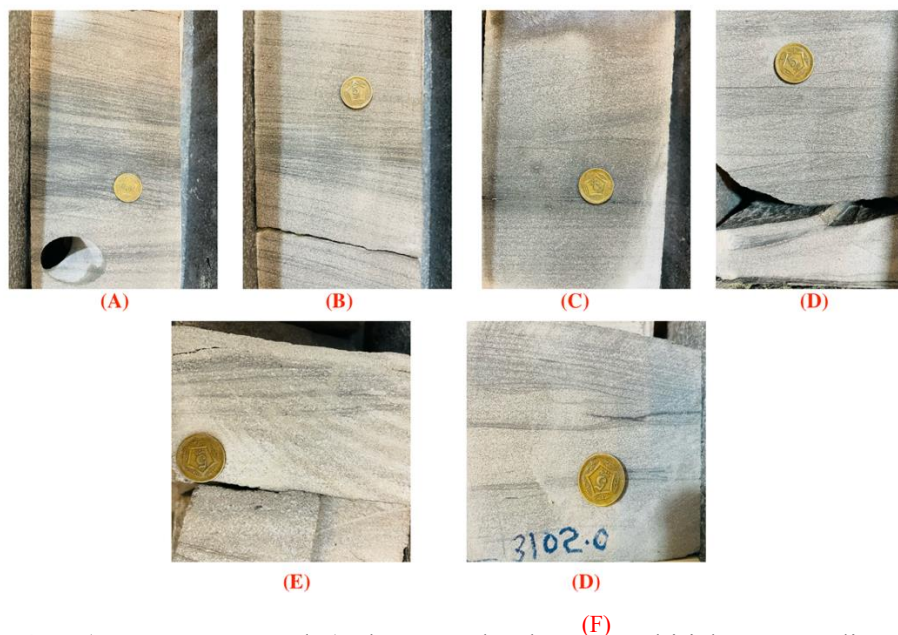


**Figure 4.15** (A, B, C, D, E and F) photographs showing whitish grey medium grained sandstone showing carbonaceous material filled laminations (planar laminations, slightly angled laminations, wavy angular laminations and trough-cross laminations).

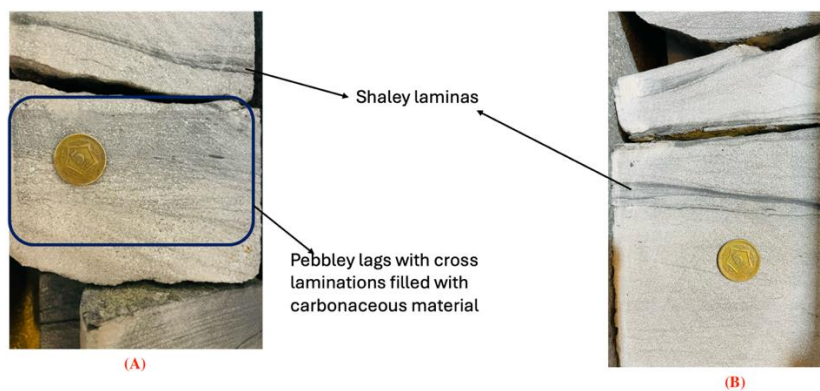


**Figure 4.16** Photographs showing (A) Pebbley lags with cross laminations filled with carbonaceous material. (B) Shaley laminas.

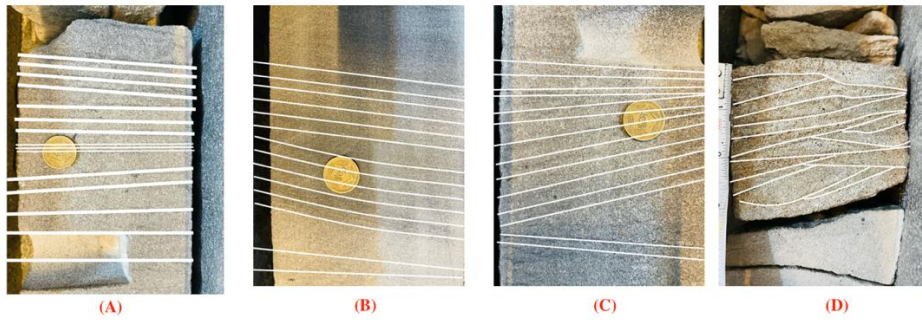


**Figure 4.17** Photograph showing (A, B and C) Medium coarse to upper coarse sandstone Showing planner laminations, slightly angled laminations, wavy angular laminations and cross laminations. Some are filled with carbonaceous material. (D) Perfect visual display of trough-cross bedding.

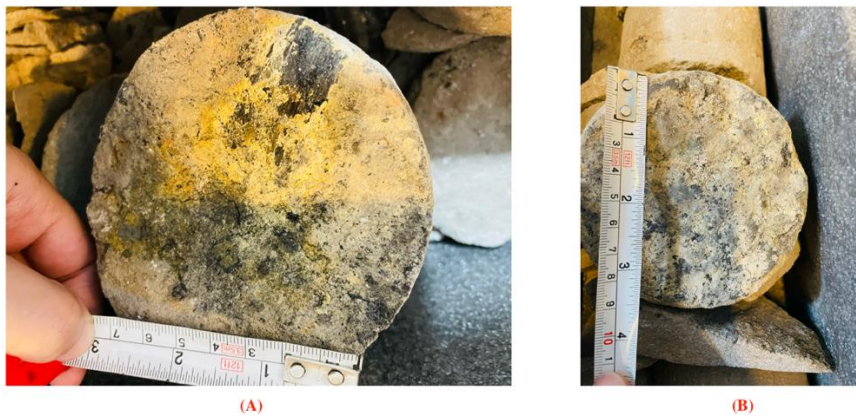


**Figure 4.18** (A and B) Brownish grey unconsolidated coarse grained fissile sandstone present with Sulphur i.e. greenish yellow in color and organic matter/ coaly material i.e. blackish in color.



**Figure 4.19** (A to H) Marked stains showing rigorous bubbling when reacted with 10% HCl due to the presence of calcareous material. Coarse to vary coarse grained brownish grey unconsolidated sandstone is visible.

The figures above showcase a variety of sandstone lithologies with distinct sedimentary features, bioturbation levels, and the presence of organic and calcareous materials. Figures 4.10 and 4.11 highlight brownish grey to blackish grey sandstones with visible laminations, burrows, and varying degrees of bioturbation, including features like Planolites, Thalassinoides, and pebbly lags. Figures 4.12 to 4.17 emphasize the ranges from heavily bioturbated to well-preserved structures such as flaser bedding and cross laminations, often filled with carbonaceous material. Figures 4.14 to 4.18 focus on fractures and fissile sandstones with carbonaceous and sulphur-rich inclusions. Figure 4.19 illustrates the reaction of calcareous materials within coarse-grained sandstones when exposed to HCl.

#### **4.8 Core Logs**

Core logs generated through the use of EasyCore and WellCAD software are essential tools in the detailed analysis and interpretation of geological core samples. These logs are produced after meticulous core analysis and serve as critical resources for visualizing and quantifying subsurface geological properties. EasyCore and WellCAD is instrumental in creating detailed core descriptions and capturing measurements and offers sophisticated log processing and visualization capabilities. The integration of these software platforms results in high-resolution core logs that provide a comprehensive overview of core characteristics, including lithology, mineralogy, ichnofacies, etc.

The importance of these core logs lies in their ability to transform raw core data into accessible and interpretable formats. By meticulously documenting sedimentary structures, grain size distributions, and bioturbation features, these logs facilitate a deeper understanding of the subsurface geology. This enhanced clarity aids geologists in identifying key geological units, correlating core data with well logs, and assessing reservoir properties with greater precision. Moreover, the use of core logs significantly improves the efficiency of data interpretation. The detailed visualizations and quantitative analyses provided by these logs streamline the process

of evaluating core samples, reducing the potential for errors and enabling more accurate assessments.

In summary, core logs are indispensable for the effective analysis of geological core samples. They not only enhance the readability and interpretability of core data but also support informed decision-making in exploration and production activities. By providing a clear and detailed representation of subsurface conditions, these logs are vital tools for geologists seeking to optimize reservoir management and improve the accuracy of geological models.

Based on the detailed description and analysis of cores obtained from three different wells within the basal sands of the Lower Goru Formation, general core logs were generated using two software platforms. The gamma-ray log was integrated with the core description data to produce comprehensive core logs. This integration was accomplished using EasyCore and WellCAD software. EasyCore was employed for the initial log preparation for Core 1 from Well A and Core 3 from Well C, as depicted in Figures 4.20 and 4.22, respectively. Meanwhile, WellCAD was used for the initial log preparation of Core 2 from Well B, as illustrated in Figure 4.21. These logs were crucial for correlating core data with well logs and for providing a visual representation of the subsurface geology.



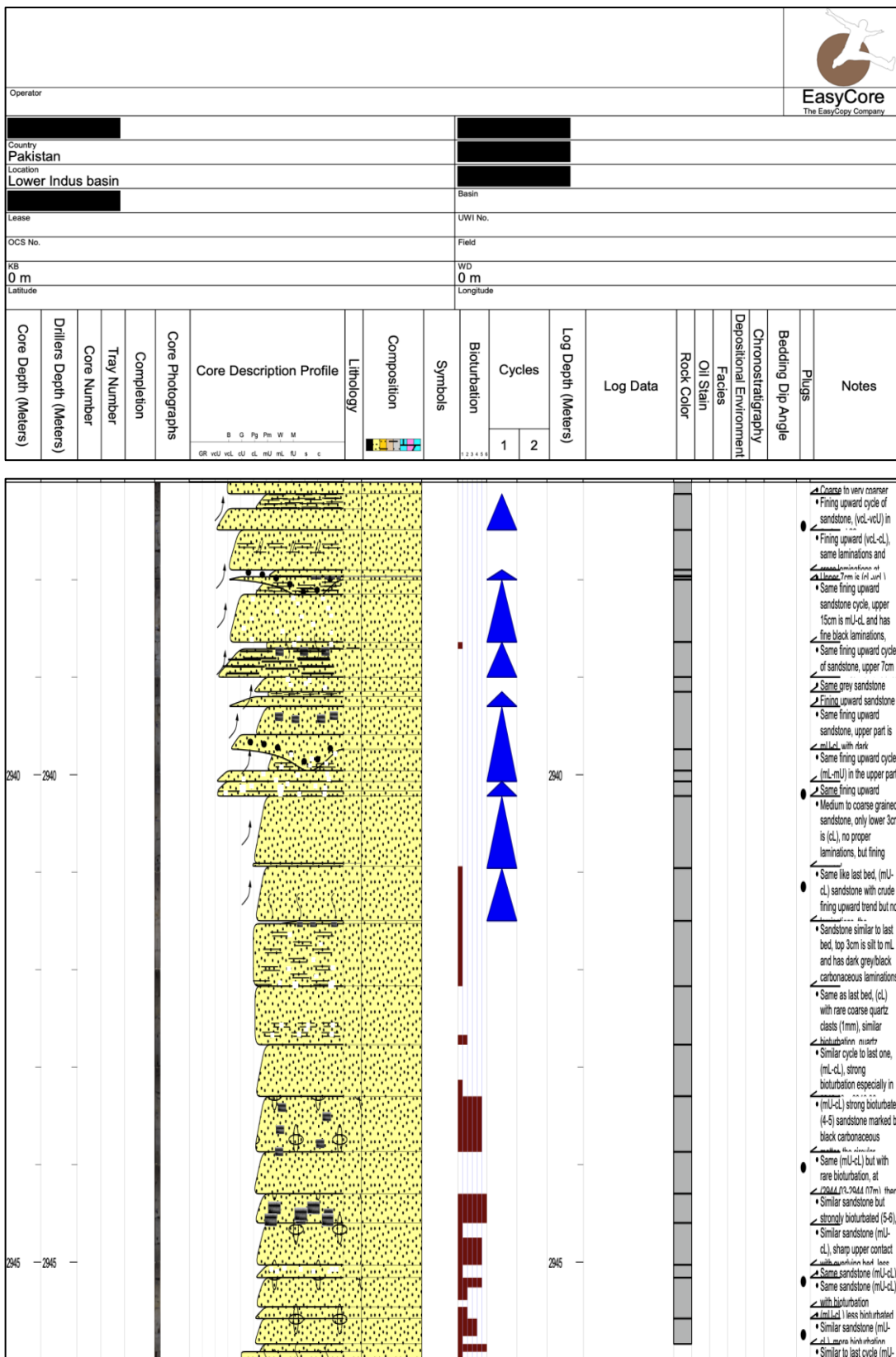
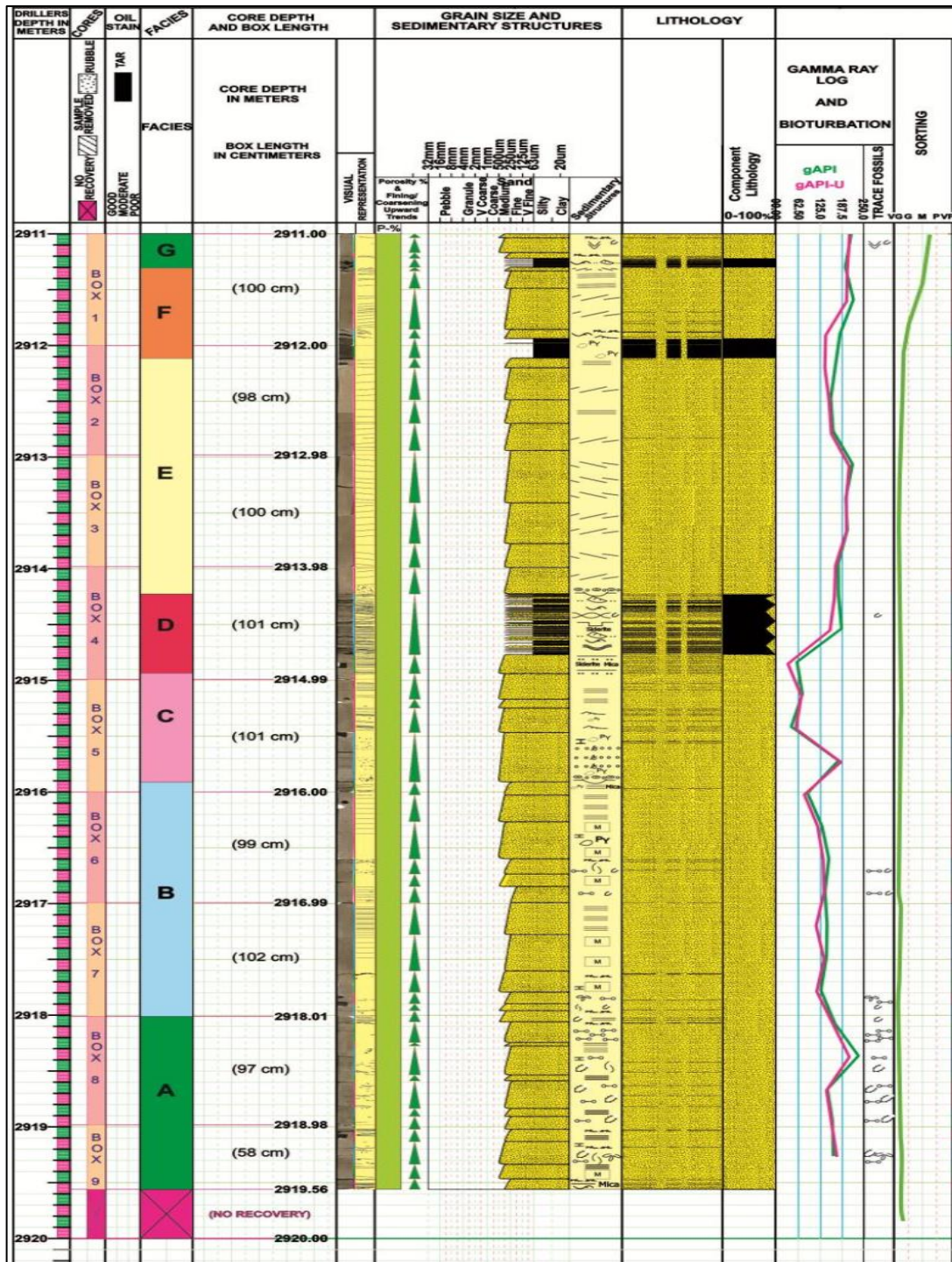


Figure 4.20 Core log of Core-1 (Well A) generated by using Easycore software



**Figure 4.21** Core log of Core-2 (Well B) generated by using WellCAD software. Facies A in green colour represents intensely bioturbated sandstone. Facies B in blue colour represents finer to medium grained sandstone with moderate bioturbation. Facies c in pink colour represents less bioturbated sandstone. Facies D in red colour represents an interbedded sand and shale. Facie E in yellow colour represents massive sandstone. Facie F in orange colour represents coarser sandstone with shaley patches. Facie G in green colour represents coarser grained sandstone.

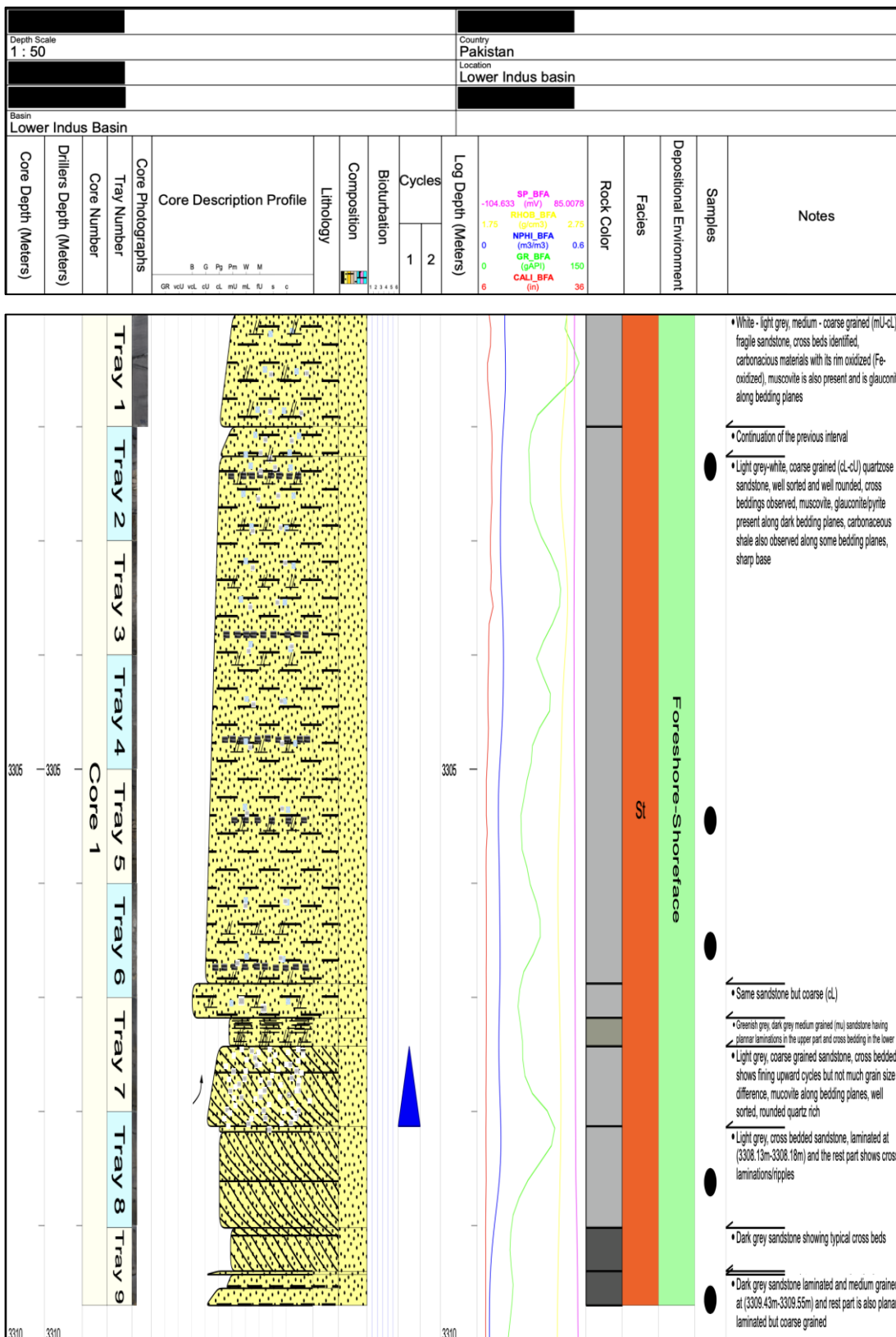


Figure 4.22 Core log of Core-3 (Well C) generated by using Easycore software

## **4.9 Gamma Ray Logs**

Gamma ray logging of core samples is a pivotal technique in subsurface geology, providing critical insights into the lithological and mineralogical composition of geological formations (Smith et al., 2019). This logging method measures the natural gamma radiation emitted by rocks, which is indicative of the concentration of radioactive elements, primarily potassium, uranium, and thorium (Jones and Roberts, 2018). One of the primary features of gamma ray logging is its ability to differentiate between clay-rich and sand-rich intervals, as clay-rich sediments typically exhibit higher gamma ray readings due to their higher radioactive content (Doe et al., 2020). This feature is instrumental in characterizing sedimentary environments and correlating core data with well logs (Brown and Wilson, 2017). The usage of gamma ray logs extends beyond lithological classification; they are also valuable in identifying boundaries between different rock types, assessing the presence of mineral deposits, and enhancing the understanding of geological formations (Miller, 2016). By providing a continuous, detailed record of gamma radiation along the length of the core, gamma ray logging facilitates accurate interpretation of subsurface geology, supports reservoir characterization, and aids in the evaluation of hydrocarbon potential (Johnson, 2015).

### **4.9.1 Gamma Ray Spectroscopy**

Gamma-ray spectrometry is a widely utilized method for detecting and measuring radioactivity within various samples (Smith et al., 2020). This technique plays a crucial role in identifying and characterizing different lithologies, particularly in subsurface geological studies (Johnson and Lee, 2018). During the process, gamma-ray spectroscopy is employed to distinguish between shale and sand formations (Brown et al., 2017). An arbitrary shale baseline is established on the gamma-ray log, serving as a reference point. Peaks that exceed this baseline are indicative of shale formations, while those that fall below it suggest the presence of sand (Miller and Thompson, 2016).

The height of the peaks on the gamma-ray log is primarily influenced by the concentrations of thorium and potassium, which are typically more abundant in shale than in sand (Doe, 2019). Therefore, a higher peak corresponds to a shale lithology, characterized by elevated levels of these radioactive elements. Conversely, a lower peak indicates a sand lithology, where these elements are less prevalent (Wilson and Green, 2015). The variation in peak heights across the gamma-ray log reflects changes in lithology, with each peak representing a different subsurface material (Jones, 2017). This contrast between high and low peaks allows geologists to differentiate between shale and sand layers, providing valuable insights into the geological structure and composition of the subsurface (Roberts et al., 2018). Ultimately, gamma-ray spectrometry is a fundamental tool in the interpretation of well logs, aiding in the identification and analysis of distinct lithological units (Smith et al., 2020).

The gamma-ray log is a crucial tool in differentiating between shale and sandstone formations based on their natural radioactivity. Typically, shale exhibits higher gamma-ray readings due to its higher content of radioactive minerals, particularly potassium, uranium, and thorium, which are concentrated in clay minerals. The reference range for shale generally exceeds 75 API units, indicating a high concentration of these radioactive elements (Rider and Kennedy, 2011). In contrast, sandstone, which is composed mainly of quartz and feldspar with minimal clay content, typically displays lower gamma-ray readings, usually below 75 API units, reflecting its lower radioactivity (Asquith and Krygowski, 2004). These reference ranges are essential for accurate lithological interpretation and reservoir characterization, as they help distinguish between clean sandstone reservoirs and shale-dominated intervals (Serra, 1984).

#### **4.9.2 GR-Spectroscopy analyses results**

The gamma-ray analysis of samples from Core 1 as shown in Appendix A reveals a range of API values that highlight significant variations in lithology and the presence of distinct sedimentary features. From sample 1 to sample 9, the API values

fluctuate between 4.4 and 96.6, indicative of primarily sand-dominated lithologies with some potential clay or shale content. However, a notable increase is observed in sample 10, which records an API value of 126.4, suggesting a shift towards a more shale-rich interval. This pattern continues with the next three samples, where API values of 88.8, 96.4, and 73.1 reflect a return to sandier lithologies. The subsequent samples show a mix of higher API values, with 107.1 and 161.8 API, indicating increased shale content or the influence of finer-grained sediments. The alternating API values continue, with a drop to 83.6 API followed by higher values between 101.3 and 146.1 API across the next five samples, pointing to further lithological changes. The pattern persists with sample 23 showing an API value of 81.8, followed by a series of higher API values ranging from 109.7 to 160.2 in the next seven samples, likely reflecting continued variability in sediment composition. The final two samples show a sharp decline in API values to 44.3 and 7, signalling a return to predominantly sandy lithologies. The elevated API values observed in certain intervals are attributed to the presence of bioturbation and burrows, along with carbonaceous laminations, which contribute to the higher concentrations of radioactive elements.

The gamma-ray spectroscopy analysis of Core 2 as shown in Appendix B reveals distinct variations in API values that correspond to changes in lithology and sedimentary features. The initial section, encompassing samples 1 through 13, exhibits elevated API values ranging from 159.5 to 224.3, indicative of a shale-dominated lithology with potential contributions from carbonaceous materials and fine-grained sediments. These high API values suggest the presence of significant amounts of radioactive elements, likely associated with the intense bioturbation and carbonaceous laminations observed in the core. Following this, the next three samples show a marked decrease in API values indicating a transition to a sandy lithology, characterized by lower gamma-ray responses. This shift suggests the presence of cleaner, coarser-grained sandstones. The subsequent sample, with an API value of 183.3, signals a return to a more shale-rich interval. The next two samples display intermediate API values of 92.1 and 134, reflecting a mix of sand and shale components. The core then continues with 10 samples having API values between 131.3 and 239.8, reinforcing the presence of shale-rich layers interspersed with

bioturbated zones and carbonaceous laminations. Additionally, from samples 1 to 9, two shaley patches are identified, further emphasizing the heterogeneity within the core. These findings illustrate the complex depositional environment and lithological variability within Core 2.

The gamma-ray spectroscopy analysis of Core 3 as shown in Appendix C reveals consistently low API values, reflecting the predominance of massive, unconsolidated, and clean sandstone throughout the core. The absence of bioturbation and minimal carbonaceous laminations further supports this interpretation. Samples 1 and 3 exhibit API values of 54.3 and 43, respectively, with Sample 4 showing a slightly higher value of 76.8 API, indicative of relatively cleaner sandstone sections. A notable exception is Sample 5, which records an API value of 128.3 due to the presence of a shaley lamina, briefly interrupting the otherwise sandy composition. The following four samples display significantly low API values of 21.9, 11.9, 2.9, and 26.6, consistent with the dominance of clean sandstone. This trend continues with three subsequent samples registering API values below 10, emphasizing the non-shaley, sandstone-rich nature of this interval. Sample 13 records an API value of 11, followed by seven samples with API values ranging from 0.6 to 8.8, further indicating an extensive section of very clean sandstone. A slight increase is observed in the next sample with a value of 12.2 API, followed by 36.6 API in the subsequent sample, potentially reflecting minor variations in lithology. However, this is followed by a return to low API values in the next sample, which records 7.4 API. The final eight samples show a modest increase in API values, ranging from 30.2 to 73.2, suggesting the presence of slightly more heterogeneous sandstone, potentially with minor shale or carbonaceous content. Overall, the low API values throughout Core 3 underscore the dominance of clean, massive sandstone with limited shale or bioturbation influences.

#### **4.9.3 GR-Spectroscopy analyses correlation**

The gamma-ray spectroscopy analysis of cores from the three wells reveals distinct lithological variations and sedimentary features that underscore the complexity of the subsurface geology within the Lower Goru Formation. Core 1

displays fluctuating API values, reflecting a mix of sandy and shale-rich intervals, with higher readings indicating the presence of bioturbation and carbonaceous laminations. Core 2 shows a dominance of shale-rich lithologies, particularly in the initial section, with significant bioturbation and carbonaceous material, while also revealing transitions to cleaner sandstones. In contrast, Core 3 is characterized by consistently low API values, indicative of massive, clean sandstone with minimal shale content, except for a few intervals marked by shaley laminations. The correlation of these results highlights the heterogeneity across the wells, with Core 1 and Core 2 showing more complex depositional environments compared to the more homogeneous sandstone-dominated sequence in Core 3.



## CHAPTER 5

### DEPOSITIONAL SEDIMENTARY FACIES AND THE ENVIRONMENTS

#### 5.1 Background

Depositional sedimentary facies represent distinct bodies of sediment with specific physical, chemical, and biological attributes that reflect the conditions of their depositional environment. These facies are fundamental to understanding the depositional processes and environments that shaped the sedimentary record, ranging from continental to marine settings. Each facies is characterized by unique features, such as grain size, sedimentary structures, fossil content, and mineralogy, which are direct responses to the energy conditions, sediment supply, and biological activity at the time of deposition (Walker and James, 1992).

For example, a fluvial facies typically features well-sorted, cross-bedded sandstones, indicative of deposition by rivers in a high-energy environment, whereas a marine shale facies might display fine-grained, laminated sediments rich in organic matter, reflecting deposition in a low-energy, anoxic marine setting (Miall, 2010). The interpretation of depositional facies is crucial for reconstructing past environments and for predicting the spatial distribution of reservoir rocks, source rocks, and seals in hydrocarbon exploration (Reading, 2009).

Facies models are often used to predict the lateral and vertical distribution of these environments in the subsurface, providing a framework for understanding the heterogeneity within sedimentary basins (Boggs, 2011). By analyzing depositional facies, geologists can infer paleogeographic settings, recognize changes in sea level, identify potential reservoirs, and assess the quality of source rocks, all of which are essential for effective exploration and production strategies in sedimentary basins (Nichols, 2009).

## 5.2 Sedimentary Facies

The rocks of Cores 1, 2 and 3 from the Basal Sands of the Lower Goru Formation can be categorized into eleven sedimentary facies, labelled Facies A to K, based on various sedimentary structures and their depositional environments.

### 5.2.1 Facies-A (intense bioturbation)

This facies is the zone of intense biogenic activity in terms of burrows and bioturbation. This facies begins with coarse to medium, light greenish-grey sandstone that is slightly to moderately calcareous. It is heavily bioturbated, primarily featuring horizontal and sub-vertical burrows, which are mostly filled with clean, dirty white sand. Occasionally, there are dark grey to black shale stringers. Noticeable white calcite laminations, which are horizontal and erosive, mark different sedimentary deposition events.

The majority of the burrows in this facies are *Thalassinoides*, with some *Skolithos* burrows of vertical to sub-vertical orientation. Concentrated lenses of calcite cement are observed along horizontal bedding planes. In areas with intense bioturbation, original sedimentary structures are almost entirely destroyed, with the light greenish-grey to light brownish-grey sandstone continuing and featuring some *Skolithos* burrows. These sandstones have a non-erosive base, and small, mud-dominated burrows, predominantly horizontal, are present. Two well-preserved vertical *Skolithos* burrows are noted.

Weak horizontal laminations, caused by differences in grain size and capped by calcite leached lamina, are present in some parts. Some sections appear massive, with minimal burrows of vertical to sub-vertical orientation and a few weak shale fragments. *Siphonichnus* burrows, primarily horizontal and lined with black shale, are filled with clean sand. Wavy mud drapes are preserved in parts of the unit.

The obliteration of laminations and homogenization of the sediments by bioturbation shows prevailing low energy fair-weather conditions in a shallow water setting. Presence of horizontal laminated bedding and suspension-feeder and deposit-feeder traces *thalassinoides suevicus* (predominantly horizontal), represents the depositional result of a shoaling zone of beach, termed here as lower shoreface setting

(Figs. 5.1 and 5.2). It is the most suitable depositional setting for this facies to be placed in. Several horizons that are completely bioturbated medium to coarse grained sandstone with *Thalassinoides* has preserved that also support the notion of interpretation for this zone. The erosive bases could be the result of storm generated waves in lower shoreface environment.

### **5.2.2 Facies-B (moderate bioturbation)**

This facies exhibits less bioturbation and more burrowing, with the presence of physical sedimentary structures. The sandstone is medium-grained, slightly brownish-grey, and massive, featuring lag deposits or granular lamina of coarse grains at its base. The facies includes a few horizontal burrows and numerous small, mud-dominated specimens, along with wavy, curvy, and slightly convex shale laminations or mud drapes that transition into horizontal laminations upward.

Granular lamina composed of coarse to very coarse sand grains are observed. The facies also contains small, mud-dominated specimens and horizontal burrows. Some units have erosive and planar horizontal bases. Wavy mud drapes and a few horizontal burrows are present, along with scattered coarse grains and occasional horizontal and vertical burrows. Notably, *Thalassinoides* (horizontal burrow) and *Skolithos* (vertical burrow) structures are present.

The lower half of the facies contains dispersed coarse grains in a horizontal bedding or lamination arrangement, with slightly shaly fragments found throughout. The entire unit has very few horizontal to sub-horizontal burrows. Above this, a small bed of granular to very coarse lower whitish-grey sandstone lies, overlain by light brownish-grey sandstone with weak, wavy, and irregular mud drapes and scattered coarse sand grains. A flame or escape structure is noted over the gritty unit, and a granular to very coarse lower, whitish-grey sandstone, wedge-shaped from the front and appearing as trough cross-bedded from the back, is also present.

The above cited characteristics i.e. physical sedimentary structures like trough cross laminations/beddings, erosive bases, slight wedged shapes, medium to coarse grain, well sorted nature of the rocks, lag/granular base of coarse upper to very coarse lower sized sand grains and biogenic structures like *skolithos* and vertical

ophiomorpha indicates deposition of these sediments in a middle shoreface environment (Figs. 5.1 and 5.2), under higher energy conditions. Such higher energy conditions in middle shoreface environment is due to breaking waves and associated longshore and rip currents. Also, the effect of storm waves is particularly important on the middle and lower shoreface environment, causing severe erosion and redeposition of sediment. Erosive bases and lag/coarse grains deposits on the bases of several beds in the lower part of this facies is the result of bottom scouring by waves, putting the sediments in suspension and its redeposition after waning of the storm. It is also the zone of longshore-bar development.

### **5.2.3 Facies-C (finer to very coarse-grained sandstone)**

This facies begins with medium-grained, light grey sandstone that is horizontally laminated and contains a horizontal burrow filled with coarse-grained sandstone. There are small, fining-upward sandstone beds, ranging in thickness from 2 to 3 cm, composed of very coarse to coarse grains. A notable feature is a single unit with a large *Conichnus* burrow or a collapsed *Ophiomorpha* tunnel-like structure, which leads to converging laminae. The sediments in this area appear to have been reworked and slightly mixed.

The coarse unit of this facie consists of gritty to very coarse sandstone with a wedge shape, while the upper bed has similar grain size, with a concentration of coarser grains and calcite cement. Both gritty units are mottled, slumped, or reworked and are separated by trough cross-beds. A 5 cm long vertical burrow is also present. This is overlain by a bed of very coarse upper to coarse lower, whitish-grey sandstone that is calcite-cemented, with symmetrical wave-topped bedding. This bed consists of interlaminated white very coarse upper and coarse lower brownish-grey sandstone. Small *Macaronichnus* burrows filled with brownish material are present within the light grey, fine-grained ground mass.

This facies includes coarse lower to medium upper light brownish-grey massive sandstone, capped by wavy shale stringers. There are a few horizontal burrows and scattered very coarse lower-sized grains. Upward, it transitions into a coarse upper to coarse lower whitish-grey, massive, well-sorted, and single wedge-

shaped sandstone bed. This bed contains wavy shale laminae and a horizontal burrow near its base. *Macaronichnus* burrows filled with light brown sand and disseminated coarse quartz grains are also observed. In some areas, a *Conichnus* burrow or collapsed structure over an *Ophiomorpha* tunnel is observed, which is overlain by coarse lower to medium upper, light brownish-grey sandstone with scattered very coarse grains. Further upward, it grades into coarse lower to medium upper, light brownish-grey sandstone, with scattered very coarse lower to very coarse upper grains. Some grits are present in the wedge-shaped top unit. Disseminated coarse grains and a 5 mm thick black shale lamina are found in the unit. In terms of grain size, some units within this facies are coarser than others and are divided into smaller units.

The facies also contain a thinly trough cross-bedded sandstone unit composed of very coarse upper to very coarse lower grains, featuring curvy bases and a significant amount of calcite cement. Thick shale laminae, mud drapes, and scattered coarse sand grains are also observed. The facies include a bed of whitish-grey trough cross-bedded sandstone, composed of very coarse upper to coarse lower grains. Another bedded sandstone unit, which fines upward from very coarse upper to coarse upper, is thinly bedded or laminated, with well-developed horizontal mud drapes on every bed.

A coarsening-upward sandstone unit, with very coarse upper to coarse upper grains, overlies this and is whitish-grey in color and wedge-shaped. This transitions into another coarsening-upward, well-preserved trough cross-bedded, whitish-grey unit with slightly concave bed bases. The second-to-last unit consists of coarse to medium, slightly brownish-grey sandstone with patches of very coarse sand. The top of this facies unit is composed of very coarse upper to coarse upper whitish-grey sandstone, with a very coarse upper wedge-shaped bed in the lower part. A sub-vertical to vertical *Ophiomorpha* burrow is also present. The upper half of the last unit is mostly massive, with a slightly bedded nature at the base.

Abundance of bi-directional and multi-directional trough cross bedding, dominant coarse to very coarse and gritty, wedge-shaped sandstone, curvy and concave upward bedding surfaces, truncating laminae together with rare *ophiomorpha* burrows indicate high energy upper shoreface environment (Figs. 5.1

and 5.2). *Macaronichnus* burrows in fine sand indicate the intervening phases. These deposits form in the surf zone of beach which is dominated by variety of wave-generated currents, strong bidirectional translations waves and longshore currents.

#### **5.2.4 Facies-D (extensive biogenic activity)**

This facies represents the zone of extensive biogenic activity within Core-2, characterized by abundant burrows and bioturbation. This facies begins with light greenish-grey sandstone, ranging from medium-lower to fine-upper grain size, which is slightly to moderately calcareous. It transitions into light grey, massive sandstone with a medium-upper to medium-lower grain size.

The burrows are predominantly horizontal and sub-vertical, filled with cleaner, dirty white sand, and are present in significant quantities. Occasional dark grey to black shale stringers are also observed. The majority of the burrows in this facies belong to the *Ophiomorpha* and *Macaronichnus* ichnofacies, with a few *Asterosoma* also noted.

Most intervals are heavily burrowed and bioturbated, resulting in the complete destruction of original sedimentary structures due to biogenic reworking. The light greenish-grey to light grey sandstone continues, often containing mica, and features non-erosive bases. In less bioturbated units, weak horizontal laminations are visible, mainly due to differences in grain size. Wavy mud drapes are preserved throughout the lower part of this facies.

The obliteration of laminations and homogenization of the sediments by bioturbation shows prevailing low energy fair-weather conditions in a shallow water setting. Presence of horizontal laminated bedding, suspension-feeder and deposit-feeder traces *ophiomorpha* (predominantly horizontal), represents the depositional result of a shoaling zone of beach, termed here as lower shoreface setting (Figs. 5.1 and 5.2). It is the most suitable depositional setting for this facies to be placed in. Several horizons that are completely bioturbated, medium grained sandstone with preserved *ophiomorpha* also support the notion of interpretation for this zone. *Asterosoma* is commonly found and reported from lower shoreface to transition zone.

### **5.2.5 Facies-E (less bioturbation)**

This facies exhibits less bioturbation and fewer burrows compared to other facies within Core 2, but it contains more pronounced physical sedimentary structures. The facies is slightly coarser in grain size and has a thickness of approximately 2 meters. It consists of medium, and occasionally coarse-grained, slightly brownish-grey sandstone that is mostly massive, with intervals of horizontal laminations.

Numerous small, wavy, curvy, and slightly convex shale laminations or mud drapes are present. The facies features mottled and massive units interspersed with laminated units. The thicker laminae transition to thinner ones towards the top.

The above cited characteristics i.e. physical sedimentary structures like laminations/beddings, medium grained, well sorted nature of the rocks indicates deposition of these sediments in a middle shoreface environment (Figs. 5.1 and 5.2), under higher energy conditions. Such higher energy conditions in middle shoreface environment is due to breaking waves and associated longshore and rip currents. Also, the effect of storm waves is particularly important on the middle and lower shoreface environment, causing severe erosion and redeposition of sediment. It is also the zone of longshore-bar development.

### **5.2.6 Facies-F (coarse grained sandstone)**

This facies represents the coarsest interval of the core. It begins with sandstone that contains mudclasts (up to 1 cm in diameter), quartz granules, and pebbles, and features an erosive base. This is followed by a massive sandstone unit with no visible sedimentary structures. Over time, a band of very coarse, lower to granule-sized quartz grains and small bivalve shells is deposited, which is then overlain by a thick, massive sand unit.

Within this unit, there is a 10 cm zone containing 3 to 4 patches of granule to very coarse quartz grains, pyritized shells, and a few well-rounded quartz pebbles. These patches are primarily composed of granule to very coarse lower grains and are mostly cemented with pyrite. Another massive unit includes disseminated coarse quartz grains, while a separate unit features 3 to 4 thinning-upward bands (ranging

from 10 mm to 5 mm). These bands contain a few mudclasts/bioclasts, abundant very coarse quartz grains, and pyrite nodules/framboids. The cementing material in these coarser grains also includes precipitated pyrite. In the upper half of this facies, low-angle planar cross-bedding or laminations at the base transitions upward to planar and horizontal bedding or laminations with mud-drapes at the top. This section comprises 6-7 smaller units with both low-angle cross-bedding and horizontal planar bedding, each starting with bedding at the base and ending with laminations at the top, indicating a thinning-upward trend with decreasing energy conditions. Additionally, a few siderite granules/clasts are present at the back of this interval.

Abundance of bi-directional cross bedding, dominant coarse to very coarse and gritty, wedge shaped sandstone, pyrite grains indicate high energy upper shoreface environment (Figs. 5.1 and 5.2). These deposits form in the surf zone of beach which is dominated by variety of wave-generated currents, strong bidirectional translations waves and longshore currents. Lag deposits/coarse grains deposits on the bases of several beds in the lower part of this facies is thought to have resulted due to transgression of the sea where transgressive lag deposits have been deposited and overlain by sub tidal heterolithic deposits.

### **5.2.7 Facies-G (medium-grained sandstone)**

This facies consists of medium-grained sandstone (ranging from upper to lower medium) interbedded with dark grey silty shale. The laminations are predominantly sub-horizontal to swaly and slightly wavy, with some laminae exhibiting sideritic stains. The shale laminae contain mica and pyrite grains and show slight inverse grading, likely due to crypto-bioturbation. The disrupted mud-rich laminae exhibit similar features. This facies appears to be graded rhythmites formed by a storm sand layer in an offshore transition zone.

Overlying this is a heterolithic unit or tidal beds composed of dark grey shale and medium-lower to fine upper light grey sandstone with a slight erosive base, including siderite laminae and pyrite content. The heterolithic unit consists of two cycles: the first starts with wavy bedding and transitions upward into lenticular bedding and tidal rhythmic laminations, with sandstone intervals containing siderite



but no burrows. The upper cycle begins with wavy flaser bedding and grades upward into wavy and lenticular bedding. This cycle features a few horizontal burrows and small gutter-cast-like structures at the bases of sandstone beds/laminae, including a clear horizontal burrow filled with calcareous sand and siderite. Nearly all sandstone beds exhibit swaly and hummocky laminae in convex and concave upward positions, truncated by mud layers.

This facies represents deposits of the subtidal environment (Figs. 5.1 and 5.2). Lenticular bedding indicates sediment-starved conditions as solitary very fine sand current ripples were deposited in a mud-rich environment that exhibited an alternation of periods of tidal current and periods of tidal slack water. These ripples can result from low sediment supply or from currents lacking the energy to transport sand. The wavy bedding indicates a slightly more energetic subtidal environment where currents and sediment supply are greater than during the formation of lenticular bedding. These are concluded as offshore to offshore transition deposit with thin storm-emplaced sandstone beds, as a result of transgression. Burrowed sandstones represent short periods of fair weather reworking.

#### **5.2.8 Facies-H (medium-lower to fine-upper grained sandstone)**

This facies is characterized by medium-lower to fine-upper grained sandstone, ranging in color from light brownish to light greenish grey, and spans approximately 2 meters in thickness. The facies consists of 6 to 7 low-angle, bi-directional cross-bedded units, each separated by horizontally laminated zones. The base of this unit is distinctly erosive and contains brown siderite grains, along with clasts and well-rounded sand and mud balls. The larger clasts are well-rounded, up to 1 cm in diameter, and include foraminifera/bivalve-like clasts of dark brownish-grey to dark grey pyrite-bearing material, some of which are encased by rusty siderite grains.

Throughout the unit, the grain size remains consistent, with a slight fining-upward trend and no evidence of biogenic sedimentary structures. The primary physical sedimentary structures present are weakly preserved low-angle, bi-directional planar cross-bedding and horizontal bedding. The uppermost part of the

unit consists of greyish-white calcareous sandstone with parallel and horizontal laminations, capped by a black shale lamina or mud-drape that contains fine lenticels of sandstone and light grey sand laminae. Re-activation surfaces and horizontal laminations are present within the unidirectional and bidirectional low-angle cross-bedded units.

This facies is thought to have been deposited as subtidal marine sand bars (Figs. 5.1 and 5.2). Sand bar deposition has occurred during the highest energy periods and unidirectional currents flow, depositing wedge shaped cross-bedded sandstones on the bar crests and flanks, and sheet sandstone beds in the offshore environments.

#### **5.2.9 Facies-I (shaley patch)**

This facies consists of dark grey to black shale with faint laminations and a few lensoid pyrite formations in the lower part. Towards the top, there are a few pyritized, connected lenses of fine-grained sandstone. No other physical or biogenic structures are observed within this black shale unit.

Above this shale, the facies transitions into a medium-lower to fine-upper grained, fining-upward sandstone that is light greenish grey in color. It exhibits sub-horizontal laminations or sheet sands and low-angle planar cross-laminations, with a leftward dip. There are two units with similar characteristics, grain size, and lithology, separated by a reactivation surface, indicating two storm or wave phases. These units are capped by a black shale lamina that contains a sand lamina. Overlying this is a fine-upper to medium-lower grained sandstone unit with two sets of oppositely dipping cross-laminated thin beds, which truncate each other.

Absence of biogenic activity with dark grey to black color and pyrite spindles/lenses/clasts depict deposition of the sediments below storm wave base in a reducing, anoxic below wave base, most probably in inter sand bars/offshore setting (Figs. 5.1 and 5.2). Weak currents during moderate energy fair weather periods and low energy fair weather periods which are dominated by wave processes, could be responsible for forming largescale, low-angle, leftward inclined surfaces on the bar

flanks and wave rippled sandstone beds and flat laminated fine grained sandstone layers in the offshore environments.

#### **5.2.10 Facies-J (lenticular shaley laminations)**

This facies is another dark grey to black shale unit featuring heterolithic tidal bedding with fine-grained, swaly, wavy, and lenticular sand laminae. This unit contains well-preserved sandstone injectites. Additionally, it includes medium-lower to fine-upper grained whitish to brownish grey sandstone, which is fining upward and laminated, with subordinate black shale laminations and a thick shale lamina containing fine sand lenses.

Rightward-dipping, thin cross-laminations are present, some of which are disturbed by burrows, including two large *Conichnus* and a few *Ophiomorpha*. A thick, blackish, curvy shale lamina truncates the underlying swaly laminae or climbing ripples. The topmost unit consists of medium-upper to medium-lower grained light greenish-grey sandstone, with shale stringers and an *Ophiomorpha* collapsed tunnel structure. A *Conichnus* burrow-like structure is also observed near the top of the facies.

Presence of burrows shows fluctuation and shift of environment to lower shoreface setting from offshore/transition zone (Figs. 5.1 and 5.2). Offshore/transition zone is evidenced by sandstone injectites which is the result sandstone encasement within mudstones in a deeper marine setting. Sandstone injectites are the result of overburden and post-depositional remobilization of the sediments.

#### **5.2.11 Facies-K (unconsolidated massive sandstone)**

This facies is characterized by several distinct features: it is an unconsolidated, massive sandstone with a whitish to brownish-grey color. The sandstone exhibits trough cross-bedding, contains sulphur and organic matter, is highly calcareous with vigorous reactions to 10% dilute HCL, and is fissile with some pebble lags in certain parts. Importantly, there is no evidence of bioturbation.

The absence of bioturbation and the presence of trough cross-bedding suggest a high-energy, shoreface environment (Figs. 5.1 and 5.2), rather than a marine setting. The cross-bedding indicates deposition by strong currents, typical of wave-dominated shoreface environments where sand is transported and deposited by migrating dunes or bars. The presence of sulfur and organic matter points to periods of anoxic conditions, possibly due to restricted circulation or rapid burial in the shoreface setting. The highly calcareous nature of the sandstone, indicated by its strong reaction to dilute HCL, suggests that carbonate material was incorporated into the sediment, possibly from nearby calcareous sources such as shells or other biogenic debris. The fissility and presence of pebble lags indicate episodic changes in energy conditions, such as storm events, that caused shifts in sediment transport and deposition. These features collectively point to a dynamic shoreface environment with fluctuating energy levels and episodes of anoxia, where both clastic and carbonate materials were deposited.

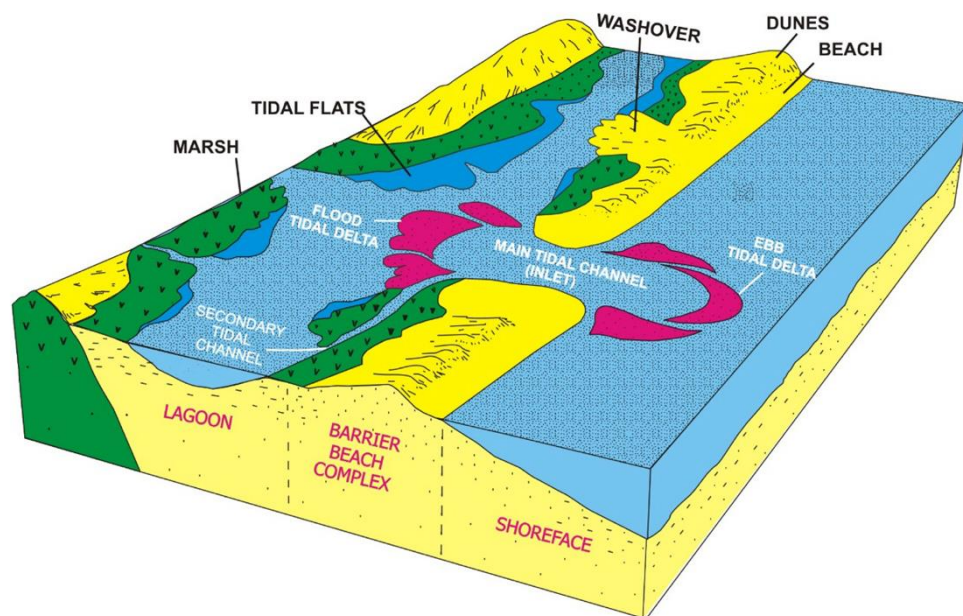


**Figure 5.1** Sub-environments of a Barrier Island System (From Reinson G. E., 1984).

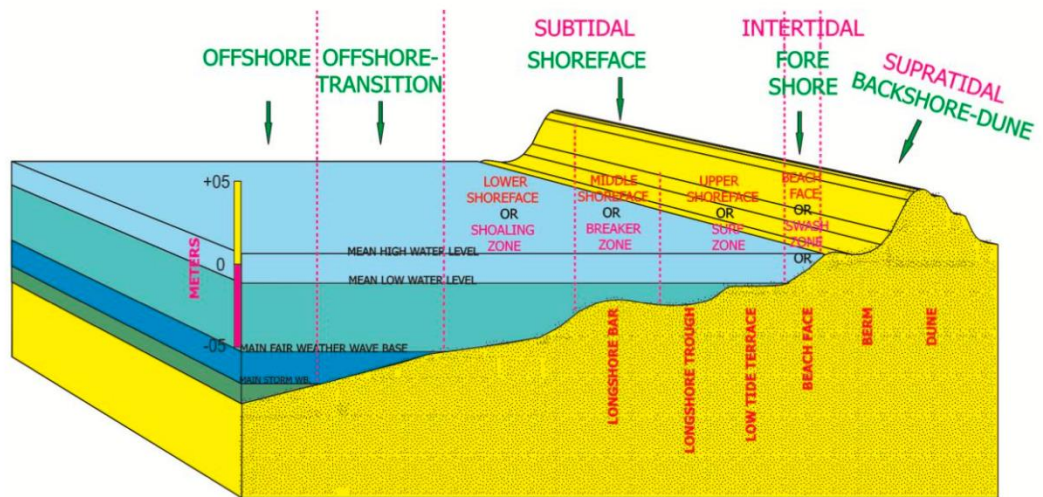


**Figure 5.2** Generalized profile of the Beach and Nearshore Zone (From Reinson, G. E., 1984).

## CHAPTER 6

### PETROGRAPHIC ANALYSIS

#### 6.1 Introduction

Petrographic analysis of core samples is a fundamental aspect of geological research, particularly in sedimentology, stratigraphy, and reservoir characterization (Smith et al., 2017). This analysis involves detailed examination through slab studies and thin section studies, which are crucial for identifying and understanding the mineralogical composition, textural features, and diagenetic alterations within the rock (Jones and Brown, 2016). Slab studies provide a macroscopic view of the core, allowing geologists to observe large-scale features such as sedimentary structures, bedding planes, and lithological variations. This helps in correlating these features with wireline logs and understanding the depositional environment (Miller et al., 2018).

Thin section studies, on the other hand, involve microscopic examination of core samples, where minerals and grain relationships are observed at a finer scale (Wilson, 2015). This level of analysis is essential for identifying mineral composition, grain size distribution, pore space, and the presence of cementing materials. Such details are vital for assessing the reservoir quality, as they directly influence porosity, permeability, and overall fluid flow within the reservoir (Roberts and Green, 2019). Petrographic analysis also aids in identifying diagenetic processes like cementation, compaction, and dissolution, which impact the reservoir's porosity and permeability (Doe et al., 2018).

The importance of petrographic analysis extends to its role in calibrating and validating petrophysical well log data (Johnson, 2016). By comparing petrographic data with log responses, geologists can enhance the accuracy of subsurface models, leading to better predictions of reservoir behaviour (Brown and Wilson, 2017).

Overall, petrographic studies are indispensable in the exploration and development of hydrocarbon resources, as they provide detailed insights into the geological history, reservoir potential, and economic viability of a given rock unit (Smith et al., 2017). This makes petrographic analysis a cornerstone in both academic research and the petroleum industry (Jones and Brown, 2016).

## **6.2 Petrographic Analysis of the Core Sections Studied**

In this research, 30 samples were selected for micromorphological analysis, focusing on depositional and diagenetic features. The mineralogical composition of the lithofacies was examined using a Leica DM750P microscope equipped with a Leica DFC 295 camera, allowing both qualitative and quantitative assessments. The results reveal that quartz is the predominant mineral, with significant quantities of feldspar and lithic fragments. The matrix typically consists of clay minerals and hematite, along with silt-sized quartz grains. Calcite cement is found to be primarily composed of calcite, clay, chlorite, hematite, and overgrowths of quartz and feldspar. The depositional characteristics observed through microscopic analysis include grain size, shape, sorting, and the nature of grain-to-grain contact. These detailed observations are crucial for understanding the mineralogical framework and diagenetic processes within the studied samples.

## **6.3 Slab Studies**

The Basal Sand of Lower Goru Formation have been studied with the aim of finding textural and mineralogical properties of the sandstones and relate them to diagenesis processes and reservoir properties. The study was conducted with the aid of petrographic studies, where thirty (30) slab samples from all three Cores were analysed by optical light microscopy. These samples were selected for their representativeness of the various lithologies, and intervals identified during the core description phase. The slab samples were prepared by slicing the cores into thin sections, allowing for a larger surface area to be examined in greater detail.

The microphotographs presented in Figures 6.1 to 6.7 reveal a diverse array of sedimentological features within the slab samples, highlighting variations in mineralogy, grain size, porosity, and cementation. Figure 6.1 displays key characteristics, including a quartz vein and a lithic fragment (Fig. 6.1A), fairly porous and permeable sandstone with iron oxide and biotite/mafic material (Fig. 6.1B), and compact sandstone with shale or sand laminations (Figs. 6.1C and 6.1D). Additionally, Figures 6.1E and 6.1F illustrate sandstone with a carbonaceous matrix, demonstrating fair porosity and permeability. In Figure 6.2, a compact sandstone with bluish-green glauconite and calcareous cementation is visible (Fig. 6.2G), while Figures 6.2H and 6.2J show poorly sorted sandstones with glauconite, lithic rock fragments, and iron oxide spots. Other notable observations include a hard sandstone with medium to coarse grains and visible cementing material (Fig. 6.2I) and sandstone with fractures likely filled with iron matrix (Figs. 6.2K and 6.2L).

Figure 6.3 highlights sub-rounded to angular grains with a vein possibly composed of carbonaceous or micaceous material (Fig. 6.3M), as well as compact, fine to very fine rock with micaceous material and laminations (Fig. 6.3N). Figures 6.3O and 6.3P depict poorly to fairly sorted sandstone with visible porosity, while Figures 6.3Q and 6.3R show the presence of a carbonaceous matrix and mica. In Figure 6.4, a fine to medium-grained sandstone abundant in iron oxide is observed (Fig. 6.4S), along with fairly sorted sandstone containing whitish lithic fragments (Fig. 6.4T). The figure also reveals sub-rounded to angular grained sandstone with cross laminations (Figs. 6.4U, 6.4V, and 6.4W), and a coarse-grained sandstone with greenish-blue glauconite (Fig. 6.4X).

Further examination in Figure 6.5 reveals medium to coarse-grained, compact rock containing micaceous material and possibly glauconite (Fig. 6.5Y), quartz fragments with iron minerals (Fig. 6.5Z), and medium to fine-grained sandstone with a calcareous matrix (Figs. 6.5A1 and 6.5B1). Quartz fragments and micaceous material are also present in Figure 6.5C1, while Figure 6.5D1 depicts fairly sorted sandstone with laminations. Figure 6.6 details brownish laminations in the upper part of a matrix, which is non-calcareous, contrasting with the highly calcareous lower matrix that reacts rigorously with 10% HCl (Figs. 6.6F1 and 6.6G1). Additionally, black carbonaceous matter is visible in a well-sorted grain matrix (Fig. 6.6G1), along



with sub-rounded to angular quartz grains (Fig. 6.6H1) and a thin pebble lag layer in finer sediments (Fig. 6.6I1). Lastly, Figure 6.7 shows trace fossils and burrows filled with carbonaceous organic matter (Figs. 6.7K1 and 6.7L1), underscoring the biological influences on the sedimentary environment.

### **6.3.1 Findings**

The microphotographs of slab samples reveal a wide range of mineralogical and textural features across various sandstone types. Quartz veins and lithic fragments are prominent, while several samples exhibit fairly porous and permeable sandstones characterized by iron oxide, biotite, carbonaceous matrix, and glauconite. Compact sandstone with distinct shale and sand laminations is observed, as well as poorly sorted sandstone containing mineral glauconite and lithic fragments.

Several samples highlight the presence of different cementing materials, including calcareous and iron-rich matrices, which significantly influence the rock's porosity and permeability. Additionally, sub-rounded to angular grains, cross-laminations, and evidence of potential oil staining are noted, reflecting varied depositional and diagenetic environments.

Trace fossils and burrows filled with carbonaceous or organic matter, along with fine to coarse grain sorting, further emphasize the complexity of the sedimentary structures. The rigorous reaction with hydrochloric acid in some samples indicates a high calcareous content, while the presence of micaceous material and pebble lags in finer sediments add to the diverse geological history recorded in these core sections. Overall, these observations provide valuable insights into the mineralogical composition, depositional processes, and diagenetic alterations within the studied lithofacies.

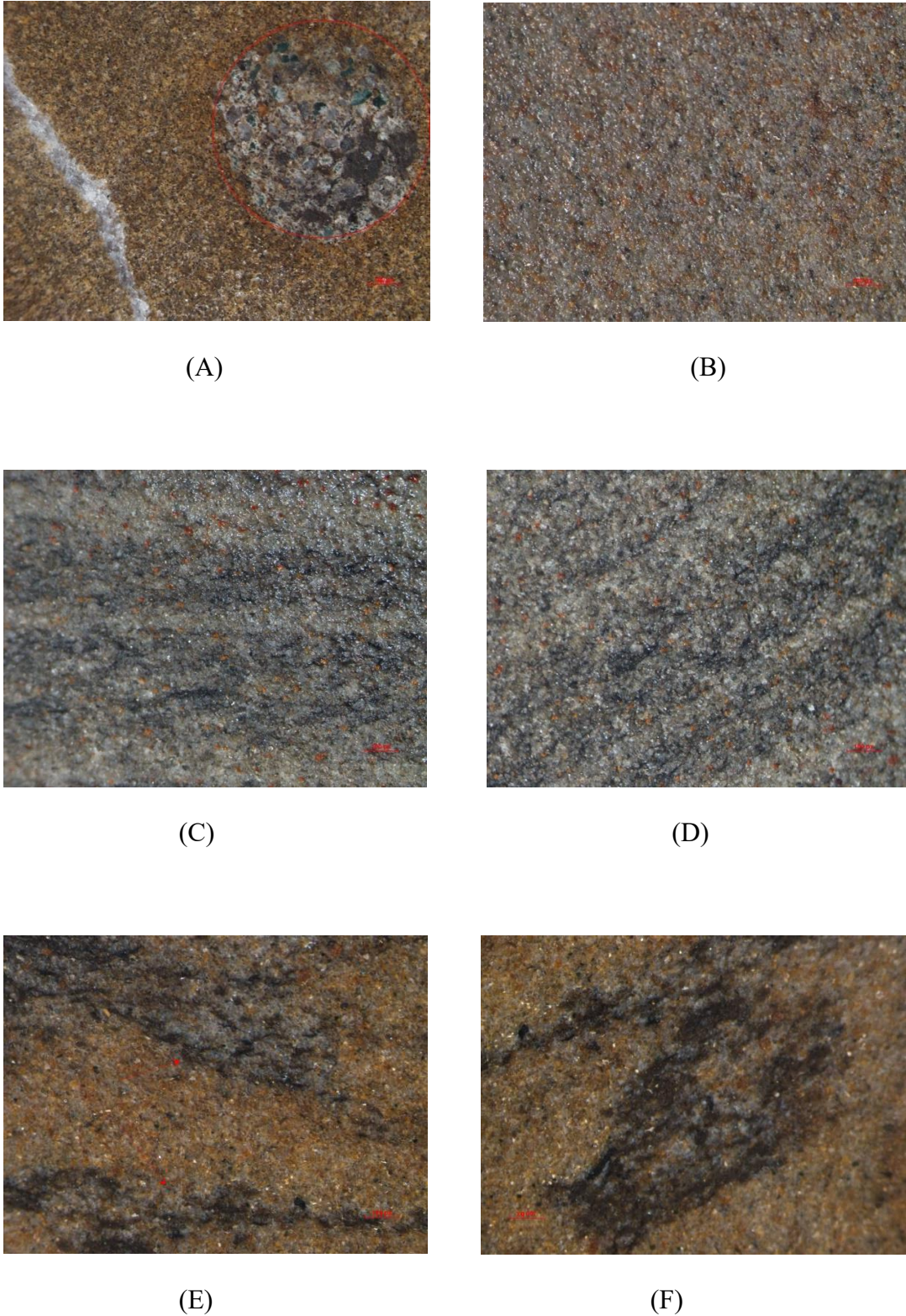
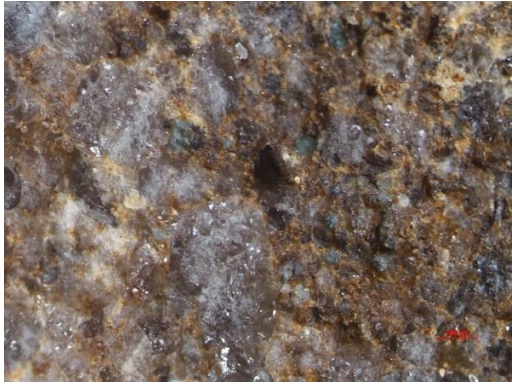
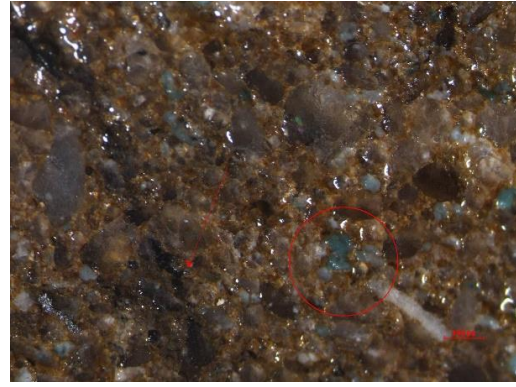


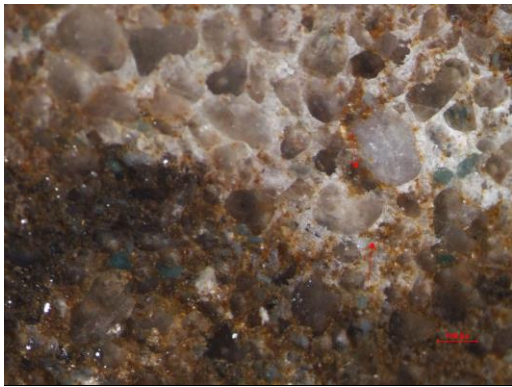
**Figure 6.1** Microphotographs of Slabs showing (A) Quartz Vein and a lithic fragment. (B) fairly porous and permeable sandstone with Iron oxide (brown spots) and biotite/mafic (black spots) material. (C and D) Compact hard sandstone with shale/sand laminae. (E and F) fairly porous and permeable sandstone with carbonaceous matrix.



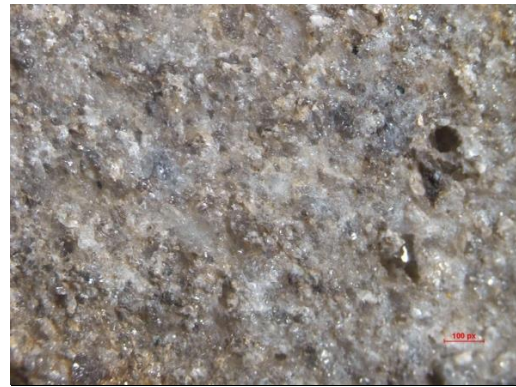
(G)



(H)



(I)



(J)



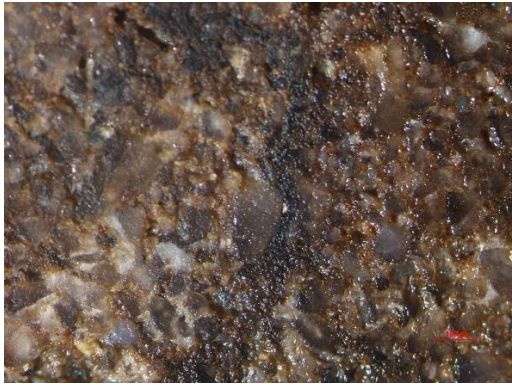
(K)



(L)

**Figure 6.2** Microphotographs of Slabs showing (G) Compact sandstone with blueish green colored Glauconite and calcareous cementation. (H) poorly sorted sandstone with mineral Glauconite and lithic rock fragment. (I) Hard sandstone rock with medium to lower coarser grains, different cementing material is visible. (J) Poorly

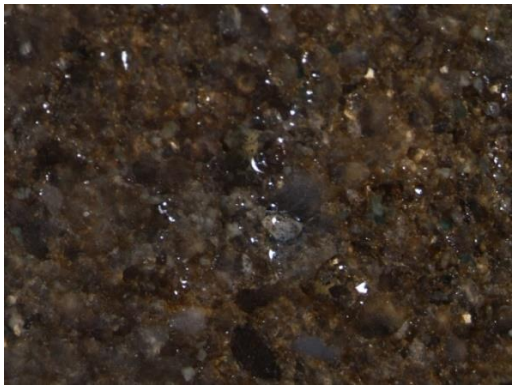
sorted greyish sandstone with a black spot maybe iron oxide. (K and L) Sandstone with fracture filled with probably Iron matrix.



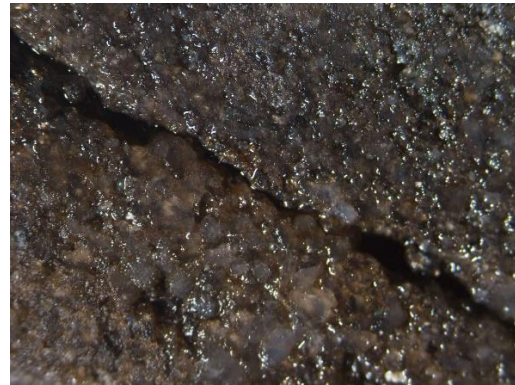
(M)



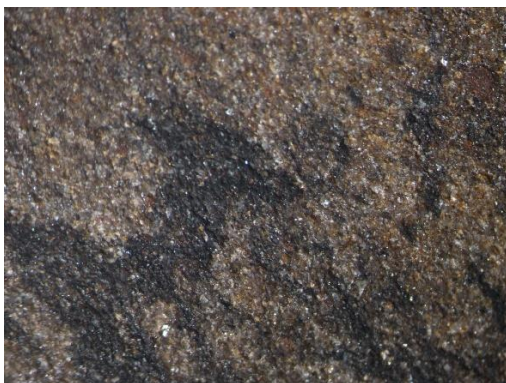
(N)



(O)



(P)



(Q)

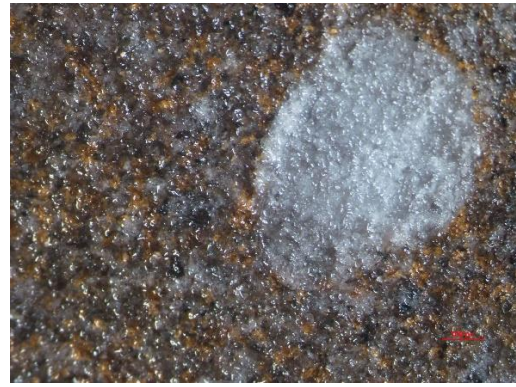


(R)

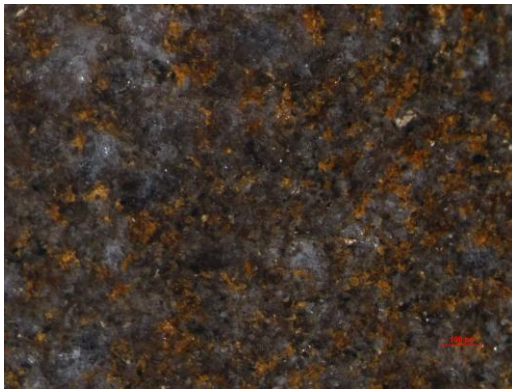
**Figure 6.3** Microphotographs of Slabs showing (M) Sub rounded to angular grains with a vein of probably carbonaceous or micaceous material. (N) Fine to very fine compact hard rock with micaceous material and laminations. (O and P) Poorly to fairly sorted sandstone with fair visible porosity. (Q and R) Carbonaceous matrix is present with a hint of Mica.



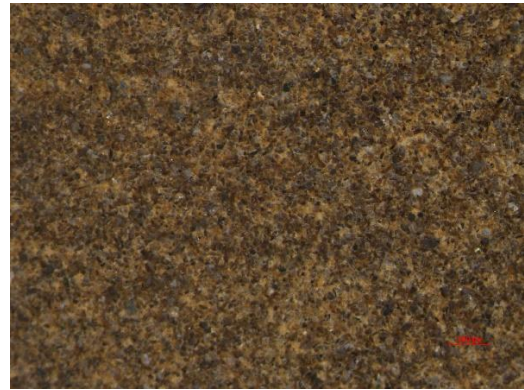
(S)



(T)



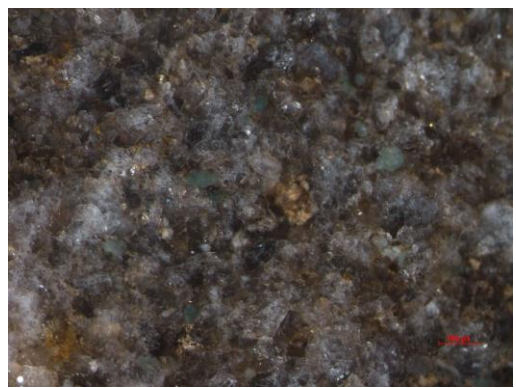
(U)



(V)

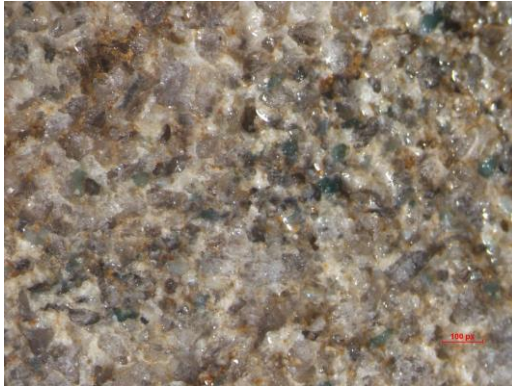


(W)

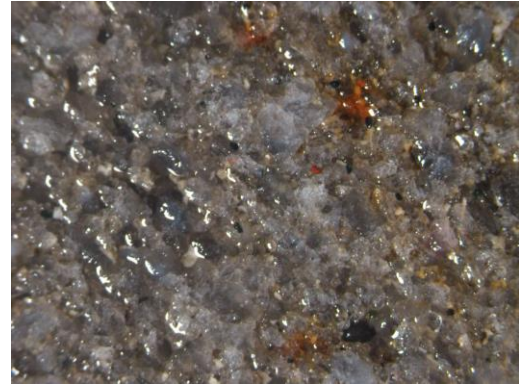


(X)

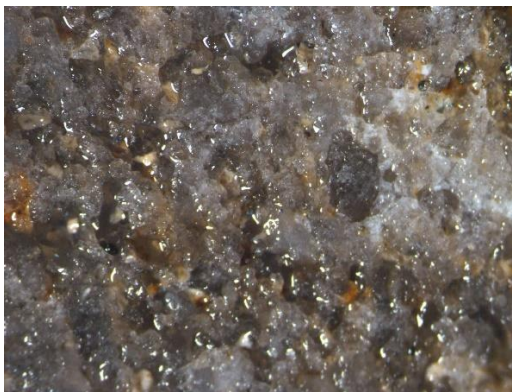
**Figure 6.4** Microphotographs of Slabs showing (S) Fine to medium grained sandstone with abundance of iron oxide. (T) fairly sorted sandstone with whitish lithic fragment. (U and V) Fine to coarse sub rounded to angular grained compact rock with fair sorting. (W) Cross laminations are visible with maybe an oil stain in the left. (X) coarse grained sandstone rock with greenish/blueish spots representing maybe glauconite.



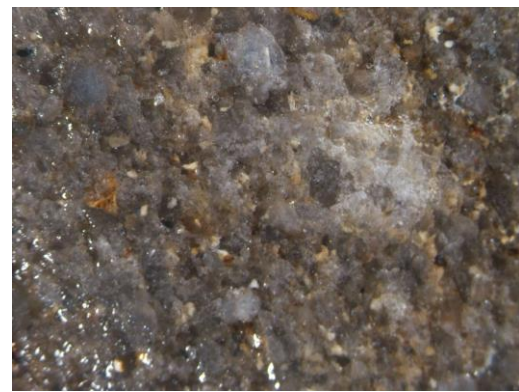
(Y)



(Z)



(A1)



(B1)

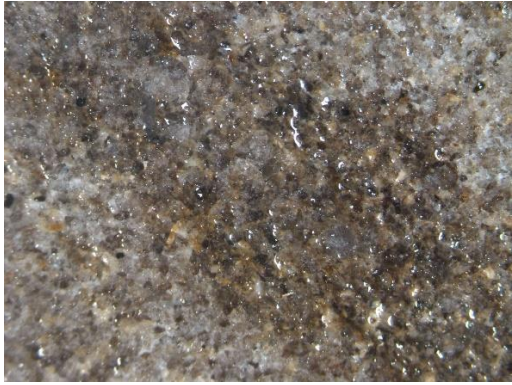


(C1)



(D1)

**Figure 6.5** Microphotographs of Slabs showing (Y) Medium to coarse grain compact rock with micaceous material and maybe Glauconite. (Z) Quartz fragments with red spots representing Iron minerals. (A1 and B1) Medium to fine grained sandstone with calcareous matrix. (C1) Quartz fragments and micaceous material is present. (D1) fairly sorted sandstone with laminations.



(E1)



(F1)



(G1)



(H1)

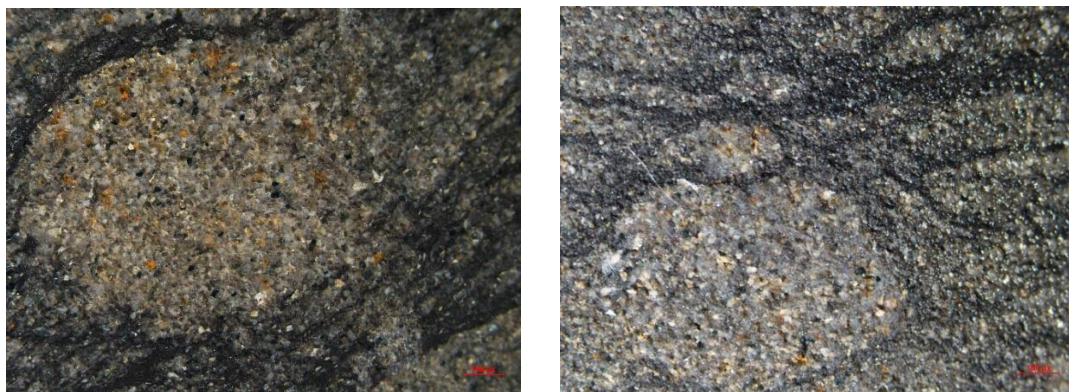


(I1)



(J1)

**Figure 6.6** Microphotographs of Slabs showing (F1) Brownish laminations in the upper part which are non-calcareous while rest of the matrix is highly calcareous. (F1) Rigorous reaction with 10% HCl, visible bubbling due to presence calcareous material. (G1) Black carbonaceous/Organic matter is present with good to fair sorting of grains. (H1) Sub rounded to angular Quartz grains. (I1) thin pebbly lags layer present in finer sediments. (J1) Ichnofacie is visible on the left bottom corner filled with some whitish material.



(K1)

(L1)

**Figure 6.7** Microphotographs of Slabs showing (K1 and L1) trace fossils/burrows filled with carbonaceous organic matter.

#### 6.4 Thin Section Studies

Following the slab studies, twelve samples were selected for detailed thin section analysis, focusing on the depositional and diagenetic characteristics of the sandstones. The three core samples under examination exhibited mineralogical and textural maturity, primarily composed of medium-grained sandstones. The dominant mineral present is monocrystalline quartz, with occasional occurrences of polycrystalline quartz. Minor components include pyrite, mica, shell fragments, lithic clasts, feldspar, and tourmaline. The primary cementing agent in these sandstones is calcite, with iron oxide and diagenetic pyrite also present in smaller amounts.

The examined sandstones displayed medium to fine grain sizes and angular to sub-angular shapes, demonstrating a generally good degree of sorting. While most samples exhibited good to fair sorting, a few from Core 3 showed poor sorting due to the presence of disseminated coarse to very coarse quartz grains and clasts. These samples also contained oyster shell fragments, mud clasts, algal fragments, pyrite granules, and a few gastropod shells (Fig. 6.8). Mechanical compaction has been identified as a significant factor influencing the coarser grains during earlier deposition and subsequent burial, as evidenced by severe fracturing. Some fractures within these coarse grains contained pyrite. In the sandstones, pyrite is found in trace amounts, typically as cement filling pore spaces and surrounding grains or clasts, with calcite remaining the dominant cementing material.



The following outlines the depositional and diagenetic characteristics observed in the thin sections.

#### **6.4.1 Thin section properties**

Micromorphological studies of the thin sections reveal that the sandstone unit exhibits a sub-arkosic nature, composed of a mix of finer to medium and medium to coarse grains that are poorly to moderately sorted. Quartz constitutes the dominant mineral, making up approximately 65-89% of the lithological unit, with feldspar and lithic fragments present in lesser quantities. The cementing materials are predominantly calcite, accompanied by a significant amount of silica in the form of quartz overgrowths, and occasional patches of siderite.

Grain morphology typically ranges from sub-angular to sub-rounded, though many grains are obscured by quartz overgrowths and calcite cement. The sandstone unit displays a sub-arkose fabric characterized by grain support, where the grain-to-grain relationship exhibits direct contact. The substantial fragmentation of framework grains indicates compaction, rearrangement, and squashing at considerable depths, resulting in a lack of preferred orientation.

Grain sizes in the studied thin sections range from medium to fine, with poor to moderate sorting. Generally, grain size decreases from the upper to lower sections, with most framework grains exhibiting sub-angular to sub-rounded shapes. Coarser grains are typically more rounded and spherical. In some intervals, grain boundaries are obscured by cementing materials, including calcite and silica in the form of quartz overgrowths.

The lithological unit displays textural maturity, as evidenced by grain size, sorting, and a lower matrix content. However, certain thin sections reveal texturally immature zones characterized by a higher proportion of matrix and easily deformable lithic fragments.

## **6.4.2 Mineralogical properties**

### **6.4.2.1 Detrital constituents**

The detrital constituents, derived from parent rocks through mechanical disintegration, include framework grains, lithic fragments, and accessory minerals. Framework grains constitute the bulk of the studied sandstone unit, comprising quartz, feldspar, and lithic fragments. Quartz makes up a significant portion of the composite minerals (66-90%) and can be distinguished as monocrystalline and polycrystalline grains, chert (lithics), and quartz overgrowths. Monocrystalline quartz grains range in size from medium to fine sand, displaying both undulatory and non-undulatory extinction, with few microlites and bubbles as inclusions. Considerable amounts of polycrystalline quartz crystals are also present.

Feldspar constitutes a smaller portion (6-11%) of the lithological unit, with alkali feldspar being the dominant type and plagioclase feldspar appearing in negligible amounts. Alkali feldspar is highly altered. Lithic fragments comprise approximately 4-28% of the studied sandstone unit, primarily consisting of chert and metamorphic rock fragments. Accessory minerals are also present, including glauconite and scattered mica, which exhibit deformation and bending between quartz grains.

### **6.4.2.2 Cementing materials**

The lithological unit contains cementing materials, which constitute a substantial part of the overall composition. Calcite, clay minerals, siderite, quartz, and feldspar overgrowths are among the cementing materials identified in the thin section analysis (Fig. 6.9). Quartz and feldspar overgrowths are easily distinguishable along the thin impurity lines at the edges of the original grains. Siderite, observed as a diagenetic product, appears in minor amounts.

### 6.4.2.3 Compaction and porosity reduction

The sandstone lithofacies exhibits porosity ranging from 2-30%. The upper zones of the lithological units demonstrate higher porosity compared to the lower sections. Both primary and secondary porosity can be observed in the microscopic analyses of the selected samples. Generally, porosity is influenced by grain rearrangement, cementation, the presence of softer grains, and compaction at greater depths. Through simple grain rearrangement, the preserved porosity of the depositional fabric diminishes from 45% to 26% (Boggs Jr. 1991). Some samples exhibit very good porosity due to extensive quartz fracturing (Fig. 6.10), while others show around 13% porosity; this loss can be attributed to compaction and the transformation of softer grains into clay minerals. Additional samples reveal proportionately low porosity (approximately 2-7%), likely due to the intense compaction of quartz grains and the effects of calcite cementation.

Optical petrographic analysis serves as a method for obtaining critical microstructural, mineralogical, and textural information for reservoir characterization. This technique effectively captures microscopic features that enhance the understanding of detrital and diagenetic minerals, alongside the compaction processes affecting sandstone reservoir rocks. Through these analyses, a comprehensive understanding of the geological history and quality of the studied reservoirs can be achieved, providing valuable insights for exploration and production in hydrocarbon contexts.

Understanding porosity and permeability is crucial for assessing reservoir rocks, as these features are integral to quantifying reservoir quality. Certain sandstones within the studied cores are characterized by coarse grains, exhibiting moderate to good porosity with effective pore connectivity. Conversely, the fine-grained sandstones do not serve as suitable reservoirs due to their low visual porosity. The detailed outcomes of the diagenetic study will significantly aid in evaluating the reservoir quality of these sandstones concerning hydrocarbon accumulation.



**Figure 6.8** Microphotographs under XPL with 4X magnification, showing (A) polycrystalline quartz, (B) fractured quartz granules (C) tourmaline (D) algal fragment (E) bioclast (F) bivalve shell (G) gastropode (H) recrystallized calcite filled shell fragment (I, J) oyster shells (K) pyritized shell (L) pyrite cement (M) pyrite cement under (PPL) (N) pyrite grain on quartz granule and (O) pyrite cement with a polycrystalline granule in medium grained sandstone.

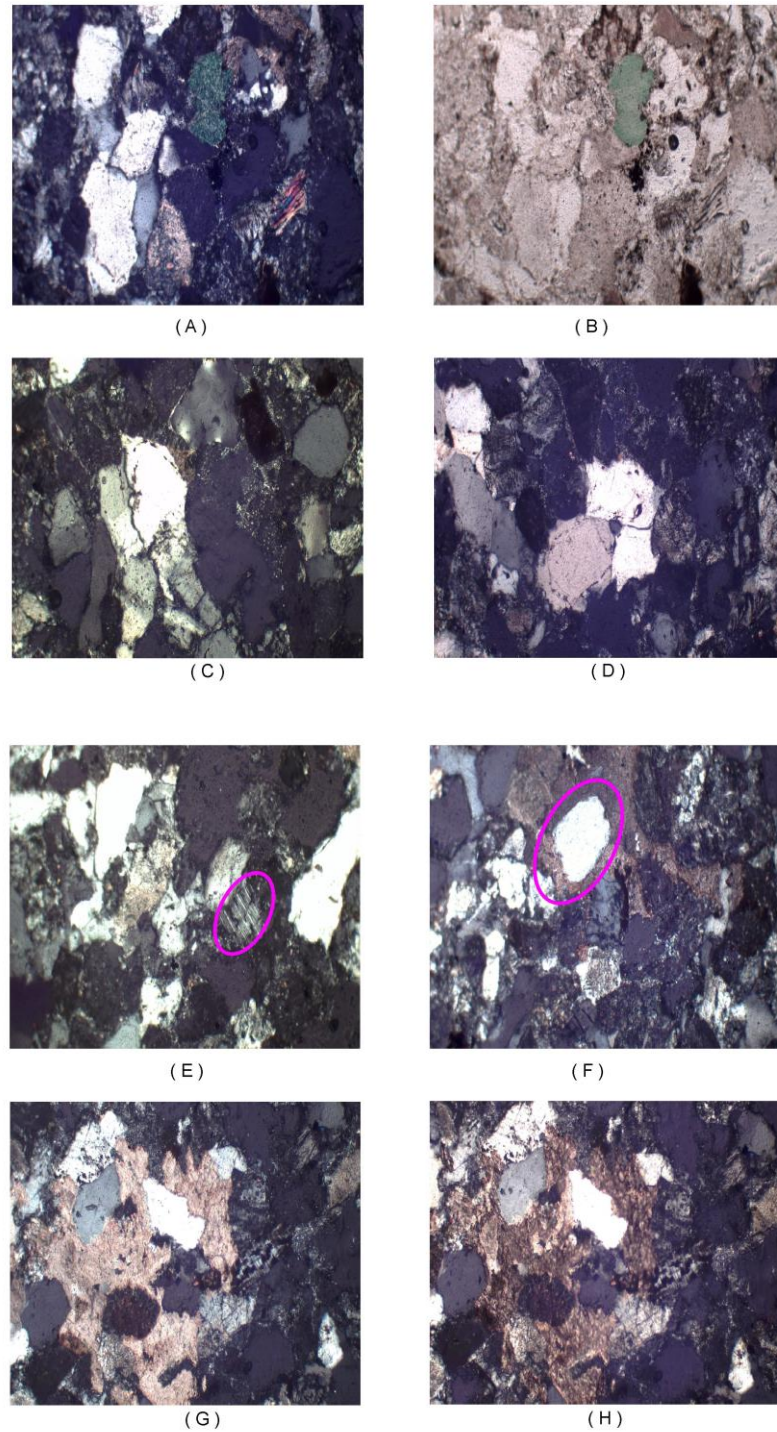
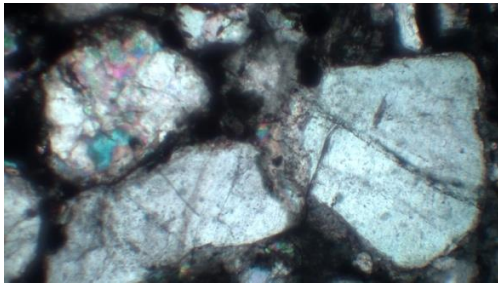
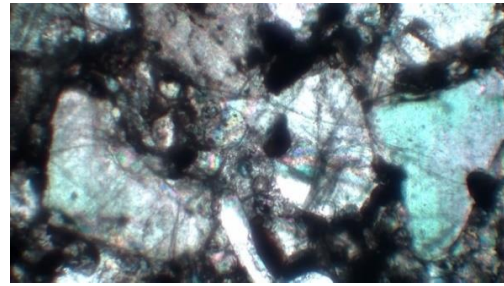


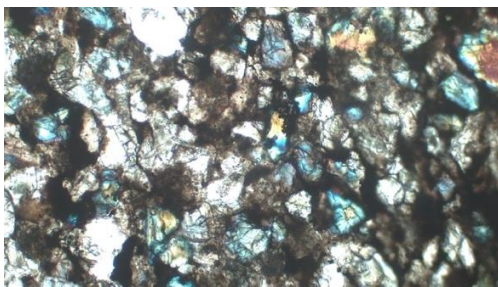
**Figure 6.9** (A) Microphotograph showing Quartz, mica and a green mineral. (B) Microphotograph showing the same minerals under PPL. (C) Microphotograph showing sutured Quartz grains. (D) Microphotograph showing excellent quartz overgrowth. (E) Microphotograph showing plagioclase with albite twinning under PPL. (F) Microphotograph showing the quartz grain surrounded and corroded by ferroan calcite cement. (G and H) Microphotograph showing ferroan calcite cementing material.



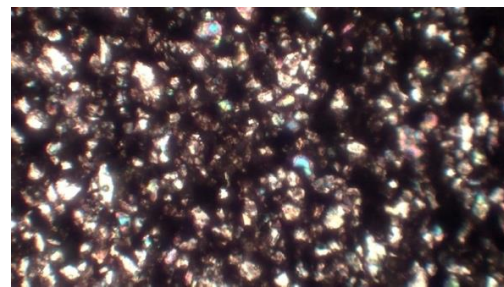
(A)



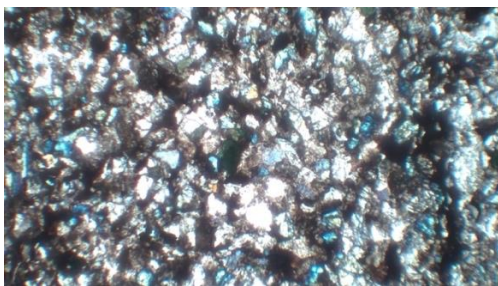
(B)



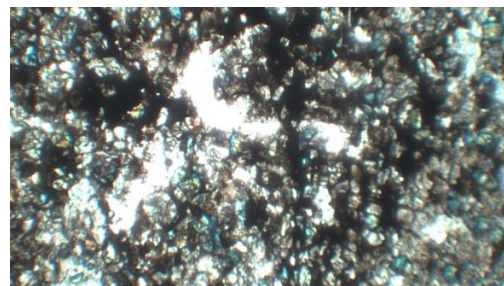
(C)



(D)



(E)



(F)

**Figure 6.10** Microphotograph showing (A) the coarse size Quartz grains which are rounded to sub rounded and are moderately sorted. (B) Quartz mineral with clear edges and corner with some microfractures on the surface. (C) moderately to fairly sorted Quartz grains (10X). (D) Texturally and mineralogically matured closely packed Quartz grains showing moderate visual porosity. (E) Closely packed and fairly sorted Quartz arenite with green color Gluconite mineral. (F). fine grained Quartz arenite closely packed with dark brown material most probably organic/carbonaceous material.

The microphotographs presented in Figures 6.8 to 6.10 offer detailed insights into the mineralogical and textural characteristics of the examined samples. Figure 6.8, under XPL at 4X magnification, showcases various mineral and fossil components, including polycrystalline quartz (Fig. 6.8A), fractured quartz granules (Fig. 6.8B), and tourmaline (Fig. 6.8C). The presence of organic and fossil fragments is highlighted by algal fragments (Fig. 6.8D), bioclasts (Fig. 6.8E), bivalve shells (Fig. 6.8F), and gastropods (Fig. 6.8G). Additionally, Figure 6.8 displays a recrystallized calcite-filled shell fragment (Fig. 6.8H), oyster shells (Figs. 6.8I and 6.8J), pyritized shells (Fig. 6.8K), and pyrite cement (Fig. 6.8L), with further emphasis on pyrite grains on quartz granules (Fig. 6.8N) and pyrite cement surrounding a polycrystalline granule in medium-grained sandstone (Fig. 6.8O).

Figures 6.9A and 6.9B depict quartz, mica, and a green mineral under XPL and PPL, respectively, while Figure 6.9C illustrates sutured quartz grains. The excellence of quartz overgrowth is shown in Figure 6.9D, followed by the presentation of plagioclase with albite twinning under PPL in Figure 6.9E. The corrosive effect of ferroan calcite cement on quartz grains is evident in Figure 6.9F, with ferroan calcite cementing material further highlighted in Figures 6.9G and 6.9H.

Figure 6.10 offers additional observations, showing coarse quartz grains that are rounded to sub-rounded and moderately sorted (Fig. 6.10A). Quartz minerals with clear edges and microfractures are depicted in Figure 6.10B, while Figure 6.10C presents moderately to fairly sorted quartz grains at 10X magnification. The textural and mineralogical maturity of closely packed quartz grains with moderate visual porosity is evident in Figure 6.10D. Furthermore, Figure 6.10E highlights a closely packed and fairly sorted quartz arenite with green glauconite mineral, and Figure 6.10F reveals fine-grained quartz arenite closely packed with dark brown material, likely organic or carbonaceous in nature.

### **6.4.3 Findings**

The thin section microphotographs reveal a diverse range of mineralogical and textural characteristics within the sandstone samples. The presence of

polycrystalline and fractured quartz granules, as observed in Figures 6.8A and 6.8B, indicates the mechanical durability and depositional history of the sediments. Tourmaline, bioclasts, and various shell fragments, including bivalves, gastropods, and oyster shells (Figs. 6.8C-G, I, J), suggest a biogenic influence in the sedimentary environment. The presence of pyrite cement and grains (Fig. 6.8L-O) points to diagenetic processes under reducing conditions. Quartz overgrowth and sutured grains, along with ferroan calcite cement (Fig. 6.9C-H), highlight significant diagenetic alteration. The moderate visual porosity in closely packed quartz arenite (Fig. 6.10D-F) underscores the varying degrees of compaction and cementation affecting reservoir quality.



## CHAPTER 7

### RESERVOIR HETEROGENEITIES THROUGH CORE ANALYSIS AND PETROPHYSICAL ANALYSIS

#### 7.1 Introduction

Reservoir heterogeneities play a pivotal role in understanding the complexity of subsurface hydrocarbon reservoirs, directly influencing reservoir performance and recovery strategies. These heterogeneities arise from variations in depositional environments, diagenetic processes, and structural modifications, which in turn impact the distribution and connectivity of reservoir properties such as porosity, permeability, and water saturation. Core analysis, particularly core plug analysis, is an indispensable tool in characterizing these heterogeneities, as it provides direct measurements of reservoir properties on a small scale. The process involves extracting cylindrical samples, or plugs, from the core, which are then subjected to a series of laboratory tests to determine porosity, permeability, and water saturation.

Porosity, a key reservoir property, refers to the volume of void spaces within the rock matrix that can store hydrocarbons. Core plug analysis enables precise determination of porosity by measuring the bulk and grain densities of the plug samples. These measurements are critical for understanding the storage capacity of the reservoir and for calibrating petrophysical models derived from well logs (Bassiouni, 1994). Permeability, which measures the ability of fluids to flow through the rock, is another fundamental property assessed through core plug analysis. The permeability of a reservoir rock is largely dependent on the size, shape, and connectivity of the pore spaces, as well as the presence of fractures and cementing materials. High-resolution permeability data from core plugs offer insights into the fluid flow dynamics within the reservoir, providing a basis for reservoir simulation and enhancing the predictability of well performance (Tiab and Donaldson, 2011).

Water saturation, the fraction of the pore space occupied by water, is also crucial in determining the hydrocarbon saturation and, consequently, the producibility of the reservoir. Core plug analysis allows for accurate measurement of water saturation by employing techniques such as Dean-Stark extraction or nuclear magnetic resonance (NMR) to quantify the water content in the rock samples. The data obtained from these analyses serve as a ground truth for interpreting water saturation from well logs, reducing the uncertainty in petrophysical evaluations (Asquith and Krygowski, 2004).

In addition to core analysis, petrophysical well logs, including gamma ray, resistivity, and neutron-density logs, are extensively used to assess reservoir heterogeneities over a larger scale. These logs provide continuous in-situ measurements of various reservoir properties along the wellbore, complementing the point-specific data obtained from core plugs. Integrating core analysis with petrophysical well logs enables a more comprehensive characterization of reservoir heterogeneities, facilitating the identification of high-quality reservoir zones, optimizing well placement, and improving recovery efficiency (Schön, 2015).

Understanding reservoir heterogeneities through core analysis and petrophysical well logs is fundamental for effective reservoir management and the optimization of hydrocarbon recovery. By providing detailed insights into the spatial distribution of porosity, permeability, and water saturation, these techniques allow for a more accurate assessment of reservoir potential and contribute to the development of more efficient extraction strategies. As the petroleum industry continues to explore increasingly complex reservoirs, the integration of core analysis and petrophysical well logs remains a critical approach in the pursuit of maximizing resource recovery (Bassiouni, 1994; Tiab and Donaldson, 2011; Asquith and Krygowski, 2004; Schön, 2015).

## **7.2 Horizontal Core Plug Analysis**

### **7.2.1 Introduction**

Horizontal core plug analysis, particularly with the CMS 300 instrument, is a specialized method used to measure the petrophysical properties of reservoir rocks, specifically porosity, permeability, and water saturation. This analysis involves extracting cylindrical samples, or "plugs," from a core along a horizontal plane, which is often more representative of the reservoir's natural conditions compared to vertical plugs. These measurements are essential for characterizing the storage and flow capacities of the reservoir rock, providing a direct assessment of its quality and performance potential (Tiab and Donaldson, 2011).

The process of acquiring horizontal core plug analysis data begins with the careful extraction of core plugs from the core sample. The 29 samples for porosity, permeability and 38 samples for water saturation were selected. The CMS 300 system was then used to conduct high-precision measurements of porosity, permeability, and water saturation. Porosity is typically determined using techniques such as helium porosimetry, where the volume of gas required to fill the pore spaces is measured (Tiab and Donaldson, 2011). Permeability is measured by flowing a fluid, usually air or brine, through the plug and recording the pressure drop across the sample. The CMS 300 is designed to perform these measurements under controlled conditions, ensuring accurate and reliable data. Water saturation is quantified using methods such as Dean-Stark extraction, where the water content is extracted and measured, or by applying nuclear magnetic resonance (NMR) techniques that offer a non-destructive way to determine fluid saturation (Bassiouni, 1994).

The data obtained from horizontal core plug analysis are crucial for various applications in reservoir engineering and management. Porosity measurements inform about the reservoir's storage capacity, indicating how much hydrocarbon the rock can hold (Tiab and Donaldson, 2011). Permeability data are used to evaluate the ease with which fluids can flow through the reservoir, which directly impacts the reservoir's productivity and the design of extraction strategies. Water saturation measurements are fundamental in determining the hydrocarbon saturation, which is

essential for estimating the recoverable reserves. These measurements are particularly valuable in constructing and calibrating reservoir models, as they provide ground-truth data that enhance the accuracy of petrophysical interpretations from well logs (Asquith and Krygowski, 2004).

Horizontal core plug analysis using the CMS 300 is critical in understanding reservoir heterogeneity and performance. The horizontal orientation of the plugs allows for a more accurate representation of the natural reservoir conditions, where fluid flow is predominantly horizontal. This approach helps in better predicting the behavior of the reservoir under production, leading to more effective reservoir management and optimized recovery strategies (Schön, 2015). Moreover, the high-resolution data obtained from this analysis are essential for reducing uncertainties in reservoir characterization, thereby improving the economic and operational decision-making process. The insights gained from horizontal core plug analysis are invaluable in developing strategies to maximize hydrocarbon recovery while minimizing production risks and costs (Bassiouni, 1994).

## **7.2.2 Calculated parameters**

### **7.2.2.1 Porosity**

The results for porosity (see Appendix D), derived from the CMS 300 horizontal core plug analysis, indicate significant variability across the samples, reflecting the heterogeneity within the reservoir. Porosity values range from 4.03% to 21.86%, with the lowest observed in sample 1057B and the highest in sample 1057R. These variations suggest differences in depositional environments, grain size, cementation, and compaction across the sampled interval. Higher porosity values, such as those in samples 1057R (21.86%) and 1057O (20.33%), imply greater pore space availability, which could translate to better hydrocarbon storage capacity. In contrast, lower porosity values, like in sample 1057B (4.03%), suggest tighter, less permeable rock. The majority of the samples exhibit porosity within the 10% to 20% range, which is typical for reservoir rocks, indicating moderate to good storage potential. The porosity data highlights the importance of core analysis in accurately

characterizing reservoir properties and understanding spatial variations within the reservoir.

The porosity results for the samples listed reveal a wide range of pore space variability, with porosity percentages spanning from as low as 4.03% in sample 1057B to as high as 21.86% in sample 1057R. Porosity is a critical factor in reservoir quality as it directly influences the capacity of the rock to store fluids, such as hydrocarbons and water. The variation in porosity among these samples can be attributed to differences in grain volume, bulk volume, and the degree of compaction under the applied overburden pressure.

For instance, sample 1057R, which exhibits the highest porosity at 21.86%, has a grain volume of 11.08 cc and a bulk volume of 14.18 cc, indicating a substantial difference between these volumes, which translates to a significant amount of void space within the rock matrix. This high porosity is further supported by the relatively lower bulk density of 2.10 gm/cc compared to other samples, such as sample 1057B with a much lower porosity of 4.03% and a bulk density of 2.50 gm/cc. The high porosity in sample 1057R suggests that this sample has a greater ability to store fluids, which could enhance its potential as a reservoir rock (Tarek Ahmed, 2010).

On the other hand, samples like 1057B, with a low porosity of 4.03%, suggest a much tighter rock fabric, with less void space available for fluid storage. This could be due to a higher degree of compaction or cementation within the rock, which reduces the effective pore space. Similarly, samples such as 1057A-1, with a porosity of 14.11%, and 1057X, with 14.28%, show moderate porosity values, indicating a balance between compaction and available pore space, which may suggest a moderate reservoir quality (Shenglai 2017).

The bulk and grain densities also play a significant role in determining porosity. For example, samples with higher grain densities, like 1057E (2.79 gm/cc), tend to have slightly lower porosities, as seen in this sample's 11.07% porosity, compared to those with lower grain densities like sample 1057O (2.58 gm/cc) with a higher porosity of 20.33%. This correlation suggests that denser grains may occupy more volume within the rock matrix, leaving less space available for pore fluids (Mark R. Curtis, 2015).

Overall, the porosity data reflects the heterogeneous nature of the reservoir, where different samples exhibit varying levels of fluid storage capacity. These variations could significantly influence reservoir performance, particularly in terms of fluid flow and recovery efficiency, underscoring the importance of detailed petrophysical analysis in reservoir characterization (Colin McPhee et al., 2015).

#### **7.2.2.2 Permeability**

The permeability results from the CMS 300 horizontal core plug analysis (see Appendix E) exhibit considerable variation, indicating significant differences in the fluid flow capacity of the reservoir rocks. The Klinkenberg permeability measurements presented here reveal significant heterogeneity across the sampled intervals, ranging from as low as 0.0145 md in sample 1057I to as high as 7.59 md in sample 1057P. This wide variation in permeability reflects substantial differences in pore structure, connectivity, and rock matrix properties among the samples. Samples such as 1057L (6.14 md), 1057N (5.5 md), 1057O (7.47 md), and 1057W (5.76 md) exhibit higher permeability, suggesting that these intervals may be more favorable for fluid flow. Such high permeability values are indicative of more porous and interconnected pore networks, which would likely enhance hydrocarbon migration and reservoir productivity in these zones.

On the other hand, the majority of samples in this dataset demonstrate considerably low permeability values, typically below 1 md, with some as low as 0.0145 md and 0.0223 md (samples 1057I and 1057B-1, respectively). These low permeability readings suggest tighter rock formations, potentially due to compaction, cementation, or the presence of fine-grained matrix materials that inhibit fluid movement. For example, samples such as 1057, 1057F, and 1057T all display permeability values under 0.05 md, which would likely hinder fluid flow and reduce reservoir quality in these intervals.

The observed permeability variability indicates a high degree of reservoir heterogeneity, a common characteristic in complex geological formations where diagenetic and depositional processes vary over short distances. This heterogeneity

could pose challenges for reservoir management, as areas of high permeability might facilitate easier extraction, while low-permeability zones could act as barriers or baffles, affecting overall productivity. Understanding these variations is crucial for effective reservoir modeling, as it helps in identifying flow pathways and potential compartmentalization within the reservoir.

In conclusion, this dataset suggests a mixed quality of reservoir potential, with certain zones offering high permeability conducive to fluid flow and others representing tight intervals with limited permeability.

### **7.2.2.3 Water saturation**

The results for water saturation (see Appendix F) from the provided data exhibit a broad range, reflecting the varying fluid retention characteristics of the samples. Water recovery, which is a direct indicator of water saturation, ranges from as low as 0.20 ml in samples such as Sample 29 and Sample 31, to as high as 1.90 ml in Sample 24, which also had the highest total fluid recovery at 2.24 ml. Samples with higher water recovery indicate higher water saturation, suggesting zones within the reservoir that are more prone to retaining water. Conversely, samples with lower water recovery, like Sample 29, indicate lower water saturation, which may point to more favorable zones for hydrocarbon extraction. Overall, the variability in water saturation underscores the heterogeneity of the reservoir, necessitating careful analysis when planning extraction strategies to optimize hydrocarbon production while managing water production.

The results for water saturation, derived from the fluid recovery data, demonstrate considerable variability across the samples. The total fluid recovered varies widely, from 0.31 ml in sample 29 to 3.36 ml in sample 34. Water recovery is consistently the dominant fluid, comprising a significant portion of the total fluid recovered in each case. The water saturation percentages can be inferred based on the proportion of water to the total fluid recovered, which indicates how much of the pore space within the samples is occupied by water as opposed to hydrocarbons.

For instance, in sample 32, a total fluid recovery of 3.22 ml was recorded, with 1.50 ml being water and 1.72 ml hydrocarbons, reflecting a more balanced distribution between water and hydrocarbons. This suggests a moderately water-wet condition, potentially indicating the presence of movable hydrocarbons alongside significant water saturation. Conversely, in sample 29, the total fluid recovery was much lower at 0.31 ml, with water accounting for 0.20 ml. The relatively high-water proportion indicates a higher water saturation, implying less hydrocarbon mobility within this sample.

Some samples exhibit particularly high-water saturation, such as sample 34, where 3.36 ml of total fluid was recovered, including 1.20 ml of water and 2.16 ml of hydrocarbons. The lower water recovery relative to the total fluid indicates that this sample has a significant hydrocarbon presence, despite the higher total fluid recovery, which may point to a lower overall water saturation (E. Donelson, 1994).

In contrast, samples like 17 and 31 show a lower total fluid recovery (0.99 ml and 0.55 ml, respectively), with water making up 0.60 ml and 0.20 ml, respectively. The higher relative proportion of water suggests these samples are more water-saturated, potentially indicating lower hydrocarbon production potential (S. T. Imoize et al., 2021).

These variations in water saturation across different samples underscore the reservoir's heterogeneity, affecting fluid distribution and potentially influencing the reservoir's productivity and management strategies (Robert F. Mitchell, 2009).

### 7.2.3 Results

**Table 7.1** Average results from the CMS-300 Horizontal Core Plug Analysis.

Properties	Porosity	Permeability (md)	Water Recorded (ml)
Average	0.14	1.491	0.90
Average (%)	14.13%	----	90%



The horizontal core plug analysis from the CMS-300 dataset reveals significant insights into the reservoir properties as shown in table 7.4. The average porosity of the core plugs is 0.14, corresponding to a 14.13% porosity in percentage terms. This indicates a moderately porous rock formation, which is crucial for evaluating fluid storage capacity within the reservoir (e.g., Cho et al., 2022).

Permeability measurements, averaged at 1.491 millidarcies (md), highlight exceptionally low permeability. This suggests that the rock formation exhibits limited fluid flow potential, which can significantly impact the efficiency of hydrocarbon extraction (e.g., Zhang et al., 2021).

The average water is recorded at 0.90 ml, which translates to a 90% saturation rate. This high water saturation implies that a large proportion of the pore space is occupied by water, influencing the reservoir's hydrocarbon productivity and recovery strategies (e.g., Smith et al., 2023).

## **7.3 Petrophysical Analysis**

### **7.3.1 Introduction**

Reservoir heterogeneities significantly influence the effectiveness of hydrocarbon recovery, as they dictate the spatial distribution of key petrophysical properties such as porosity, permeability, and water saturation. Porosity, which represents the void spaces within the rock matrix, is a primary indicator of a reservoir's storage capacity (Tiab and Donaldson, 2015). However, porosity alone is insufficient to assess a reservoir's potential; permeability, the measure of a rock's ability to transmit fluids, is equally crucial as it governs the ease with which hydrocarbons can flow through the reservoir (Lake, 2010). The interplay between these two properties often results in complex flow patterns, particularly in heterogeneous reservoirs where variations in grain size, cementation, and diagenetic processes introduce anisotropy and non-uniformity (Aydin and Eyal, 2002).

Water saturation, defined as the fraction of pore volume occupied by water, further complicates this dynamic by affecting the relative permeability of hydrocarbons. High water saturation typically reduces the effective permeability to oil and gas, necessitating a detailed analysis to optimize recovery strategies (Buckley et al., 1998). The integration of core plug analysis with petrophysical well logs allows for a more comprehensive understanding of these heterogeneities, enabling better prediction of reservoir performance and more efficient field development (Asquith and Krygowski, 2004). Through detailed petrophysical analysis, engineers and geologists can delineate zones of varying quality within the reservoir, tailor recovery methods, and ultimately enhance the economic viability of hydrocarbon production (Tiab and Donaldson, 2015).

Petrophysical analysis stands as a crucial tool in evaluating and classifying the fundamental properties of reservoir rocks, providing essential insights into the potential for hydrocarbon production. The productivity of a well is heavily influenced by several petrophysical parameters, including lithology, porosity, permeability, water saturation, and hydrocarbon maturation. These factors collectively determine the reservoir's capacity to store and transmit fluids, which are vital for successful hydrocarbon recovery (Tiab and Donaldson, 2015). The framework of petrophysics in this context is often referred to as formation evaluation, a comprehensive process involving the interpretation of borehole measurements to assess the geological and structural characteristics of subsurface formations (Schlumberger, 2018).

Formation evaluation employs a suite of well logging techniques to gather and interpret data, allowing for a detailed understanding of the reservoir's properties. Key logs used in this analysis include gamma ray logs, which help in identifying lithology and detecting shale content; density and neutron porosity logs, which are crucial for determining porosity and fluid content; and resistivity logs, such as LLD, LLS, and MSFL, which are vital for estimating water saturation and identifying hydrocarbon zones (Ellis and Singer, 2007). Photoelectric effect (PE) logs are also utilized to provide additional lithological information, particularly in differentiating between various rock types (Asquith and Krygowski, 2004).

In this dissertation study, raw well log data from three wells in the Bitrism E.L. field have been analyzed to perform a detailed petrophysical assessment (Figs.

7.2 to 7.4). By integrating these diverse data sets, the study aims to enhance the understanding of the reservoir's heterogeneities, ultimately leading to more accurate predictions of hydrocarbon potential and improved decision-making in reservoir management (Sarah et al., 2015).

### **7.3.2 Logs used in petrophysical analysis**

In the petrophysical analysis of Wells A, B, and C, several key well logs were employed to assess the reservoir's characteristics:

The gamma ray (GR) log measures the natural gamma radiation emitted by the formation. It is primarily used to differentiate between shales, which typically emit higher levels of gamma radiation, and cleaner reservoir rocks like sandstones or carbonates. This log helps in identifying lithology and determining the shale volume in the formation (Asquith and Krygowski, 2004).

The sonic (DT) log, also known as the compressional sonic log, measures the travel time of sound waves through the formation. This data is critical for evaluating porosity, as the speed of sound varies with the density and porosity of the rock. Lower travel times generally indicate higher porosity, while higher travel times suggest denser, less porous formations (Ellis and Singer, 2007).

The caliper (CALI) log records the diameter of the borehole. Variations in the borehole size can indicate the presence of washouts or caving, which can affect the accuracy of other log measurements. It also provides insights into the mechanical properties of the formation, such as its competence and stability (Rider and Kennedy, 2011).

The spherically focused log (SFLU) is a type of resistivity log that measures the resistivity of the formation near the borehole. It is particularly useful for identifying fluid content and differentiating between water-bearing and hydrocarbon-bearing zones. High resistivity values generally indicate the presence of hydrocarbons, while low values suggest water saturation (Tiab and Donaldson, 2015).

The laterolog deep (LLD) log is another resistivity measurement that investigates the deeper parts of the formation, away from the borehole's influence. This log is essential for determining the true resistivity of the formation, which is crucial for accurate water saturation calculations (Ellis and Singer, 2007).

The bulk density (RHOB) log measures the density of the formation. It is primarily used to determine porosity, as there is a direct relationship between the formation's density and its porosity. Lower density values typically correspond to higher porosity (Asquith and Krygowski, 2004).

The neutron porosity (PHIN) measures the hydrogen content in the formation, which is directly related to the presence of fluids, primarily water and hydrocarbons. This log is widely used to estimate porosity and to differentiate between gas and liquid-filled porosities (Tiab and Donaldson, 2015).

The spontaneous potential (SP) log records the natural electrical potential difference between the borehole and the formation. It is useful for identifying permeable zones and lithology, as well as for estimating formation water salinity (Schlumberger, 2018).

These logs, when integrated, provide a comprehensive view of the reservoir's petrophysical properties, enabling more accurate assessments of porosity, permeability, fluid saturation, and overall reservoir quality.

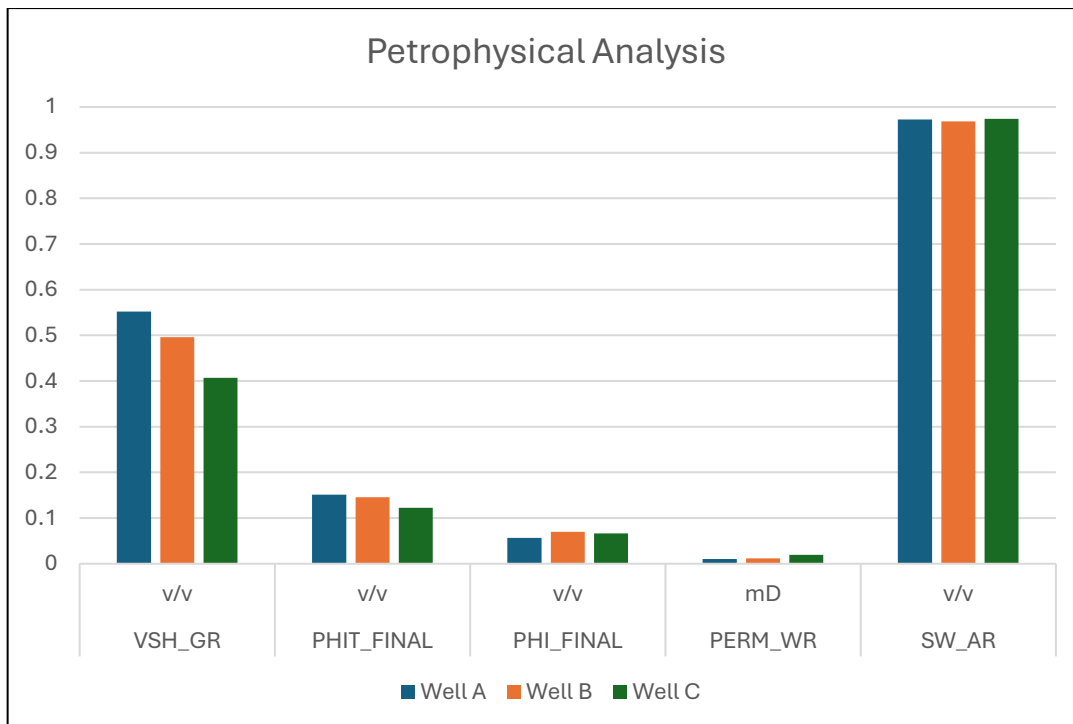


**Figure 7.1** Calculated parameters from well logs of Well A, B and C.

The bar chart in figure 7.1 shows that Well A has the highest shale volume (VSH_GR) among the three, while Wells B and C have slightly lower and comparable values. For total porosity (PHIT_FINAL) and effective porosity (PHI_FINAL), all three wells exhibit relatively low values, with Well A slightly higher than the others. Permeability (PERM_WR) is also low across the wells, with Well A showing a marginally higher value than Wells B and C. Water saturation (SW_AR) is consistent across all wells, reaching close to a maximum of 1 v/v, indicating high water content within the formations of all three wells. This analysis provides insights into the geological and reservoir quality differences among the wells, with Well A generally showing slightly higher values across most parameters except water saturation, which remains uniformly high across the board.

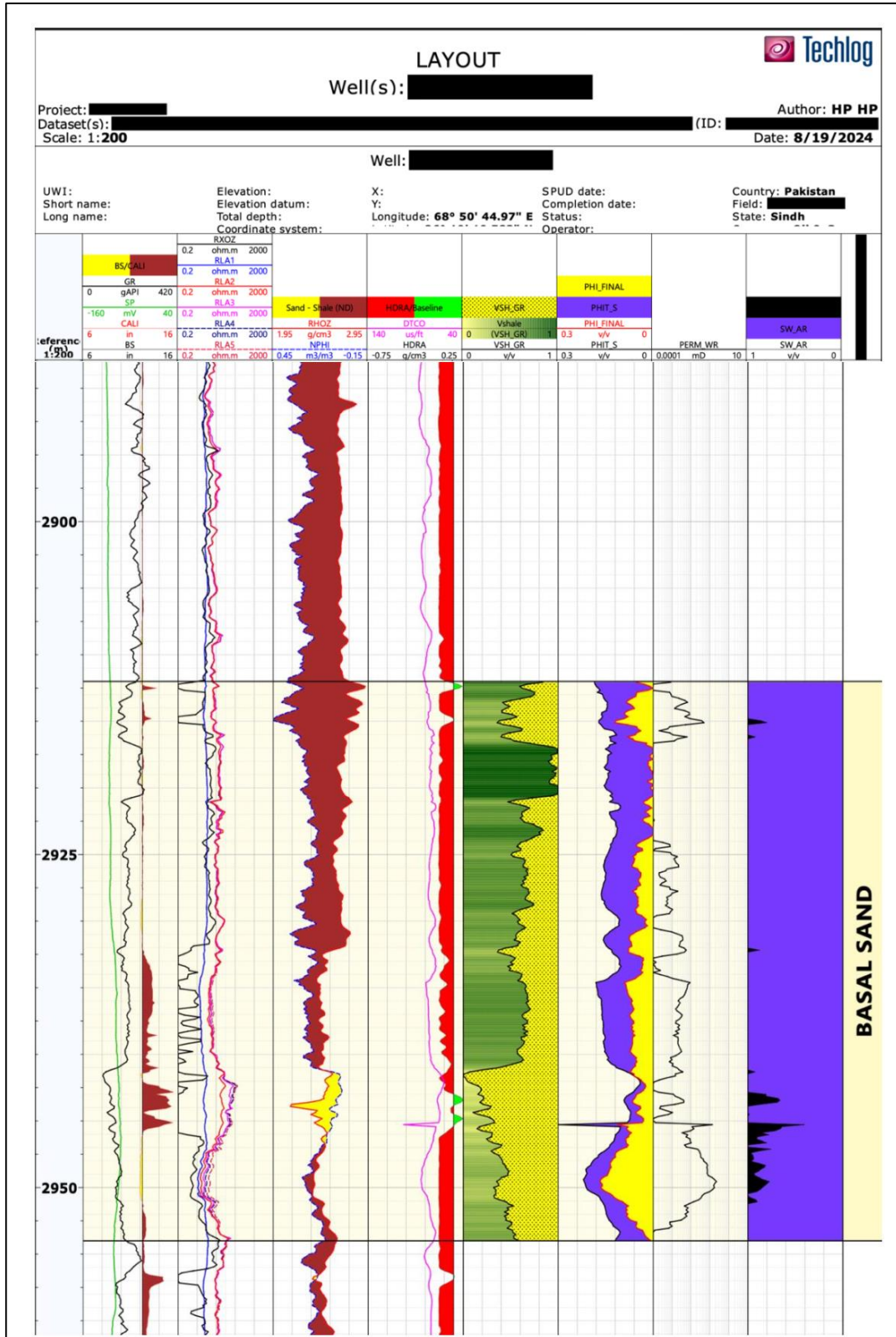


Figure 7.2 Well Log data of Well A.

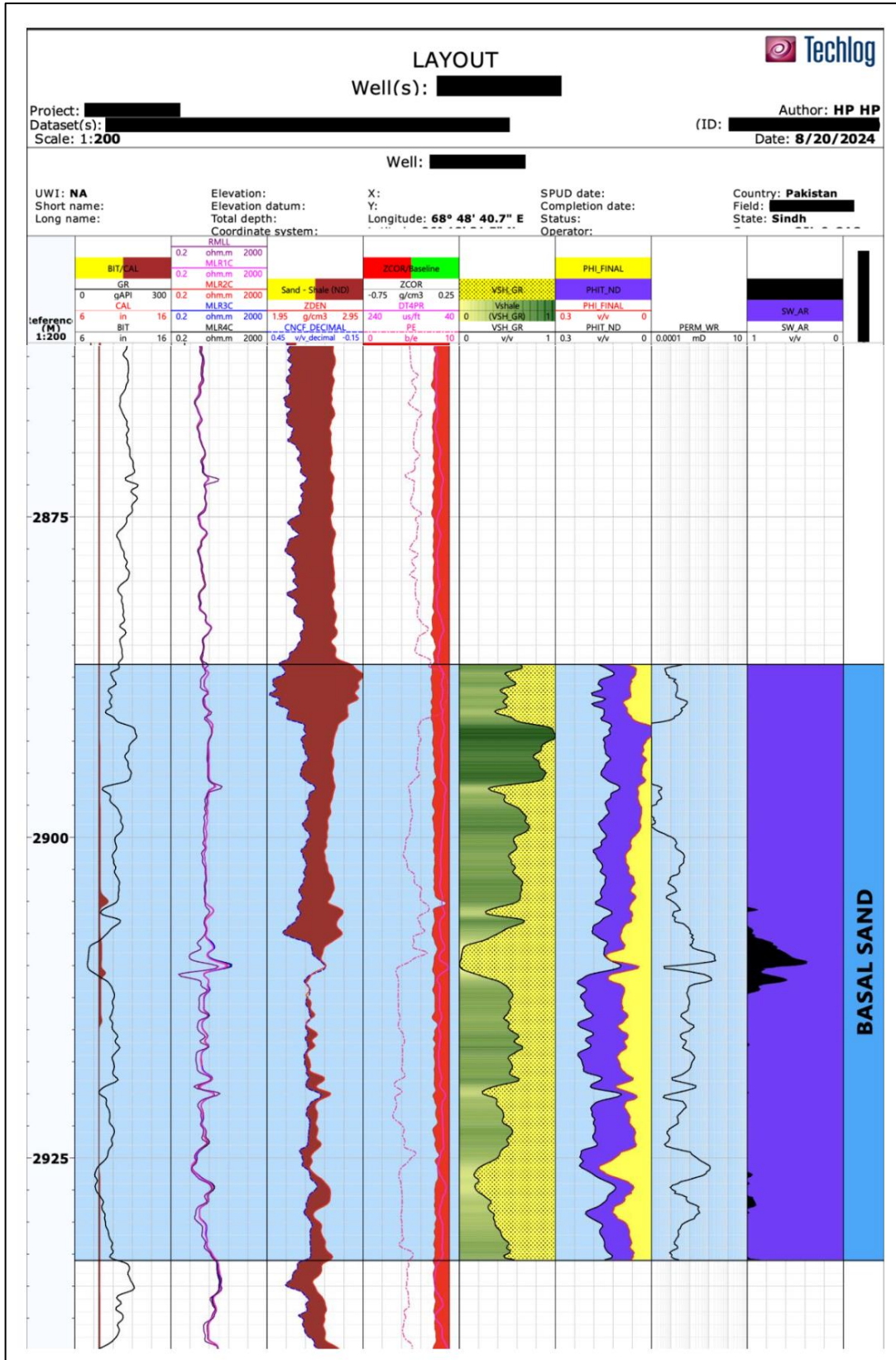


Figure 7.3 Well Log data of Well B.

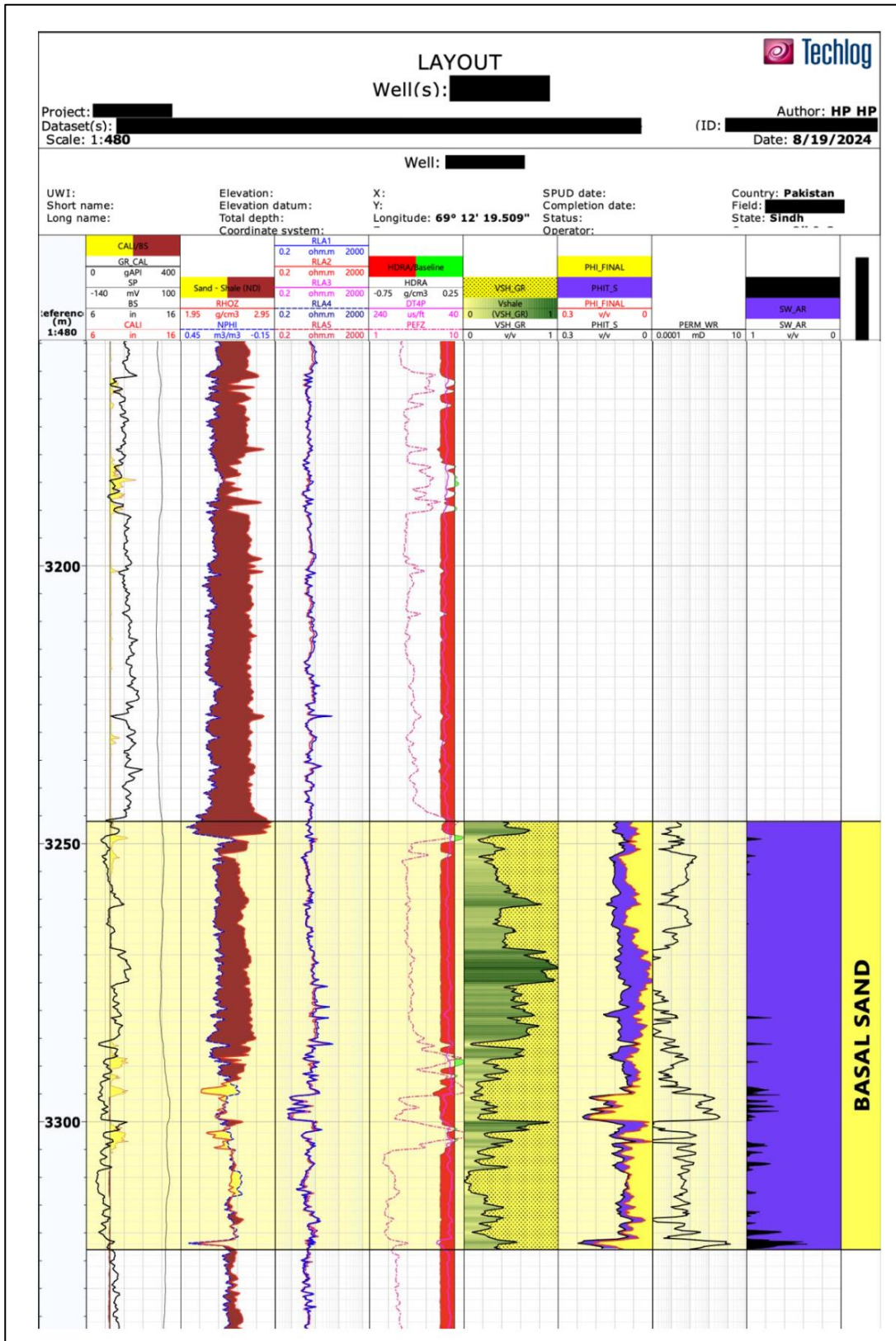


Figure 7.4 Well Log data of Well C.



### 7.3.3 Calculated Parameters

#### 7.3.3.1 Volume of shale (VSH-GR)

The volume of shale in a reservoir can be determined using a Gamma Ray (GR) log, which measures the natural radioactivity of formations. Shale, being more radioactive than other sedimentary rocks due to its clay content, produces higher GR readings. The volume of shale (Vsh) is calculated by normalizing the GR log readings between the minimum and maximum values observed in the formation. Once the IGR is obtained, it is used to estimate the volume of shale using empirical correlations such as the Larionov or Steiber methods, which are commonly applied in clastic or older formations (Ellis and Singer, 2007). The Vsh value is crucial for evaluating the net-to-gross ratio, porosity, and permeability, which are essential parameters in reservoir characterization (Schlumberger, 1991).

$$\text{IGR} = \frac{\text{GRLog} - \text{GRMin}}{\text{GRMax} - \text{GRMin}} \quad (1)$$

$$\text{Vsh} = \text{IGR} \quad (2)$$

Here,

- GRLog = Gamma ray log response in the region of concern, API units.
- GRMin = Log response in the clean sand beds, API units.
- GRMax = Log response in the shale beds, API units.
- Vsh = Volume of shale.

#### 7.3.3.2 Neutron Density porosity (PHIT-ND)

Total porosity (PHIT) can be determined using a combination of Neutron and Density logs. The Density log measures the electron density of the formation, which correlates with the bulk density, allowing for the calculation of density porosity (PHID). The Neutron log, on the other hand, measures the hydrogen content in the formation, providing a direct estimation of neutron porosity (PHIN) (Rider and

Kennedy, 2011). By cross-plotting the Neutron and Density porosities, the total porosity can be accurately estimated, considering the lithology and fluid content of the formation. The PHIT-ND is particularly effective in reducing the uncertainties associated with gas effects or lithological variations, as it compensates for the differences between the two logs (Asquith and Krygowski, 2004). The combined approach is widely used in both clastic and carbonate reservoirs to achieve a more precise evaluation of the total porosity (Schlumberger, 1989).

The total porosity using the PHIT-ND is typically calculated using the following equation:

$$\text{PHIT-ND} = \text{PHID} + \text{PHIN}/2 \quad (3)$$

Here,

PHID is the porosity derived from the Density log, calculated using the formula:

$$\text{PHID} = \rho_{ma} - \rho_b / \rho_{ma} - \rho_f \quad (4)$$

Here,

- $\rho_{ma}$  is the matrix density,
- $\rho_b$  is the bulk density from the log,
- $\rho_f$  is the fluid density.

PHIN is the porosity derived from the Neutron log, which is typically provided directly by the log, corrected for lithology and fluid content.

### 7.3.3.3 Sonic porosity (PHIT-S)

Total porosity (PHIT) can be determined using a Sonic log, which measures the travel time of acoustic waves through the formation. The travel time, known as the  $\Delta T$  or slowness, is inversely proportional to the formation's density and porosity.

To calculate total porosity from the Sonic log, the Wyllie time-average equation is commonly used:

$$\text{PHIT} - S = \frac{\Delta T_{\text{log}} - \Delta T_{\text{ma}}}{\Delta T_{\text{f}} - \Delta T_{\text{ma}}} \quad (5)$$

Here,

- $\Delta T_{\text{log}}$  = sonic log reading
- $\Delta T_{\text{ma}}$  = matrix travel time constant for sandstone
- $\Delta T_{\text{f}}$  = fluid travel time constant

#### 7.3.3.4 Average total porosity (PHIT-FINAL)

The final total porosity is typically calculated by averaging the porosity values derived from these logs, which helps mitigate the errors and uncertainties that can arise from gas effects, lithological variations, or fluid content.

The equation for the final total porosity (PHIT-FINAL) is:

$$\text{PHIT-FINAL} = \frac{(\text{PHIT-ND} + \text{PHIT-S})}{2} \quad (6)$$

Here,

- PHIT-FINAL = Average porosity
- PHIT-ND = Neutron Density Porosity
- PHIT-S = Sonic porosity

#### 7.3.3.5 Effective porosity through Neutron Density Log (PHIE-ND)

Effective porosity, which represents the interconnected pore spaces in a formation that contribute to fluid flow, can be determined using the Neutron-Density

log combination. The Neutron log measures the hydrogen content, which correlates with the presence of fluids in the pore spaces, while the Density log measures the bulk density of the formation, from which porosity can be inferred. To find effective porosity, the porosity from the Neutron log (PHIN) is first corrected for the presence of bound water and non-effective porosity (such as in clay-bound water). Similarly, the porosity from the Density log (PHID) reflects the total porosity, including non-effective components.

The effective porosity (PHIE) can be calculated using the following equation:

$$PHIE = \frac{PHIN+PHID}{2} - V_{sh} \times PH_{sh} \quad (7)$$

Here,

- PHIN is the porosity from the Neutron log,
- PHID is the porosity from the Density log,
- Vsh is the volume of shale calculated from the Gamma Ray log,
- PHsh is the assumed porosity of the shale.

#### 7.3.3.6 Effective porosity through Sonic log (PHIE-S)

Effective porosity (PHIE) can be determined using a Sonic log by analyzing the acoustic travel time through the formation, which reflects the porosity of the interconnected pore spaces that contribute to fluid flow. The Sonic log measures the interval transit time ( $\Delta t$ ) of compressional sound waves through the rock, which is influenced by the porosity and the type of fluids present in the pores. To calculate effective porosity, the Wyllie time-average equation is used, with an adjustment to account for the presence of shale or other non-effective pore spaces.

The effective porosity (PHIE) is calculated using the following equation:

$$PHIE = \frac{\Delta T_{log} - \Delta T_{ma}}{\Delta T_f - \Delta T_{ma}} - V_{sh} \times PHI_{sh} \quad (8)$$

Here,

- $\Delta T_{log}$  is the interval transit time from the Sonic log,
- $\Delta T_{ma}$  is the transit time of the rock matrix,
- $\Delta T_f$  is the transit time of the pore fluid (usually for water),
- $V_{sh}$  is the shale volume determined from the Gamma Ray log,
- $PHI_{sh}$  is the porosity associated with the shale.

### 7.3.3.7 Average Effective Porosity (PHI-FINAL)

To calculate the average effective porosity, the effective porosities from both methods are first computed and then averaged.

$$PHIE = \frac{PHIE-ND + PHIE-S}{2} \quad (9)$$

Here,

- $PHIE - ND$  = Average Neutron density effective porosity
- $PHIE - S$  = Average sonic effective porosity

### 7.3.3.8 Permeability through well regression (PERM-WR)

Permeability, a key reservoir property that indicates the ability of fluids to flow through the rock, can be estimated through well regression by correlating it with other well log-derived properties, such as porosity and water saturation. This method involves developing a statistical relationship, typically a linear or logarithmic regression model, between permeability and porosity from core data, which is then applied to well log data. The basic form of the regression equation used is:

$$K = a \times \phi^b \times SW^c \quad (10)$$

where:

- K is the permeability,
- $\phi$  is the porosity,
- a and b are regression coefficients determined through calibration with core data,
- SW is saturation of water,
- c is another regression coefficient.

### 7.3.3.9 Saturation of water (SW)

The meaning of "water saturation" describes the presence of water in pore spaces. It helps determine whether a reservoir contains hydrocarbons. A low SW value suggests a large amount of hydrocarbon in the reservoir, whereas a high SW value indicates a very small amount. The saturation of water is determined using a variety of techniques, such as the Modified Simandoux Equation, the Indonesian Equation, and Archie's Equation (Luthi et al., 2001).

Water saturation in a reservoir can be estimated using Archie's equation, a fundamental relationship in petrophysics that relates resistivity measurements to water saturation. Archie's equation is particularly useful for evaluating the volume of water in a reservoir rock by using electrical resistivity data obtained from well logs. The basic form of Archie's equation is:

$$S_w = [ (a / F_m) * (R_w / R_t) ]^{(1/n)} \quad (11)$$

where:

- $S_w$  is the water saturation,
- $R_t$  is the observed resistivity of the formation,
- $R_w$  is the resistivity of the formation water,
- F is porosity

- $m$  is the cementation exponent, which accounts for the rock's texture and structure.
- $a$  is a constant for cementation factor (often taken to be 1)
- $n$  is saturation exponent (generally 2)

Archie's equation provides a straightforward method to estimate water saturation from resistivity logs, which is essential for evaluating reservoir properties and hydrocarbon potential (Archie, 1942; Schlumberger, 1989).

#### **7.3.4 Porosity, permeability and water saturation determined through Well logs**

For each property, 30 samples were selected, with 10 samples taken from each well. In the case of water saturation, 38 samples were utilized across all three wells. The results are presented in the Appendix G and H.

#### **7.3.5 Picket plot creation**

The Picket plot is a widely used graphical tool in the petroleum and gas industry, primarily employed to evaluate the water saturation in various sections of an underground reservoir. Typically constructed using data from one or more wells, this plot visually represents the Archie equation, which is instrumental in estimating the water volume within a reservoir (Pickett et al., 1973). By plotting the relationship between formation resistivity and porosity, the Picket plot aids in determining the water saturation of the reservoir rocks.

The X-axis of the Picket plot usually represents the logarithm of porosity, while the Y-axis shows the logarithm of resistivity. This allows for the identification of trends that indicate the presence of hydrocarbons versus water in the pore spaces. The intersection and slope of the lines on the plot can reveal the water saturation, cementation exponent, and formation water resistivity, crucial parameters for reservoir characterization (Tiab and Donaldson, 2015).

The Picket plot is particularly valuable because it integrates various

petrophysical data into a single, interpretable graph, allowing geoscientists and engineers to make more informed decisions regarding reservoir management and hydrocarbon recovery. This method not only provides a clear visual representation but also enhances the understanding of complex reservoir properties, thereby facilitating the optimization of production strategies (Asquith and Krygowski, 2004).

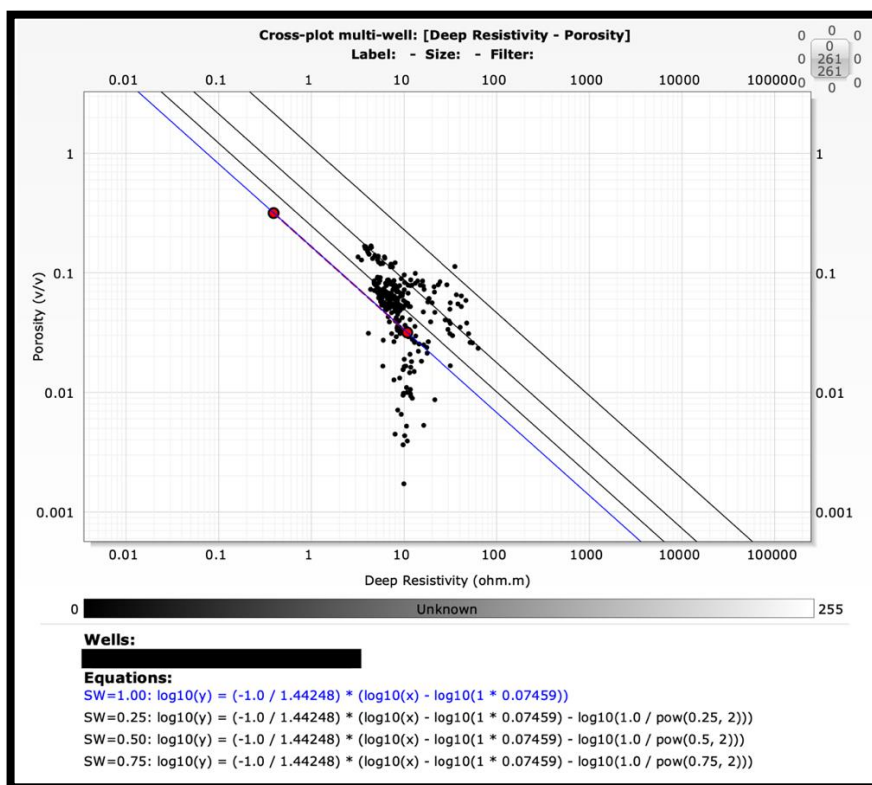


Figure 7.5 Picket Plot of Well A.

A Pickett plot, which is a graphical tool used to evaluate the water saturation (SW) in reservoir rocks. A Pickett plot typically features multiple lines, each representing different levels of water saturation within the pore space of the rock. In the context of the provided figures:

Figure 7.5 shows that the resistivity of water in Well A is 0.075 ohmmeters. Figure 7.6 indicates that the resistivity of water in Well B is 0.042 ohmmeters. Figure 7.7 reveals that the resistivity of water in Well C is 0.22 ohmmeters.



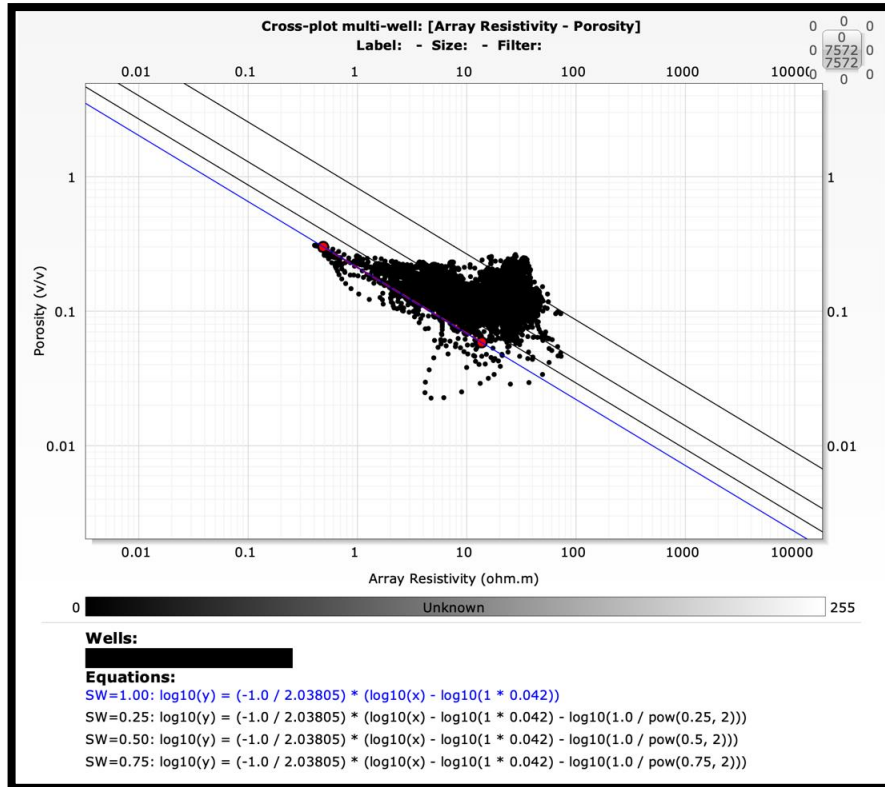


Figure 7.6 Picket Plot of Well B.

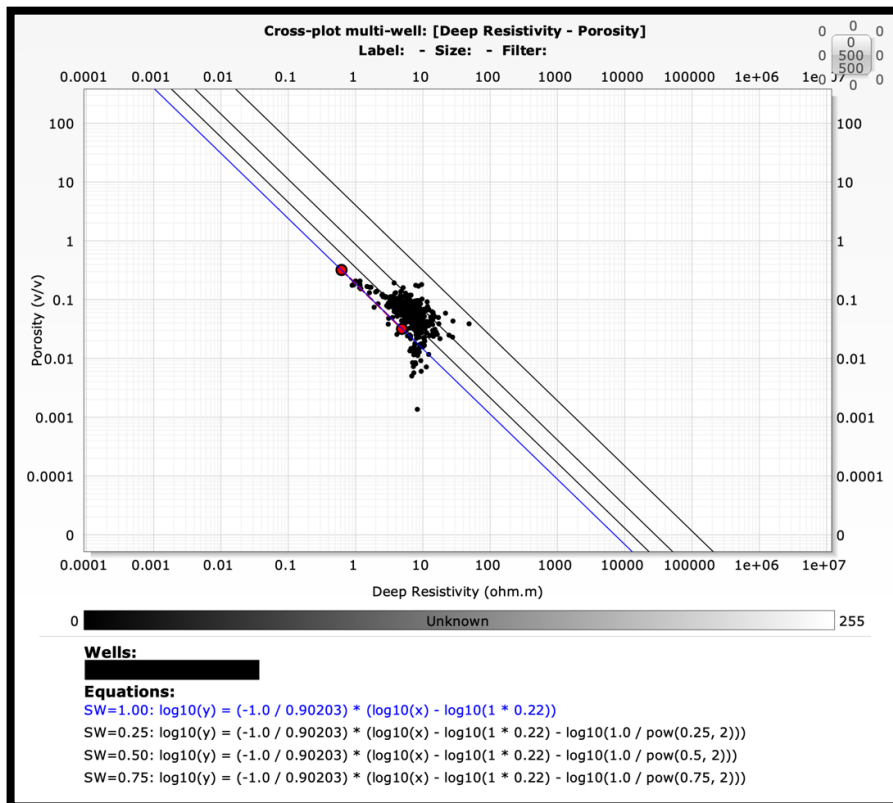


Figure 7.7 Picket Plot of Well C.

The resistivity of water varies across these wells, reflecting differences in the water's salinity or ion concentration, which impacts the overall interpretation of water saturation in the rock formations. These variations are crucial for accurately assessing reservoir characteristics and determining the potential productivity of each well.

### 7.3.6 Results

**Table 7.1** Average results from the Well log analysis.

Properties	Vsh-GR	PHIT-FINAL	PHIE-FINAL	PERM-WR (mD)	SW-AR
Average	0.3973	0.13896	0.0586	0.0064	0.9443
Average (%)	39.733%	13.896%	5.866%	----	94.43%

The well log analysis presents detailed petrophysical properties of the reservoir as shown in table 7.1. The average shale volume (Vsh) derived from gamma ray logs is 0.3973, which corresponds to 39.733% shale content in the rock formation. This high shale volume indicates a substantial presence of non-reservoir material, which can affect reservoir quality and fluid distribution (e.g., Schlumberger, 2021). The final total porosity (PHIT-FINAL) is recorded at 0.13896, or 13.896% in percentage terms. This measurement reflects the overall pore space available in the rock for fluid storage, suggesting moderate porosity within the reservoir (e.g., Asquith and Krygowski, 2004). Effective porosity (PHIE-FINAL) averages at 0.0586, translating to 5.866%. This lower value indicates the proportion of the pore space that contributes to fluid flow, highlighting potential challenges in fluid recovery (e.g., Miall, 2016). The average permeability (PERM-WR) is 0.0064 millidarcies (md), or 0.64%. This extremely low permeability suggests limited fluid flow capacity within the reservoir, which may impact hydrocarbon production efficiency (e.g., Terry and McCormick, 2022). The average water saturation (SW-AR) is 0.9443, equivalent to 94.43%, indicating that a significant majority of the pore space is occupied by water. This high water saturation is crucial for

understanding the reservoir's hydrocarbon content and guides the development strategies (e.g., Wyllie et al., 1956).

**Table 7.3** Calculated parameters from the samples through core and petrophysical Analysis.

<b>Properties</b>	<b>Vsh-GR</b>	<b>Total Porosity</b>	<b>Effective Porosity</b>	<b>Perm (md)</b>	<b>Water Saturation</b>
Through Core Analysis	-----	0.14	-----	1.491	90%
Through Petrophysical Analysis	0.3973	0.13896	0.0586	0.0064	94.43%

In table 7.3 comparison of key reservoir properties have been done derived from selected samples using core analysis and petrophysical analysis, highlighting notable differences. In core analysis, the total porosity is recorded at 0.14, permeability at 1.491 md, and water saturation at 90%. In contrast, petrophysical analysis reports a shale volume (Vsh-GR) of 0.3973, total porosity of 0.13896, effective porosity of 0.0586, permeability significantly lower at 0.0064 md, and higher water saturation of 94.43%. The disparities in permeability and water saturation suggest variability in the accuracy and resolution of each method, with core analysis generally indicating more favorable reservoir characteristics.

Overall, these results offer essential insights into the reservoir's petrophysical characteristics, guiding both exploration and production efforts. The petrophysical analysis indicates that Well A has the highest shale volume and total porosity, but all wells have very low effective porosity and permeability, suggesting limited hydrocarbon potential. Despite the high average water saturation across all three wells, there are some intervals with relatively low water saturation (~60%). These intervals are thick in Well B and C as compared to Well A. These lower water saturation intervals suggest that the formation may contain hydrocarbons; however, further analysis using advanced, high-resolution petrophysical techniques is necessary for confirmation.

## CONCLUSIONS

Based on the aforementioned findings, the study is concluded as follows:

- (1) The analysis of cores from Wells A, B, and C drilled into the Basal Sand of the Lower Goru Formation has provided a comprehensive understanding of the sedimentary and petrographic characteristics of the reservoir. The sedimentary sequence reveals a diverse range of facies, including very fine to coarse granule-sized sandstones with well-rounded mud clasts and occasional dark grey mud-drapes. Notable sedimentary structures include cross laminations, horizontal laminations, and various forms of cross bedding, alongside mud-drapes, muddy seams, and sandstone injectites. These observations indicate a shoaling-up sequence with a transgressive phase, reflecting depositional environments ranging from offshore to shoreface settings, such as wave-dominated beach or barrier bar environments. The presence of biogenic materials, including further supports a shallow marine depositional model. The reservoir exhibits significant heterogeneity due to variations in sedimentary facies, depositional environments, biogenic content, and petrographic characteristics. These variations affect reservoir quality, including porosity and permeability, leading to complex spatial distribution and challenges in hydrocarbon extraction.
- (2) Petrographic analysis highlights that the sandstones are mineralogically and texturally mature, primarily composed of medium-grained quartz with minor feldspar, lithic fragments, and accessory minerals like mica and pyrite. Calcite is the dominant cementing material, with occasional iron oxide, quartz overgrowths, and diagenetic pyrite. Visual porosity varies between 2-30%, with higher values in the upper zones and lower values in more compacted and cemented sections. The presence of texturally immature zones with increased matrix content and deformation-prone lithic fragments, along with the impact of mechanical compaction, has led to a reduction in porosity and an overall tight reservoir rock. Sorting ranges from good to fair, with some samples showing poor sorting due to coarse grains, clasts, and shell fragments.

- (3) Integration of core analysis data with petrophysical data reveals significant heterogeneity in reservoir quality. The CMS-300 horizontal core plug analysis and well log data indicate moderate porosity, with values of 14.13% and 13.896%, respectively. However, both analyses show exceptionally low permeability, with the CMS-300 reporting 1.491 millidarcies and well logs showing 0.0064 millidarcies, suggesting very restricted fluid flow. High water saturation, with values of 90% from the CMS-300 and 94.43% from well logs, further complicates hydrocarbon extraction. The high shale volume of 39.733% correlates with elevated water content, emphasizing the tight nature of the reservoir rock. These findings underline the need for enhanced recovery techniques and optimized production strategies to address the reservoir's tightness and high water saturation, aiming to improve hydrocarbon extraction and management.

## **FUTURE SUGGESTIONS**

It is recommended that future development plans incorporate a detailed reservoir characterization study, integrating both core and petrophysical data to refine the understanding of heterogeneities within the reservoir. This approach would help identify specific zones with better permeability and lower water saturation, allowing for targeted stimulation and completion strategies. By combining these insights with tailored production methods, operators can optimize hydrocarbon recovery while mitigating the challenges associated with low permeability and high water saturation in the reservoir.

## REFERENCES

- Abbas, S., Mirza, K., and Arif, S. (2015). Lower Goru formation-3D modeling and petrophysical interpretation of Sawan Gas field, Lower Indus basin, Pakistan. *The Nucleus*, 52(3), 138-145.
- Ahmed, R. (1991). Pishin Basin: Status and prospects. *Pakistan Journal of Hydrocarbon Research*, 3(1), 27-33.
- Alpay, O. A. (1972). A practical approach to defining reservoir heterogeneity. *Journal of Petroleum Technology*, 24(07), 841-848.
- Ashraf, U., Zhang, H., Anees, A., Ali, M., Zhang, X., Shakeel Abbasi, S., and Nasir Mangi, H. (2020). Controls on reservoir heterogeneity of a shallow-marine reservoir in Sawan gas field, SE Pakistan: Implications for reservoir quality prediction using acoustic impedance inversion. *Water*, 12(11), 2972.
- Asquith, G. B., and Krygowski, D. (2004). *Basic Well Log Analysis*. AAPG Methods in Exploration Series.
- Aydin, A., and Eyal, Y. (2002). Morphology and Hydromechanical Properties of Shear Faults in Sandstone. *Tectonophysics*, 357(1-4), 99-116.
- Baig, M. O., Harris, N., Ahmed, H., and Baig, M. (2016). Controls on reservoir diagenesis in the Lower Goru sandstone formation, Lower Indus Basin, Pakistan. *Journal of Petroleum Geology*, 39(1), 29-47.
- Bassiouni, Z. (1994). *Theory, Measurement, and Interpretation of Well Logs*. SPE Textbook Series, Vol. 4.
- Berger, A., Gier, S., and Krois, P. (2009). Porosity-preserving chlorite cements in shallow-marine volcanoclastic sandstones: Evidence from Cretaceous sandstones of the Sawan gas field, Pakistan. *AAPG bulletin*, 93(5), 595-615.
- Boggs Jr., S. (1991). *Principles of Sedimentology and Stratigraphy*. Prentice Hall.
- Boggs, S. (2011). *Principles of Sedimentology and Stratigraphy*. Pearson.
- Boggs, S. Jr. (1987). *Principles of Sedimentology and Stratigraphy*. Merrill Publishing Company.
- Boggs, S., Jr. (2006). *Principles of Sedimentology and Stratigraphy*. Pearson.
- Brown, A., and Wilson, R. (2017). *Gamma-Ray Logging and Core Analysis*. Geological Society Publishing House.

- Brown, A., and Wilson, R. (2017). *Petrophysical Data Calibration: Methods and Applications*. Geological Society Publishing House.
- Brown, A., Jones, R., and Wilson, R. (2017). *Gamma-Ray Spectrometry in Geological Studies*. Geological Society Publishing House.
- Buckley, J. S., Liu, Y., and Monsterleet, S. (1998). Mechanisms of Wetting Alteration Caused by Crude Oils. *SPE Journal*, 3(1), 54-61.
- Colin McPhee, Julian A. T. C. Matthews, Roy Franklin (2015). *Core Analysis: A Best Practice Guide*. 1st Edition. Elsevier.
- Doe, J. (2019). *Thorium and Potassium in Sedimentary Rocks: Analysis and Interpretation*. Springer.
- Doe, J., Smith, L., and Johnson, M. (2018). *Diagenesis in Sedimentary Rocks: Impact on Reservoir Properties*. Springer.
- Doe, J., Smith, L., and Johnson, M. (2020). *Clay-Rich and Sand-Rich Sediments: Gamma-Ray Insights*. Springer.
- Duke, W. L. (1985). Hummocky cross-stratification, tropical hurricanes, and intense winter storms. *Sedimentology*, 32(2), 167-194.
- E. Donaldson (2012). *Advanced Petrophysics*. 1st Edition. Elsevier Science.
- E. Donelson, 1994. *Saturation Concepts in Reservoir Engineering*. Society of Petroleum Engineers.
- Ellis, D. V., and Singer, J. M. (2007). *Well Logging for Earth Scientists*. Springer.
- Farooq, M., et al. (2015). Organic geochemistry and hydrocarbon potential of the Lower Goru Formation. **Marine and Petroleum Geology**, 61, 129-140.
- Frank E. Eames, 1952. A Contribution to the study of Eocene in western Pakistan and Western India: A. The Geology of standard sections in the western Punjab and in the Kohat District. *Quarterly Journal of the Geological society*, 107, 159-171.
- Friend, P. F. (1997). MIALL, AD 1996. *The Geology of Fluvial Deposits. Sedimentary Facies, Basin Analysis, and Petroleum Geology*.
- G. R. Thompson and J. Turk. (1976). *Introduction to physical Geology*. Published by Brooks Cole.

<https://geology.com/world/pakistan-satellite-image.shtml>

<https://tribune.com.pk/story/612493/tectonic-tragedy-balochistan-earthquake>



- Hussain, M., Ahmed, N., Chun, W. Y., Khalid, P., Mahmood, A., Ahmad, S. R., and Rasool, U. (2017). Reservoir characterization of basal sand zone of lower Goru Formation by petrophysical studies of geophysical logs. *Journal of the Geological Society of India*, 89(3), 331-338.
- Ilyas, M. U. (2019). Seismic interpretation and determination of hydrocarbon potential by petrophysical analysis of Bitrism field, Lower Indus Basin of Pakistan.
- Jawad A., Jan, et al. (2024) Depositional and diagenetic studies of clastic reservoirs zone in the Cretaceous Lower Goru Formation, Sindh Monocline, South Pakistan", *Journal of Earth System Science*.
- J.H. Doveton (1994). *Petrophysical Properties of Reservoir Rocks*. 1st Edition. Springer.
- Johnson, J. W. (2010). *Core Analysis: A Best Practice Guide*. Society of Petrophysicists and Well-Log Analysts.
- Johnson, L. (2015). *Reservoir Characterization Using Gamma-Ray Logs*. Elsevier.
- Johnson, L. (2016). *Advanced Petrographic Techniques in Reservoir Analysis*. Elsevier.
- Johnson, L., and Lee, M. (2018). *Subsurface Lithology and Gamma-Ray Logs*. Elsevier.
- Johnsson, M. J. (1990). Tectonic versus chemical-weathering controls on the composition of fluvial sands in tropical environments. *Sedimentology*, 37(4), 713-726.
- Jones, R. (2017). *Advanced Gamma-Ray Logging Techniques*. Wiley-Blackwell.
- Jones, R., and Brown, A. (2016). *Sedimentology and Stratigraphy*. Wiley-Blackwell.
- Jones, R., and Roberts, D. (2018). *Gamma-Ray Spectrometry in Geology: Principles and Applications*. Wiley-Blackwell.
- Jones, R.H., and Roberts, C. (2018). *Discourse Analysis: A Resource Book for Students*.
- Kadri, I.B, 1995. *Petroleum geology of Pakistan*. Karachi: Ferozsons (Pvt) Ltd.
- Kazmi, A.H, and Jan, M.Q,1997. *Geology and tectonics of Pakistan*, graphic publishers, Karachi Pakistan.

- Kazmi, A.H., and Rana, R.A. (1982). Tectonic Map of Pakistan. Geological Survey of Pakistan.
- Kemal, A. (1991). Geology and new trends for petroleum exploration in Pakistan. PAPG Bulletin, 16-57.
- Kennedy, W. J. (1967). Burrows and surface traces from the Lower Chalk of southern England. Bull. Br. Mus. nat. Hist.(Geol.), 15, 125-167.
- Khan, M. A., et al. (2007). Stratigraphy and reservoir potential of the Lower Goru Formation in the Lower Indus Basin. *Journal of Petroleum Geology*, 30(3), 241-258.
- Khan, M. J., Ali, M., and Khan, M. (2017). Gamma ray-based facies modelling of lower Goru formation: A case study in Hakeem Daho Well Lower Indus Basin Pakistan. *Bahria Univ. Res. J. Earth Sci*, 2(1), 40-45.
- Khattak, N., Akram, M., Ullah, K., Qureshi, A., and Qureshi, I. (2004). Recognition of Emplacement Timke of Jambil Carbonatities from Nw Pakistan-Constraints from Fission-Track Dating of Apatite Using Age Standard Approach (The S Method). *Journal of Himalayan Earth Sciences*, 37.
- Knaust, D. (2017). Atlas of trace fossils in well core: appearance, taxonomy and interpretation. Springer.
- Knaust, D. (2018). The ichnogenus *Teichichnus* Seilacher, 1955. *Earth-Science Reviews*, 177, 386-403.
- Knaust, D., and Bromley, R. G. (2012). Trace fossils as indicators of sedimentary environments. Newnes.
- Lake, L. W. (2010). Enhanced Oil Recovery. Society of Petroleum Engineers.
- Malkani, M. S., and Mahmood, Z. (2016). Revised stratigraphy of Pakistan. Geological Survey of Pakistan, Record, 127, 1-87.
- Mark R. Curtis (2015). Applied Petrophysics. 1st Edition. Elsevier Science.
- Matsumoto, R., and Iijima, A. (1981). Origin and diagenetic evolution of Ca–Mg–Fe carbonates in some coalfields of Japan. *Sedimentology*, 28(2), 239-259.
- Miall, A. D. (1977). Lithofacies types and vertical profile models in braided river deposits: a summary.

- Miall, A. D. (2006). Reconstructing the architecture and sequence stratigraphy of the preserved fluvial record as a tool for reservoir development: A reality check. AAPG bulletin, 90(7), 989-1002.
- Miall, A. D. (2010). *The Geology of Stratigraphic Sequences*. Springer.
- Miall, A. D. (2016). *Sedimentary Rocks in the Field*. Springer.
- Miller, J. (2016). *Advanced Techniques in Gamma-Ray Logging*. CRC Press.
- Miller, J., and Thompson, H. (2016). *Core Analysis and Gamma-Ray Log Interpretation*. CRC Press.
- Miller, J., Roberts, D., and Green, P. (2018). *Core Analysis and Reservoir Characterization*. CRC Press.
- Mohsin, S. I., Minhas, M. S. T., and Rafi, S. (2010). Diagenesis of basal sands of the cretaceous lower goru formation of the Badin Area, Sindh, Pakistan. *Pakistan Journal of Hydrocarbon Research*, 20, 27-35.
- Molnar, P., and Tapponnier, P. (1975). Cenozoic tectonics of Asia: effects of a continental collision. *science*, 189(4201), 419-426.
- Morad, S., Ketzer, J., and De Ros, L. F. (2000). Spatial and temporal distribution of diagenetic alterations in siliciclastic rocks: implications for mass transfer in sedimentary basins. *Sedimentology*, 47, 95-120.
- Munir, K., Iqbal, M. A., Farid, A., and Shabih, S. M. (2011). Mapping the productive sands of Lower Goru Formation by using seismic stratigraphy and rock physical studies in Sawan area, southern Pakistan: a case study. *Journal of Petroleum Exploration and Production Technology*, 1(1), 33-42.
- Nichols, G. (2009). *Sedimentology and stratigraphy*. John Wiley and Sons.
- Oldham, R. D. (1892). Report on the geology of Thal Chotiali and part of the Mari Country. Geological Survey of India.
- Pemberton, S. G. (2012). Murray K. Gingras, James A. MacEachern, Shahin E. Dashtgard, John-Paul Zonneveld, Jesse Schoengut, Michael J. Ranger.
- Pemberton, S. G., and Frey, R. W. (1982). Trace fossil nomenclature and the Planolites-Palaeophycus dilemma. *Journal of Paleontology*, 843-881.
- Pickett, G. R., et al. (1973). *The Use of the Archie Equation in Well Log Analysis*. Petroleum Engineer International.
- Powell, C. M. (1979). A speculative tectonic history of Pakistan and surroundings. *Geodynamics of Pakistan*.

- Quadri, V.-u.-N., and Shuaib, S. (1986). Hydrocarbon prospects of southern Indus basin, Pakistan. AAPG bulletin, 70(6), 730-747.
- Raza, H., and Ahmed, R. (1990). Hydrocarbon potential of Pakistan. Journal of Canada Pakistan Cooperation, 4(1), 9-27.
- Reading, H. G. (2009). Sedimentary Environments: Processes, Facies, and Stratigraphy. Wiley-Blackwell.
- Reinson, G.E. (1984). Barrier Island and Associated Strand-Plain Systems. In R.G. Walker (Ed.), Facies Models (pp. 119-140). Geological Association of Canada.
- Rider, M. H., and Kennedy, M. (2011). The Geological Interpretation of Well Logs. Rider-French Consulting Ltd.
- Robert F. (Bob) Mitchell, 2009. Advanced Core Analysis in Petroleum Reservoirs. Elsevier
- Roberts, D., and Green, P. (2019). Reservoir Quality Assessment: A Petrographic Perspective. AAPG Memoir.
- Roberts, D., Green, P., and Brown, A. (2018). Geological Structure and Lithology through Gamma-Ray Spectrometry. AAPG Memoir.
- S. T. Imoize, N. H. Al-Kaabi, R. M. Alhassan, 2021. Petrophysical Analysis Techniques. Springer
- Sahito, A. G., Solangi, S. H., Usmani, P., Brohi, I. A., Napar, L. D., and Khokhar, Q. (2013). Sedimentologic studies of Upper sands of Lower Goru Formation based on well cuttings and wireline logs from wells of X Field in the subsurface of Sindh Monocline, Southern Indus Basin, Pakistan. Sindh University Research Journal-SURJ (Science Series), 45(2).
- Sarah, et al. (2015). Advanced Petrophysical Techniques in Hydrocarbon Reservoir Characterization. Petroleum Geoscience, 21(2), 123-136.
- Schlumberger. (1989). Log Interpretation Charts. Schlumberger Educational Services.
- Schlumberger. (1991). Log Interpretation Principles/Applications.
- Schlumberger. (2018). Log Interpretation Charts. Schlumberger Limited.
- Schlumberger. (2021). Log Interpretation Principles/Application. Schlumberger Educational Services.

- Schön, J. H. (2015). *Physical Properties of Rocks: A Workbook*. 2nd Edition. Elsevier.
- Searle, M. (1983). Stratigraphy, structure and evolution of the Tibetan–Tethys zone in Zaskar and the Indus suture zone in the Ladakh Himalaya. *Earth and Environmental Science Transactions of the Royal Society of Edinburgh*, 73(4), 205-219.
- Serra, O. (1984). *Fundamentals of Well-Log Interpretation*. Elsevier.
- Shah, S. (2009). Stratigraphy of Pakistan (memoirs of the geological survey of Pakistan). *The Geological Survey of Pakistan*, 22.
- Shenglai Yang (2017). *Fundamentals of Petrophysics*. 1st Edition. Elsevier
- Siddiqui, N. K. (2004). Sui Main Limestone: Regional geology and the analysis of original pressures of a closed-system reservoir in central Pakistan. *AAPG bulletin*, 88(7), 1007-1035.
- Siyar, S. M., Waqas, M., Mehmood, S., Jan, A., Awais, M., and Islam, F. (2017). Petrophysical characteristics of lower Goru formation (Cretaceous) in Sawan gas field, central Indus basin, Pakistan. *Journal of Biodiversity and Environmental Sciences (JBES)*, 10(5), 260-266.
- Smith, L., Johnson, M., and Lee, K. (2020). *Fundamentals of Gamma-Ray Spectrometry*. Academic Press.
- Smith, L., Jones, R., and Brown, A. (2017). *Fundamentals of Petrographic Analysis*. Academic Press.
- Smith, L., Jones, R., and Brown, A. (2019). *Fundamentals of Gamma-Ray Logging*. Academic Press.
- Solangi, S. H., Nazeer, A., Abbasi, S. A., Napar, L. D., Usmani, P. A., and Sahito, A. G. (2016). Sedimentology and petrographic study of b-sand of upper sands of lower Goru formation, based well cuttings and wire line logs from wells of southern Sindh monocline, lower Indus basin, Pakistan. *Bahria Uni Res. J. of Earth Sci*, 1(1).
- Suttner, L. J. (1974). *Sedimentary petrographic provinces: an evaluation*.
- Tarek Ahmed (2010), *Reservoir Engineering Handbook*. Gulf Professional Publishing, 4th Edition.

- Terry, R. D., and McCormick, C. R. (2022). Permeability and its relationship to fluid flow in petroleum reservoirs. *Journal of Petroleum Technology*, 74(3), 55-65.
- Tiab, D., and Donaldson, E. C. (2012). **Petrophysics: Theory and Practice of Measuring Reservoir Rock and Fluid Transport Properties**. Gulf Professional Publishing.
- Tiab, D., and Donaldson, E. C. (2015). *Petrophysics: Theory and Practice of Measuring Reservoir Rock and Fluid Transport Properties*. Gulf Professional Publishing.
- Tucker, M. E., and Wright, V. P. (2009). *Carbonate sedimentology*. John Wiley and Sons.
- Walker, R. G., and James, N. P. (1992). *Facies Models: Response to Sea Level Change*. Geological Association of Canada.
- Weber, K. (1982). Influence of common sedimentary structures on fluid flow in reservoir models. *Journal of Petroleum Technology*, 34(03), 665-672.
- Wells, N. A., and Gingerich, P. D. (1987). Paleoenvironmental interpretation of Paleogene strata near Kotli, Azad Kashmir, Northeastern Pakistan. *Kashmir Journal of Geology*, 5, 23-41.
- Wetzel, A. (1984). Bioturbation in deep-sea fine-grained sediments: influence of sediment texture, turbidite frequency and rates of environmental change. *Geological Society, London, Special Publications*, 15(1), 595-608.
- Williams, M. (1959). 19. Stratigraphy of the Lower Indus Basin, West Pakistan. 5th World petroleum congress.
- Wilson, R. (2015). *Thin Section Microscopy: Techniques and Applications*. Cambridge University Press.
- Wilson, R., and Green, P. (2015). *Gamma-Ray Logging and Lithological Analysis*. Cambridge University Press.
- Wyllie, M. R. J., Gregory, A. R., and Gardner, L. W. (1956). Elastic Wave Velocities in Heterogeneous and Porous Media. *Geophysics*, 21(1), 41-70.
- Zaigham, N. A., and Mallick, K. A. (2000). Regional framework and hydrocarbon prospects of Pakistan. **Journal of Asian Earth Sciences**, 18(3), 749-753.

## APPENDIX A

Table Showing Spectral Gamma Ray report of samples from Core 1 Well A.

Sample Name	K (%)	U (ppm)	Th (ppm)	Total (gAPI)	Total (gAPI-U)
Sample no.1	2.72	1.3	5.8	52.2	43.8
Sample no.2	2.58	0	6.2	31.3	43.3
Sample no.3	0	1.9	0	4.4	0
Sample no.4	0.6	0	7.1	16.7	24.5
Sample no.5	2.51	2.8	6.5	61.7	43.1
Sample no.6	1.52	0.9	4.3	33.2	27.2
Sample no.7	3.81	3	4.4	72	51.6
Sample no.8	6.93	2.1	3.4	96.6	82.5
Sample no.9	1.33	0	12.4	44.1	45.7
Sample no.10	10.12	2.2	1.5	126.4	111.7
Sample no.11	6.11	2.7	2.3	88.8	70.9
Sample no.12	6.42	0	12.7	96.4	100.8
Sample no.13	4.01	0.1	11.6	73.1	72.3
Sample no.14	7.09	0.2	11.8	107.1	105.6
Sample no.15	9.91	2.4	15.8	161.8	145.9
Sample no.16	5.1	0	13.2	83.6	87.8
Sample no.17	7.11	2.4	3.8	101.3	85.3

Sample no.18	11.46	1.2	6.2	146.1	137.8
Sample no.19	9.69	0.7	7.7	127.1	122.7
Sample no.20	7.65	0.3	7.9	103.6	101.7
Sample no.21	10.49	0.5	8.1	135.8	132.5
Sample no.22	4.42	0.2	13	81.8	80.1
Sample no.23	7.39	2.8	4.9	109.7	91.2
Sample no.24	11.91	2.1	0.4	142.1	127.7
Sample no.25	12.56	0	10.9	160.2	161.5
Sample no.26	10.56	2.8	10.6	158.3	139.6
Sample no.27	10.05	0	12.9	137.3	139.8
Sample no.28	8.71	1.8	7.7	124.2	112.4
Sample no.29	11.91	0.4	11.5	159.2	156.3
Sample no.30	3.85	1.5	0	44.4	34.2
Sample no.31	0	1.9	0	7	0



## APPENDIX B

Table Showing Spectral Gamma Ray report of samples from Core 2 Well B.

Sample Name	K (%)	U (ppm)	Th (ppm)	Total (gAPI)	Total (gAPI-U)
Sample no.1	18.33	1.1	5.7	217.5	209.8
Sample no.2	16.27	0	12	200.2	203.9
Sample no.3	18.33	3.3	2.7	224.3	202.3
Sample no.4	8.47	6.5	20.6	186.3	142.7
Sample no.5	11.28	4.7	7.9	172.2	140.4
Sample no.6	11.12	1.1	13.2	159.5	152
Sample no.7	12.68	1.1	9.1	165.8	158.3
Sample no.8	17.57	1.9	8.6	221.8	209.2
Sample no.9	16.23	0.3	10.9	202.5	200.6
Sample no.10	16.71	0.7	9.3	206.5	201.6
Sample no.11	13.99	1.5	8.5	180.8	170.6
Sample no.12	10.68	2	21.2	181.2	167.6
Sample no.13	11.45	5.3	12.9	190.5	154.7
Sample no.14	1.39	4.4	7.5	63.4	34
Sample no.15	4.14	0.9	11.5	79.2	73.4
Sample no.16	3.94	0	5.9	46.2	56.9
Sample no.17	17.75	0	0	183.3	187

Sample no.18	4.83	1.7	11.5	92.1	80.7
Sample no.19	11.28	2	0.2	134	120.6
Sample no.20	11.56	2.9	4.9	154.7	135.5
Sample no.21	9.71	0.9	13.6	143.8	138
Sample no.22	9.52	5	5.4	149.1	115.3
Sample no.23	11.39	1.4	6.6	147.1	138.1
Sample no.24	8.96	2.3	8.1	131.3	116.1
Sample no.25	12.7	1.1	11.2	171	163.9
Sample no.26	20.61	4.3	0	239.8	210.8
Sample no.27	12.39	0.9	4.9	150.3	144.5
Sample no.28	13.86	0.8	4.6	164.9	159.3
Sample no.29	14.51	0	7.4	166.7	173.5

### APPENDIX C

Table Showing Spectral Gamma Ray report of samples from Core 3 Well C.

Sample Name	K (%)	U (ppm)	Th (ppm)	Total (gAPI)	Total (gAPI-U)
Sample no.1	0.99	4.6	5.1	54.3	23.5
Sample no.2	0	0	0	0	0
Sample no.3	1.94	0	8.8	43	43
Sample no.4	4.55	1.4	7.5	76.8	67.6
Sample no.5	2.33	13.5	5.2	128.3	38.1
Sample no.6	1.12	0	3.9	21.9	21.9
Sample no.7	1.02	0	0.4	11.9	11.9
Sample no.8	0	0.4	0.1	2.9	0.3
Sample no.9	0	4	0	26.6	0
Sample no.10	0.36	0	0	3.9	3.9
Sample no.11	0.83	0	0	8.8	8.8
Sample no.12	0	0.3	0	1.7	0
Sample no.13	0	1.5	0.5	11	1.2
Sample no.14	0.05	0	0	0.6	0.6
Sample no.15	0.37	0	0.1	4.1	4.1
Sample no.16	0	0	0.1	0.3	0.3
Sample no.17	0.02	0	3.1	8.2	8.2
Sample no.18	0	0	1	2.7	2.7

Sample no.19	0.48	0	1.4	8.8	8.8
Sample no.20	0.32	0.1	0.2	4.4	3.8
Sample no.21	0	1.6	0.5	12.2	1.4
Sample no.22	0.92	3.4	1.7	36.6	14.1
Sample no.23	0.53	0	0.7	7.4	7.4
Sample no.24	1.57	2.9	8.6	58.2	38.7
Sample no.25	1.16	1.3	3.5	30.2	21.2
Sample no.26	1.7	5.3	0.4	54.6	19.2
Sample no.27	2.26	0.8	1.2	32.3	27.1
Sample no.28	1.91	0	8.7	42.6	42.6
Sample no.29	3.35	0	4.4	46.8	46.8
Sample no.30	2.05	7.7	0	73.2	21.8
Sample no.31	3.23	0	13.1	67.9	67.9

## APPENDIX D

Table Showing CMS 300-Horizontal Core Plug Analysis result for Porosity.

Sample I.D.	Weight (g)	Grain Volume (cc)	Bulk Volume (cc)	Requested Overburden (psi)	Act Overbur. During Pore Vol (psi)	Pore Volume (cc)	Bulk Density (g/cc)	Grain Density gm/cc	Porosity (%)
1057	45.05	16.98	18.35	1000	943	1.36	2.46	2.65	7.46
1057A	43.56	16.52	18.15	1000	953	1.62	2.40	2.64	8.96
1057B	46.09	17.66	18.40	1000	968	0.74	2.50	2.61	4.03
1057D	41.25	15.81	18.30	1000	1066	2.48	2.25	2.61	13.58
1057E	45.23	16.23	18.25	1000	1066	2.02	2.48	2.79	11.07
1057F	41.72	16.15	18.44	1000	959	2.29	2.26	2.58	12.42
1057G	40.39	15.39	18.40	1000	1043	3.00	2.20	2.62	16.34
1057H	42.16	16.13	18.30	1000	922	2.17	2.30	2.61	11.86
1057I	46.42	17.50	18.45	1000	1048	0.94	2.52	2.65	5.12
1057J	40.72	15.28	18.01	1000	950	2.72	2.26	2.66	15.13
1057K	39.36	15.20	18.40	1000	920	3.20	2.14	2.59	17.4
1057L	30.57	11.74	14.02	1000	953	2.27	2.18	2.60	16.23
1057M	42.32	15.92	18.30	1000	916	2.37	2.31	2.66	12.98
1057N	39.67	15.00	18.30	1000	947	3.30	2.17	2.65	18.05
1057O	37.89	14.70	18.45	1000	913	3.75	2.05	2.58	20.33
1057P	38.55	14.98	18.45	1000	938	3.46	2.09	2.57	18.78

1057Q	39.95	15.13	18.25	1000	919	3.11	2.19	2.64	17.07
1057R	29.75	11.08	14.18	1000	1030	3.10	2.10	2.69	21.86
1057S	39.22	15.01	18.45	1000	938	3.43	2.13	2.61	18.63
1057T	42.46	16.08	18.40	1000	911	2.32	2.31	2.64	12.62
1057U	41.54	15.68	18.25	1000	976	2.56	2.28	2.65	14.06
1057V	40.03	15.30	18.40	1000	1021	3.10	2.18	2.62	16.85
1057W	30.08	11.73	14.39	1000	1025	2.65	2.09	2.56	18.45
1057X	41.67	15.86	18.50	1000	1019	2.64	2.25	2.63	14.28
1057Y	40.67	15.54	18.50	1000	1010	2.95	2.20	2.62	15.97
1057Z	41.71	15.91	18.45	1000	1018	2.54	2.26	2.62	13.77
1057A-1	42.45	15.76	18.35	1000	1010	2.59	2.31	2.69	14.11
1057B-1	44.26	16.64	18.45	1000	1000	1.81	2.41	2.66	9.83
1057C-1	42.69	16.19	18.50	1000	996	2.31	2.31	2.64	12.49

### APPENDIX E

Table showing CMS 300-Horizontal Core Plug Analysis result for Permeability.

Sample I.D.	Requested Overburden (psi)	Act Overbur. During Pore Vol (psi)	Air Perm (md)	Klinkenberg (Perm md)	b psi	beta 1/ft	alpha microns
1057	1000	943	6.49E-02	0.0419	4.23E+01	3.08E+13	4.18E+03
1057A	1000	953	2.34E-01	0.165	2.92E+01	6.60E+11	3.53E+02
1057B	1000	968	2.42E+00	2.07	1.00E+01	1.21E+11	8.09E+02
1057D	1000	1066	2.77E-01	0.182	3.67E+01	2.32E+12	1.37E+03
1057E	1000	1066	4.29E-01	0.311	2.56E+01	3.84E+11	3.86E+02
1057F	1000	959	2.12E-01	0.136	3.95E+01	1.93E+12	8.49E+02
1057G	1000	1043	1.66E+00	1.36	1.32E+01	2.37E+10	1.05E+02
1057H	1000	922	1.27E-01	0.0766	4.83E+01	1.27E+13	3.16E+03
1057I	1000	1048	2.59E-02	0.0145	6.48E+01	4.65E+14	2.19E+04
1057J	1000	950	2.64E-01	0.17	3.85E+01	1.60E+12	8.85E+02
1057K	1000	920	2.03E+00	1.9	4.02E+00	1.14E+11	2.03E+02
1057L	1000	953	6.43E+00	6.14	2.64E+00	5.66E+09	1.13E+02
1057M	1000	916	9.79E-02	0.0786	1.81E+01	8.24E+13	2.10E+04
1057N	1000	947	6.01E+00	5.5	5.22E+00	6.59E+09	1.17E+02
1057O	1000	913	7.80E+00	7.47	2.44E+00	4.85E+09	1.17E+02

1057P	1000	938	7.99E+00	7.59	2.94E+00	2.87E+09	7.06E+01
1057Q	1000	919	3.91E-01	0.257	2.78E+01	5.17E+11	4.30E+02
1057R	1000	1030	2.58E-01	0.178	3.17E+01	5.33E+10	3.06E+01
1057S	1000	938	3.14E+00	2.8	7.04E+00	2.28E+10	2.07E+02
1057T	1000	911	6.07E-02	0.0332	6.47E+01	1.71E+14	1.84E+04
1057U	1000	976	7.60E-02	0.0422	6.17E+01	2.26E+13	3.09E+03
1057V	1000	1021	4.97E-01	0.365	2.41E+01	2.99E+11	3.54E+02
1057W	1000	1025	6.25E+00	5.76	4.85E+00	4.68E+09	8.71E+01
1057X	1000	1019	1.48E-01	0.0983	3.69E+01	2.46E+12	7.83E+02
1057Y	1000	1010	2.78E-01	0.193	3.08E+01	8.05E+11	5.02E+02
1057Z	1000	1018	2.61E-01	0.219	1.30E+01	1.95E+11	1.38E+02
1057A-1	1000	1010	8.62E-02	0.0486	5.90E+01	1.26E+13	1.98E+03
1057B-1	1000	1000	4.13E-02	0.0223	6.83+01	5.00E+14	3.61E+04
1057C-1	1000	996	6.87E-02	3.82E-02	6.18E+01	5.99E+13	7.42E+03



### APPENDIX F

Table showing CMS 300-Horizontal Core Plug Analysis result for Water Saturation.

S/NO.	WEIGHT OF CRUSIBLE (g)	WT. OF CRUS+ SAMPLE (g)	WT. OF CRUS+ SAMPLE A(Ext.) (g)	TOTAL FLUID (ml)	WATER REC. (ml)	H.C REC. (ml)
1	83.32	107.31	106.29	1.02	1.00	0.02
2	62.06	94.51	93.02	1.49	1.30	0.19
3	87.07	108.57	107.58	0.99	0.80	0.19
4	61.31	95.45	94.88	0.57	0.50	0.07
5	82.09	102.65	101.89	0.76	0.60	0.16
6	82.22	111.23	110.47	0.76	0.20	0.56
7	61.79	82.75	82.00	0.75	0.70	0.05
8	86.40	109.41	108.62	0.79	0.60	0.19
9	82.99	115.55	114.70	0.85	0.80	0.05
10	92.40	132.12	130.66	1.46	1.40	0.06
11	62.76	89.57	88.52	1.05	0.80	0.25
12	65.51	106.57	105.21	1.36	1.20	0.16
13	86.66	112.50	111.67	0.83	0.30	0.53
14	61.61	95.32	94.18	1.14	0.90	0.24
15	61.86	84.75	84.08	0.67	0.60	0.07
16	86.53	107.13	106.44	0.69	0.30	0.39

17	83.94	116.34	115.35	0.99	0.60	0.39
18	62.57	96.66	95.47	1.19	0.80	0.39
19	82.63	115.00	113.72	1.28	1.00	0.28
20	84.35	121.02	119.93	1.09	0.90	0.19
21	84.05	118.78	117.25	1.53	1.20	0.33
22	86.09	117.68	116.28	1.40	1.20	0.20
23	84.01	103.18	102.28	0.90	0.80	0.10
24	82.57	131.27	129.03	2.24	1.90	0.34
25	61.31	84.96	83.94	1.02	0.90	0.12
26	83.26	103.61	102.79	0.82	0.60	0.22
27	86.32	111.77	110.79	0.98	0.80	0.18
28	85.83	113.80	112.74	1.06	0.90	0.16
29	86.70	112.67	112.36	0.31	0.20	0.11
30	83.25	103.32	102.31	1.01	0.80	0.21
31	66.17	96.51	95.96	0.55	0.20	0.35
32	62.05	98.50	95.28	3.22	1.50	1.72
33	61.35	97.98	96.37	1.61	1.30	0.31
34	61.99	111.08	107.72	3.36	1.20	2.16
35	62.42	95.08	93.26	1.82	1.40	0.42
36	65.37	115.69	113.52	2.17	1.50	0.67
37	65.85	108.22	106.18	2.04	1.70	0.34
38	62.58	86.06	84.99	1.07	0.70	0.37

### APPENDIX G

Table showing results of estimated porosity and permeability through Well logs.

Sample	VSH_ GR	PHIT_ ND	PHIT_ _S	PHIT_FIN AL	PHIE_ ND	PHIE_ _S	PHI_FIN AL	PERM_ WR
no.	v/v	v/v	v/v	v/v	v/v	v/v	v/v	mD
1	0.62	0.19	0.162	0.176	0.099	0.074	0.074	0.003515
2	0.65	0.216	0.161	0.188	0.12	0.068	0.068	0.002478
3	0.62	0.204	0.157	0.18	0.112	0.068	0.068	0.002526
4	0.65	0.206	0.157	0.181	0.11	0.064	0.064	0.001955
5	0.68	0.207	0.158	0.182	0.107	0.061	0.061	0.001510
6	0.68	0.186	0.153	0.17	0.086	0.057	0.057	0.001156
7	0.61	0.197	0.152	0.174	0.107	0.065	0.065	0.002035
8	0.62	0.186	0.155	0.17	0.095	0.066	0.066	0.002218
9	0.57	0.188	0.153	0.171	0.104	0.072	0.072	0.003233
10	0.57	0.206	0.148	0.177	0.121	0.067	0.067	0.002308
11	0.62	0.21	0.141	0.176	0.119	0.053	0.053	0.000820
12	0.61	0.186	0.138	0.162	0.096	0.051	0.051	0.000717
13	0.53	0.19	0.132	0.161	0.112	0.057	0.057	0.001104
14	0.37	0.193	0.116	0.154	0.139	0.063	0.063	0.001797
15	0.03	0.094	0.044	0.069	0.089	0.039	0.039	0.000208
16	0.05	0.093	0.041	0.067	0.085	0.033	0.033	0.000109
17	0.16	0.072	0.046	0.059	0.048	0.023	0.023	0.000022

18	0.19	0.078	0.053	0.065	0.05	0.026	0.026	0.000037
19	0.18	0.084	0.063	0.074	0.058	0.038	0.038	0.000190
20	0.15	0.086	0.074	0.08	0.063	0.052	0.052	0.001160
21	0.21	0.1	0.084	0.092	0.07	0.055	0.055	0.001454
22	0.2	0.126	0.092	0.109	0.096	0.064	0.064	0.004246
23	0.28	0.22	0.079	0.149	0.178	0.039	0.039	0.000222
24	0.1	0.146	0.071	0.108	0.131	0.056	0.056	0.001040
25	0.3	0.128	0.073	0.101	0.084	0.031	0.031	0.000077
26	0.26	0.15	0.355	0.252	0.112	0.318	0.112	0.136105
27	0.31	0.121	0.112	0.117	0.076	0.069	0.069	0.003466
28	0.3	0.127	0.119	0.123	0.083	0.076	0.076	0.006763
29	0.41	0.143	0.136	0.14	0.083	0.078	0.078	0.004649
30	0.39	0.146	0.138	0.142	0.089	0.083	0.083	0.005877

**APPENDIX H**

Table showing results of estimated Saturation of Water (Archie's Equation) through Well logs.

Sample	SW_AR
no.	v/v
1	1
2	1
3	1
4	0.94
5	0.809
6	0.841
7	0.782
8	0.896
9	1
10	1
11	1
12	1
13	1
14	0.913
15	0.832
16	0.944
17	0.966

18	0.962
19	0.973
20	1
21	1
22	1
23	1
24	1
25	1
26	1
27	0.822
28	0.749
29	0.77
30	0.84
31	0.986
32	0.972
33	1
34	1
35	0.932
36	0.956
37	1
38	1

## ORIGINALITY REPORT

---

10%

SIMILARITY INDEX

4%

INTERNET SOURCES

7%

PUBLICATIONS

3%

STUDENT PAPERS

---

## PRIMARY SOURCES

---

**1** Submitted to Higher Education Commission Pakistan 1%  
Student Paper

---

**2** Dirk Knaust. "Atlas of Trace Fossils in Well Core", Springer Nature, 2017 1%  
Publication

---

**3** Jawad Ahmed Jan, Mumtaz Muhammad Shah, Hamad ur Rahim, Shahid Iqbal, Samina Jahandad, Muhammad Jamil, Rayan Khalil, Yawar Amin. "Depositional and diagenetic studies of clastic reservoirs zone in the Cretaceous Lower Goru Formation, Sindh Monocline, South Pakistan", Journal of Earth System Science, 2024 1%  
Publication

---

**4** Submitted to Asia Pacific University College of Technology and Innovation (UCTI) <1%  
Student Paper

---

**5** docplayer.net <1%  
Internet Source

---

6

"Petroleum Reservoir Rock and Fluid Properties", CRC Press, 2019

Publication

<1 %

7

Mureed Hussain, Nisar Ahmed, Wang Yan Chun, Perveiz Khalid, Azhar Mahmood, Sajid Rashid Ahmad, Umair Rasool. "Reservoir characterization of basal sand zone of lower Goru Formation by petrophysical studies of geophysical logs", Journal of the Geological Society of India, 2017

Publication

<1 %

8

Albuloushi, Asmaa. "Sequence Stratigraphy of Lower Cretaceous Carbonates in Umm Gudair Oil Field, West Kuwait.", Southern Illinois University at Carbondale, 2019

Publication

<1 %

9

[systems.uomisan.edu.iq](http://systems.uomisan.edu.iq)

Internet Source

<1 %

10

Mahdi K. Aswad, Muhamed F. Omer, Srood F. Naqshabandi. "Unlocking the hydrocarbon potential: Formation evaluation and petrophysical properties of the upper Triassic Kurra Chine Formation in Sarta Oil Field, Kurdistan Region, Northern Iraq", Heliyon, 2024

Publication

<1 %



- 11 Madof, Andrew S. "Sequence stratigraphic analysis of high frequency sequences: Cozzette sandstone member, Mount Garfield formation, Book Cliffs, Colorado", Proquest, 20111108  
Publication <1 %
- 
- 12 THEOPENUNIVERSITY. "Principles and Processes of Sediment Transport", Waves Tides and Shallow-Water Processes, 1999  
Publication <1 %
- 
- 13 [ntnuopen.ntnu.no](http://ntnuopen.ntnu.no)  
Internet Source <1 %
- 
- 14 N.D. Webb, B. Seyler, J.P. Grube. "Geologic reservoir characterization of Carboniferous fluvio-tidal deposits of the Illinois Basin, USA", Elsevier BV, 2015  
Publication <1 %
- 
- 15 [www.researchgate.net](http://www.researchgate.net)  
Internet Source <1 %
- 
- 16 Muhammad Naeem, Muhammad Kamran Jafri, Sayed S. R. Moustafa, Nassir S. AL-Arifi, Shazia Asim, Farhan Khan, Nisar Ahmed. "Seismic and well log driven structural and petrophysical analysis of the Lower Goru Formation in the Lower Indus Basin, Pakistan", Geosciences Journal, 2015  
Publication <1 %
-

87

riunet.upv.es

Internet Source

&lt;1 %

88

"Biological Consequences of Plate Tectonics",  
Springer Science and Business Media LLC,  
2020

Publication

&lt;1 %

89

El-Azabi, M.H.. "Depositional framework and  
sequence stratigraphic aspects of the  
Coniacian-Santonian mixed  
siliciclastic/carbonate Matulla sediments in  
Nezzazat and Ekma blocks, Gulf of Suez,  
Egypt", Journal of African Earth Sciences,  
200704

Publication

&lt;1 %

90

Qamar UZ Zaman Dar, Renhai Pu, Christopher  
Baiyegunhi, Ghulam Shabeer et al. "The  
impact of diagenesis on the reservoir quality  
of the early Cretaceous Lower Goru  
sandstones in the Lower Indus Basin,  
Pakistan", Journal of Petroleum Exploration  
and Production Technology, 2021

Publication

&lt;1 %

91

Spears, Justin D.. "Horizons in Unconventional  
Energy: Examples From the Anadarko Basin  
and Gulf of Mexico", Oklahoma State  
University, 2024

Publication

&lt;1 %